

This item was submitted to Loughborough's Institutional Repository (<https://dspace.lboro.ac.uk/>) by the author and is made available under the following Creative Commons Licence conditions.



CC creative commons
COMMONS DEED

Attribution-NonCommercial-NoDerivs 2.5

You are free:

- to copy, distribute, display, and perform the work

Under the following conditions:

BY: **Attribution.** You must attribute the work in the manner specified by the author or licensor.

Noncommercial. You may not use this work for commercial purposes.

No Derivative Works. You may not alter, transform, or build upon this work.

- For any reuse or distribution, you must make clear to others the license terms of this work.
- Any of these conditions can be waived if you get permission from the copyright holder.

Your fair use and other rights are in no way affected by the above.

This is a human-readable summary of the [Legal Code \(the full license\)](#).

[Disclaimer](#) 

For the full text of this licence, please go to:
<http://creativecommons.org/licenses/by-nc-nd/2.5/>

Active vibration control of flexible bodied railway vehicles via smart structures

by
Xiang Zheng

A doctoral thesis submitted in partial fulfilment of the requirements
for the award of Doctor of Philosophy of
Loughborough University

November 2011

©Xiang Zheng 2011

Abstract

Future railway vehicles are going to be designed lighter in order to achieve higher speed. Suppressing the flexible modes becomes a crucial issue for improving the ride quality of the light-weight high speed railway vehicles. The concept of smart structure brings structural damping to flexible structures by integrating smart actuators and sensors onto the structure. Smart structure eliminates the need for extensive heavy mechanical actuation systems and achieves higher performance levels through their functionality for suppressing the flexible modes. Active secondary suspension is the effective conventional approach for vibration control of the railway vehicle to improve the ride quality. But its ability in suppressing the flexible modes is limited. So it is motivated to combine active structural damping for suppressing the flexible modes and the vibration control through active secondary suspension which has an effect on both rigid and flexible modes.

The side-view model of the flexible-bodied railway vehicle integrated with piezoelectric actuators and sensors is derived. The procedure for selection of placement configurations of the piezoelectric actuators and sensors using structural norms is presented. Initial control studies show that the flexibility of the vehicle body will cause a considerable degradation in ride quality if it is neglected in the design model. Centralized and decentralized control strategies with various control approaches (e.g. modal control with skyhook damping, LQG/ \mathcal{H}_2 control, \mathcal{H}_∞ control and model predictive control (MPC)) are applied for the combined control of active structural damping and active suspension control. The active structural damping effectively suppresses the flexible modes as a complement to the work of the active suspension control.

Acknowledgement

I would like to express my gratitude to my supervisors Dr. Argyrios Zolotas and Prof. Roger Goodall for giving me this opportunity to do this research in control systems group of Loughborough University. Big thanks to them for their guidance, support, encouragements and patience during all the years of my research study, which are invaluable to me.

I also would like to thank my group members for being willing to help on many problems that I encountered in my research and their encouragements during the period of my research study.

Thanks to Dr. Orukpe Patience whom I met in summer school. Thank her for sharing her knowledge of model predictive control with me and her interest in applying it in railway vehicle systems, which make the paper *Model Predictive Control based on Mixed H_2/H_∞ Control Approach for Active Vibration Control of Railway Vehicles* possible. I would like to acknowledge that the research study is supported by the departmental studentship from Department of Electronic and Electrical Engineering of Loughborough University.

I also would like to mention my friends and brother and sisters, Xiaoyao Lu, Yiyi Mo, Derek&Tina, Angela, Aaron, Victor&Ivy, Rachel, Joanna, Audrey, Eva, Xinhai Lin, Jiang Long, Star&Laofan, Clive, Frances, Nick, Xinmiao Zhong (and many more to mention)... from Loughborough Chinese Christian fellowship. Thank them all for your love, support, sharing and prayers. Thanks to Malcolm and Margaret King from Holywell Free Church for their hospitality, trust, support and always being ready to help. Thanks to my lovely housemates Yoke, Rima and Yetta. I appreciate very much the friendship and bond that we build up during my stay in Loughborough.

I am very grateful to all my families. Special thanks to my parents for their unreserved love and support, which are so precious and important for me to complete this thesis and thanks to my grandpa who is very dear to me and passed away during this period of my research study

Last but the most important to remember, thank God for His faithfulness, His grace and unfailing love in Jesus Christ He gives to us.

Contents

Contents	iv
List of Tables	viii
List of Figures	x
1 Introduction	1
1.1 Railway transportation	1
1.2 Problems of high speed railway vehicles	3
1.3 Secondary suspensions of railway vehicles	4
1.4 Smart materials and smart structures	8
1.5 Motivations of the Research	9
1.6 Research aims and objectives	10
1.6.1 Thesis structure	11
1.7 Summary	12
2 Literature Review	13
2.1 Vibration control of railway vehicles	13
2.1.1 Active suspension control	13
2.1.2 Vibration suppression of the flexible modes	15
2.2 Smart materials and structures	16
2.2.1 Piezoelectric materials	17
2.2.2 Control with piezoelectric actuators and sensors	19
2.2.3 Piezoelectric technology for flexible-bodied vehicles	22
2.2.4 Modeling and analysis of smart structures	24

2.3	Actuator and sensor placement	25
2.4	Summary	26
3	Assessment Methods	27
3.1	Track profile	28
3.1.1	Track irregularities	28
3.2	Frequency domain analysis	30
3.3	Covariance analysis	31
3.4	Time domain analysis	33
3.5	Summary	33
4	Derivation of the Model	35
4.1	Overview	35
4.2	Rigid model of a railway vehicle	36
4.3	Model of the flexible structure	41
4.4	Flexible model of the railway vehicle	46
4.5	Coupling between rigid motion and flexible motion	49
4.6	Model analysis and simulations	50
4.7	Summary	54
5	Actuators and Sensors	57
5.1	Electro-servo Hydraulic Actuator	57
5.1.1	Spool valve	59
5.1.2	Hydraulic primary actuator	60
5.1.3	Simplified model of spool valve and torque motor	61
5.1.4	Load equation	61
5.1.5	State-space model of hydraulic actuator	61
5.1.6	Control of the hydraulic actuator	62
5.2	Piezoelectric actuators and sensors	66
5.2.1	Piezoelectric actuators	66
5.2.2	Piezoelectric sensors	68
5.3	Placement of actuators and sensors	69
5.3.1	Norms of a flexible structure	69
5.3.2	Placement indices	71

5.3.3	Placement of actuators and sensors for flexible body of a railway vehicle	71
5.4	Summary	77
6	Preliminary Studies with Active Suspension Control	78
6.1	Modal control with skyhook damping	78
6.1.1	Control method	79
6.1.2	Control design	80
6.1.3	Results and discussion	82
6.2	LQG Control	86
6.2.1	LQG Preliminaries	86
6.2.2	Control design	89
6.2.3	Results and discussion	93
6.3	Effect of actuator dynamics	98
6.4	Concluding remarks	103
7	Control Design I: Decentralized Control	104
7.1	Introduction of active structural damping	104
7.2	Structure of decentralized control	105
7.3	Control design	107
7.3.1	Active structural damping (design of K_1)	107
7.3.2	Active suspension control (design of K_2)	116
7.4	Combined active damping and active suspension control . . .	117
7.4.1	$K_1 + K_{sky}$	117
7.4.2	$K_1 + K_{rLQG}$	117
7.4.3	$K_1 + K_{LQG}$	123
7.5	Summary	125
8	Control Design II: Centralized Control	126
8.1	Structure of centralized control	126
8.2	\mathcal{H}_2 and \mathcal{H}_∞ control preliminaries	128
8.3	\mathcal{H}_2 optimal control for vibration control of railway vehicles . .	129
8.3.1	Control design with constant weights	130
8.3.2	Control design with frequency dependent weights . . .	132

8.3.3	Simulation results and analysis	134
8.3.4	Summary	141
8.4	\mathcal{H}_∞ optimal control for vibration control of railway vehicles . .	141
8.4.1	Choice of weight	142
8.4.2	Simulation results	143
8.4.3	Summary	145
8.5	Model predictive control based on mixed $\mathcal{H}_2/\mathcal{H}_\infty$ control approach for vibration control of railway vehicles	148
8.5.1	Control design	149
8.5.2	Problem Formulation	151
8.5.3	Simulation results and discussion	154
8.5.4	Parameter tuning	154
8.5.5	Conclusions	160
8.6	Concluding remarks	161
9	Conclusions and Future Work	162
9.1	Conclusions	162
9.2	Suggestions for future work	165
	Appendices	175
A	Railway Vehicle parameters	176
B	Actuator and sensor parameters	177
C	Publications of research work	179

List of Tables

1.1	Categorization of materials and systems	8
4.1	RMS results for a passive system	51
5.1	\mathcal{H}_2 and \mathcal{H}_∞ norms of individual modes of investigated actuator and sensor configurations	77
6.1	RMS results: modal control with skyhook damping	83
6.2	RMS results: LQG control design with rigid model with $q_1 =$ $1/(0.1)^2$ and $q_2 = 1/(0.012)^2$	94
6.3	RMS results: LQG control designed with flexible model with $q_2 = 1/(0.012)^2$	97
6.4	RMS results with actuator dynamics: $G + K_{sky}$	98
6.5	RMS results with actuator dynamics: $G + K_{LQG}$	100
7.1	Eigenvalues and damping ratios of the first two flexible modes of system $(G + K_1)$	113
7.2	RMS results for system $(G + K_1)$	113
7.3	RMS results for system $(G + K_1 + K_{sky})$:	117
7.4	RMS results: comparison between $G + K_1$ (config.3), $G + K_{sky}$ and $G + K_1 + K_{sky}$ (config.3)	118
7.5	RMS results for system $(G + K_1 + K_{rLQG})$:	120
7.6	RMS results: comparison between $G + K_1$ (config.3), $G + K_{rLQG}$ and $G + K_1 + K_{rLQG}$ (config.3)	120
7.7	RMS results: comparison between $G + K_{LQG}$ and $G + K_1 +$ K_{LQG} (config.3)	123

8.1	RMS results for centralized control: \mathcal{H}_2 control with constant weights	135
8.2	RMS results for centralized control: \mathcal{H}_2 control with dynamic weights	135
8.3	RMS results for \mathcal{H}_∞ control	145
8.4	RMS results for MPC control based on mixed $\mathcal{H}_2/\mathcal{H}_\infty$ control approach	156
9.1	Percentage improvement in ride quality compared with the passive system	165
B.1	Specifications of electro-servo hydraulic actuator	177
B.2	Specification of piezoelectric stack actuator	178
B.3	Specification of piezoelectric sensor patch	178

List of Figures

1.1	Dynamic elements in a high speed rail vehicle	2
1.2	Vibration modes of analytical beam	4
1.3	Passive suspension	5
1.4	Bode diagram of passive suspension	6
1.5	Active suspension	6
1.6	General active suspension scheme	7
1.7	Smart materials and structure system	9
2.1	Piezoelectric element and notations	17
2.2	Electrical equivalent of a piezoelectric	20
2.3	PZT patch actuator	20
2.4	PZT stack actuator	21
2.5	Piezoelectric stack actuator	21
4.1	Sideview model of a typical high speed passenger railway vehicles	36
4.2	Mode shapes of the free-free beam of a railway vehicle	45
4.3	Step track inputs	51
4.4	Step responses of passive rigid system: vertical accelerations .	52
4.5	Step responses of passive rigid system: deflections	52
4.6	Step responses of passive flexible system: vertical accelerations	53
4.7	Step responses of passive flexible system: deflections	53
4.8	PSD of centre acceleration for passive system	54
4.9	PSD of left acceleration for passive system	55
4.10	PSD of right acceleration for passive system	55
5.1	Servo-valve electro-hydraulic actuator	58

5.2	Controller Structure of a railway suspension system	62
5.3	Open loop uncompensated hydraulic actuator	63
5.4	Controller design for hydraulic actuator	63
5.5	Open loop of controlled hydraulic actuator	64
5.6	Closed-loop of controlled hydraulic actuator	64
5.7	Closed-loop hydraulic actuator force following	65
5.8	Closed-loop hydraulic actuator disturbance rejection	65
5.9	Piezoelectric actuator	66
5.10	Piezoelectric element	67
5.11	Relation between Ψ_r and actuator position with $L_p = 0.194m$	74
5.12	Normalized \mathcal{H}_∞ indices as a function of actuator location with fixed sensor	75
5.13	Normalized \mathcal{H}_2 indices as a function of actuator location with fixed sensor	75
5.14	Actuator and sensor placement configurations	76
6.1	Skyhook damping system	79
6.2	Intuitive control configuration: skyhook damping	80
6.3	Structure of modal control	81
6.4	Control system of modal control with skyhook damping	81
6.5	Modal control with skyhook damping with $c_b = 12 \times 10^4$ and $c_1 = 4$: Step responses	84
6.6	Modal control with skyhook damping with $c_b = 12 \times 10^4$ and $c_1 = 4$: Center acceleration PSDs	84
6.7	Modal control with skyhook damping with $c_b = 12 \times 10^4$ and $c_1 = 4$: Left acceleration PSDs	85
6.8	Modal control with skyhook damping with $c_b = 12 \times 10^4$ and $c_1 = 4$: Right acceleration PSDs	85
6.9	Modal control with skyhook damping with $c_b = 12 \times 10^4$ and $c_1 = 4$: Control Force PSDs	86
6.10	The separation principle	88
6.11	Linear quadratic control structure for the railway vehicle	90

6.12	LQG control designed with rigid model, with $q_1 = 1/(0.1)^2$ and $q_2 = 1/(0.012)^2$:closed-loop step response	95
6.13	LQG control designed with rigid model, with $q_1 = 1/(0.1)^2$ and $q_2 = 1/(0.012)^2$: Center acceleration PSDs	95
6.14	LQG control designed with rigid model, with $q_1 = 1/(0.1)^2$ and $q_2 = 1/(0.012)^2$: Left accelerations PSDs	96
6.15	LQG control designed with rigid model, with $q_1 = 1/(0.1)^2$ and $q_2 = 1/(0.012)^2$: Right acceleration PSDs	96
6.16	LQG control designed with rigid model, with $q_1 = 1/(0.1)^2$ and $q_2 = 1/(0.012)^2$:Control force PSDs	97
6.17	LQG control designed with flexible model, with $q_1 = 1/(0.1)^2$ and $q_2 = 1/(0.012)^2$:closed-loop step response	97
6.18	LQG control designed with flexible model, with $q_1 = 1/(0.1)^2$ and $q_2 = 1/(0.012)^2$: Center acceleration PSDs	98
6.19	LQG control designed with flexible model, with $q_1 = 1/(0.1)^2$ and $q_2 = 1/(0.012)^2$: Left accelerations PSDs	99
6.20	LQG control designed with flexible model, with $q_1 = 1/(0.1)^2$ and $q_2 = 1/(0.012)^2$: Right acceleration PSDs	99
6.21	LQG control designed with flexible model, with $q_1 = 1/(0.1)^2$ and $q_2 = 1/(0.012)^2$:Control force PSDs	100
6.22	Effect of actuator dynamics ($G + K_{sky}$) :Center acceleration PSDs	101
6.23	Effect of actuator dynamics ($G + K_{sky}$): Left accelerations PSDs	101
6.24	Effect of actuator dynamics ($G + K_{sky}$): Right acceleration PSDs	102
6.25	Ratio of real force/ideal force of hydraulic actuator	102
7.1	Structure of the decentralized control	106
7.2	Control system for design of $K_1(s)$	107
7.3	Closed-loop system with controller K_1 : centre acceleration PSDs	114
7.4	Closed-loop system with controller K_1 : left acceleration PSDs	114
7.5	Closed-loop system with controller K_1 : right acceleration PSDs	115
7.6	Piezoelectric actuator input voltages (configuration 3)	115
7.7	Control system for design of $K_2(s)$	116

7.8	comparison between $G + K_1$ (config.3), $G + K_{sky}$ and $G + K_1 + K_{sky}$ (config.3) : centre acceleration PSDs	118
7.9	comparison between $G + K_1$ (config.3), $G + K_{sky}$ and $G + K_1 + K_{sky}$ (config.3): left acceleration PSDs	119
7.10	comparison between $G + K_1$ (config.3), $G + K_{sky}$ and $G + K_1 + K_{sky}$ (config.3): right acceleration PSDs	119
7.11	comparison between $G + K_1$ (config.3), $G + K_{rLQG}$ and $G + K_1 + K_{rLQG}$ (config.3): centre acceleration PSDs	121
7.12	comparison between $G + K_1$ (config.3), $G + K_{rLQG}$ and $G + K_1 + K_{rLQG}$ (config.3): left acceleration PSDs	121
7.13	comparison between $G + K_1$ (config.3), $G + K_{rLQG}$ and $G + K_1 + K_{rLQG}$ (config.3): right acceleration PSDs	122
7.14	Acceleration step responses of system $G + K_1 + K_{rLQG}$ (config.3)	122
7.15	comparison between $G + K_1$ (config.3), $G + K_{LQG}$ and $G + K_1 + K_{LQG}$ (config.3): centre acceleration PSDs	123
7.16	comparison between $G + K_1$ (config.3), $G + K_{LQG}$ and $G + K_1 + K_{LQG}$ (config.3): left acceleration PSDs	124
7.17	comparison between $G + K_1$ (config.3), $G + K_{LQG}$ and $G + K_1 + K_{LQG}$ (config.3): right acceleration PSDs	124
8.1	Structure of centralized control	127
8.2	Configuration of piezoelectric actuators for centralized control	128
8.3	General control configuration	129
8.4	The LQG problem formulated in the general control configuration	130
8.5	Structure diagram of \mathcal{H}_2 (/ \mathcal{H}_∞) control design	133
8.6	Weights on control inputs for \mathcal{H}_2 control with $k_{u1} = 0.004$ and $k_{u2} = 0.001$	134
8.7	\mathcal{H}_2 control with constant weights: centre acceleration PSDs . .	136
8.8	\mathcal{H}_2 control with constant weights: left acceleration PSDs . . .	136
8.9	\mathcal{H}_2 control with constant weights: right acceleration PSDs . .	137
8.10	\mathcal{H}_2 control with constant weights: force PSDs	137

8.11 \mathcal{H}_2 control with constant weights: piezoelectric actuator voltage PSDs	138
8.12 \mathcal{H}_2 control with dynamic weights: centre acceleration PSDs	138
8.13 \mathcal{H}_2 control with dynamic weights: left acceleration PSDs	139
8.14 \mathcal{H}_2 control with dynamic weights: right acceleration PSDs	139
8.15 \mathcal{H}_2 control with dynamic weights: force PSDs	140
8.16 \mathcal{H}_2 control with dynamic weights: piezoelectric actuator voltage PSDs	140
8.17 Weights on outputs for \mathcal{H}_∞ control with $k_{z1} = 33.33$, $k_{z2} = 50$, $k_{u1} = 0.0016$ and $k_{u2} = 0.005$	144
8.18 \mathcal{H}_∞ control: centre acceleration PSDs	145
8.19 \mathcal{H}_∞ control: left acceleration PSDs	146
8.20 \mathcal{H}_∞ control: right acceleration PSDs	146
8.21 \mathcal{H}_∞ control: force PSDs	147
8.22 \mathcal{H}_∞ control: piezoelectric actuator voltage PSDs	147
8.23 MPC with piezoelectric actuators: centre acceleration	156
8.24 MPC with piezoelectric actuators: left acceleration	157
8.25 MPC with piezoelectric actuators: right acceleration	157
8.26 MPC with piezoelectric actuators: suspension forces	158
8.27 MPC with piezoelectric actuators: piezoelectric actuator voltages	158
8.28 Comparisons between MPC controllers: Center acceleration PSDs	159
8.29 Comparisons between MPC controllers: Left acceleration PSDs	159
8.30 Comparisons between MPC controllers: Right acceleration PSDs	160

Chapter 1

Introduction

In this chapter, the background knowledge of this research is introduced. Motivations of this research and deriving of the concept of smart structure for vibration control of flexible structures are traced. The challenges in future railway vehicle design to meet the requirement of faster speed with improved ride quality are revealed and the specific problems to be solved in this research are addressed.

1.1 Railway transportation

A typical conventional passenger train, as shown by Figure 1.1, consists of the vehicle body, two bogies and two wheelsets per bogie. Through the primary suspension, the wheelsets are connected to the bogie, and the bogie is connected to the vehicle body by secondary suspension. The primary suspension is so stiff that the bogie will more or less follow the way in which the track moves vertically as the train travels along. The secondary suspension is comparatively softer and is aimed to transmit the low frequency intended movements so the vehicle follows the track, but at the same time to isolate the higher frequency irregularities. Briefly speaking, the suspension system provides guidance of the train and helps to maintain the ride comfort of the passengers.

The vehicle body has 6 degrees of freedom: longitudinal, which is the

1.1. RAILWAY TRANSPORTATION

speed of the train, lateral, and vertical, plus three rotational modes: roll, pitch and yaw. Each bogie has the same degrees of freedom as the vehicle body. More degrees of freedom come from the springs and dampers. And extra modes are added if the flexibility of the vehicle body is taken into account. For vertical suspension control, the side-view model of the railway vehicle is usually used, which will be described in detail in the Modeling Chapter (Chapter 4).

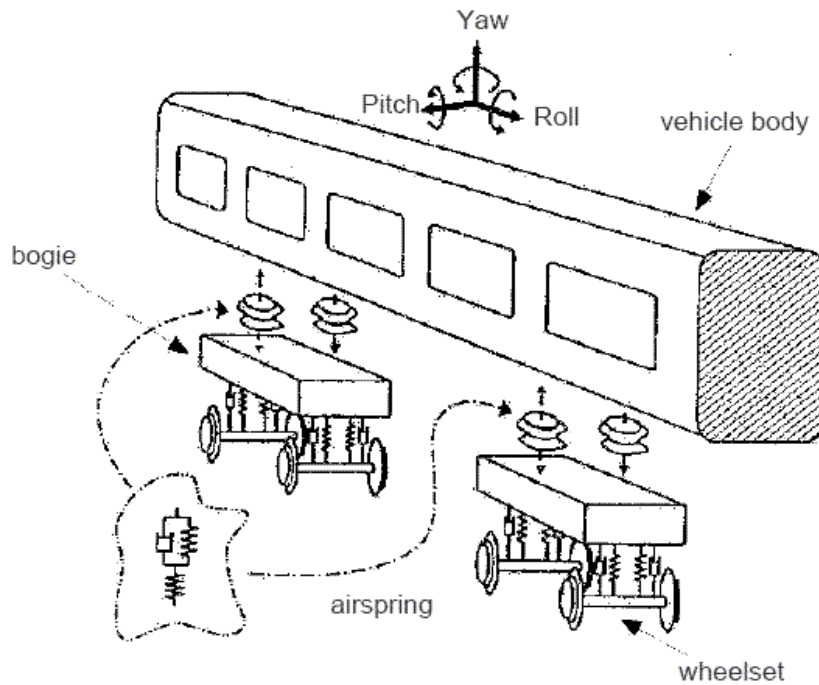


Figure 1.1: Dynamic elements in a high speed rail vehicle

In order to keep the competitive position in the whole transportation industry, there is an impetus for railway vehicles to be increasingly faster. High speed rail, by definition, is public transport by rail at the speed over 125 km/hour. The first high-speed train in the world, Japan's Tokaido Shinkansen built by Kawasaki heavy industries officially launched in 1964, achieved the speeds of 200km/h. The French TGV set in 1990 reached a speed of 515 km/h (320 mph), the world speed record for a conventional

wheeled train. The Japanese magnetic levitation (maglev) train has reached 581 km/h (361 mph). High speed train has been proved to be a very efficient and economical way of transportation.

According to Goodall and Kortum [2002], in a prospective view, future railway design is aimed to be more cost-effective and energy-efficient. Faster speed and lighter bodies are the objectives. This becomes feasible both theoretically and practically with the development of electronics and feedback control. Actuators, sensors and controller will be at the heart of future railway vehicles. Furthermore, to take full advantage of control, it is pointed out that re-design of the mechanical system is needed rather than just adding electronic control to an existing mechanical system. Thereafter, the system becomes lighter and mechanically more straightforward by making use of new lightweight designs and straightforward mechanical configurations.

1.2 Problems of high speed railway vehicles

In order to increase the speed of the railway vehicle and reduce energy consumption, the vehicle body needs to be designed as light as possible because heavy bodies limit the operating speed and require actuators of increased size and power. Due to the light-weight strategy for future high speed railway vehicle design, the impact of flexibilities of the vehicle body on ride quality can not be ignored anymore.

The problem with flexible structures lies in the reduced stiffness of the body, which results in lower natural frequencies. Therefore, increased flexibility and structural vibrations are easily excited by disturbances from the outside. This will result in increased levels of high frequency vibrations, which significantly affect ride quality. Normally vehicle bodies are built heavier than the bogies so that bogie movements are filtered via the secondary suspension effectively and do not excite body frequencies. However, as bodies become lighter, the problem of further excitation of body flexible frequencies from bogies is evident. Hence the light vehicle bodies regarded as flexible structures becomes an important issue and suppression of the vibration of both the rigid modes and flexible modes is required in order

to maintain an acceptable ride comfort or achieve improved ride quality. Also, the uncertainties associated with flexible structures require the designed controller to be sufficiently robust.

Flexible modes are bending and twisting of the vehicle body due to external forces acting on it. In this thesis, it is focused on the vertical ride quality of the vehicle and only the vertical bending modes are considered. Figure 1.2 shows the vibration modes of the vehicle body when assumed as a beam. The first vertical bending mode has the largest influence on ride comfort (Orvnas [2010]).

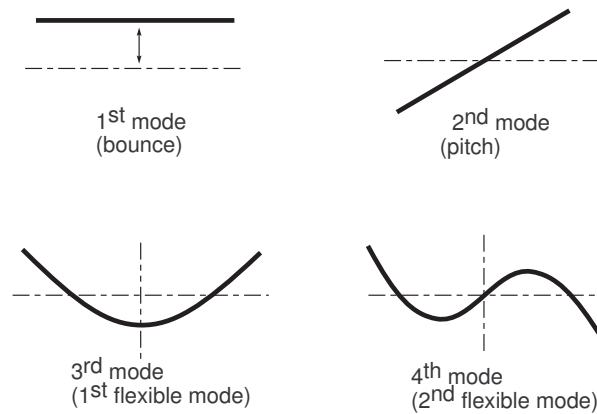


Figure 1.2: Vibration modes of analytical beam

1.3 Secondary suspensions of railway vehicles

The two main objectives of the secondary suspensions of the railway vehicle (including primary suspension and secondary suspension as shown in Figure 1.1) are

- Achieving good ride quality
- Maintaining adequate suspension clearance

The above can be interpreted as minimizing the acceleration of the vehicle body experienced by passengers without causing large suspension deflections. The track excitations can be categorized into two types: stochastic, which

1.3. SECONDARY SUSPENSIONS OF RAILWAY VEHICLES

is due to track irregularities and deterministic, e.g the gradient or steps of the track, which is designed by the civil engineers. Ride quality problem is mainly caused by the track irregularities.

The control design is a multi-objective procedure and there are trade-offs for the designers to make. In general, the suspension systems in railway vehicles can be classified into three types:

Passive suspensions (e.g Figure 1.3) usually employ springs and pneumatic or oil dampers. They are simple and cost effective. However, the performance on the wide frequency range is limited.

Active suspension (e.g Figure 1.5) has high control performance over wide frequency range while it requires high power and sophisticated control implementation

Semi-active damping was formally proposed by Karnopp [1974]. It is based on passive components and its implementations modify the stiffness and the damping characteristics of the suspension system without the need to supply a substantial amount of external energy Kallio et al. [2002]. Most commonly used are switched or variable dampers. The control action of the switched or continuously variable damper attempts to emulate a fully active control law

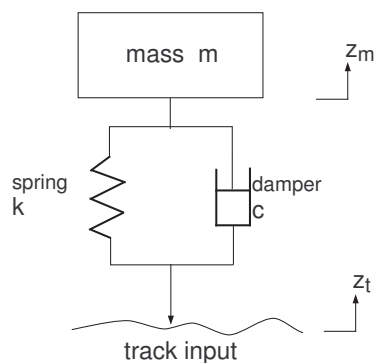


Figure 1.3: Passive suspension

1.3. SECONDARY SUSPENSIONS OF RAILWAY VEHICLES

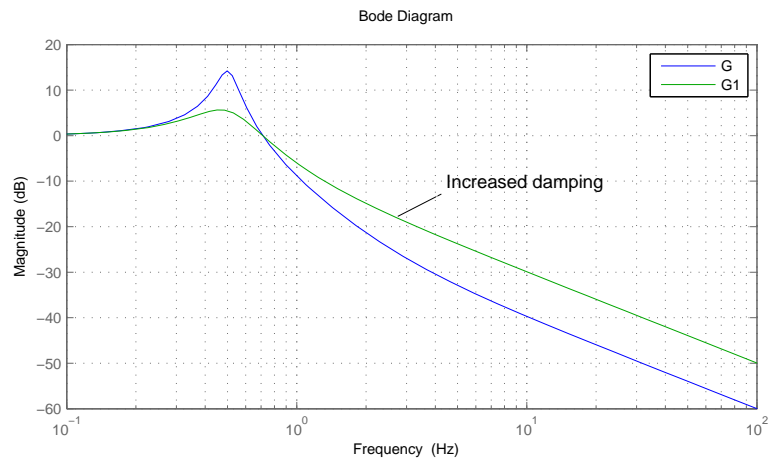


Figure 1.4: Bode diagram of passive suspension

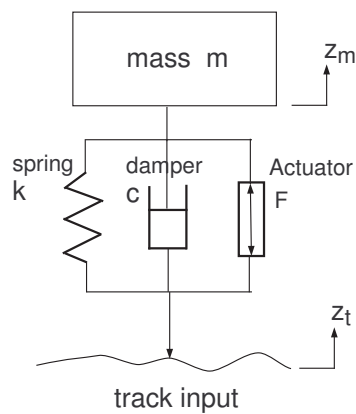


Figure 1.5: Active suspension

With passive suspensions, the performance limits have been reached due to the inherent trade-offs to be met in the design process, such as increase in the levels of damping reduces the resonance peak, but it will increase the transmissibility at higher frequencies as it is shown by Figure 1.4, which is the Bode diagram of the passive suspension system of Figure 1.3. Also, if the damping value is too low, it will increase the maximum suspension deflection during the transient period.

Semi-active control is claimed to be able to offer significant improvements in performance over passive suspensions whilst avoiding the main drawbacks

1.3. SECONDARY SUSPENSIONS OF RAILWAY VEHICLES

associated with the use of active schemes, such as complexity, weight and cost.

The technology of active suspensions of vehicles has received a great deal of attention and developments have been made over many decades. In active suspension, actuators that could provide the function of damping are used in place of dampers. However, rather than replacing the dampers and springs by actuators, the actuators are usually added in parallel with an already optimized passive suspension. Active suspension can ease the inherent trade-offs. For example, the resonance can be attenuated without increase the high frequency transmissibility (e.g.skyhook damping). Moreover, active suspension is especially more effective in suppressing the flexible motions of a flexible structure, so active suspension make possible the design of lighter-bodied higher speed railway vehicles. However, it is noted that actuators are limited in magnitude and bandwidth of forces they can produce. The bandwidth of the actuator and its ability to avoid having any effect on the system at higher frequencies is a crucial issue for active suspension control (Yusof et al. [2011]).

Figure 1.6 is a block diagram representation of a railway vehicle dynamic system. The controller is designed to govern the response of the vehicle to track inputs. The overall performance of system depends on the sensors, actuators and the software of the controller (Goodall [1997])

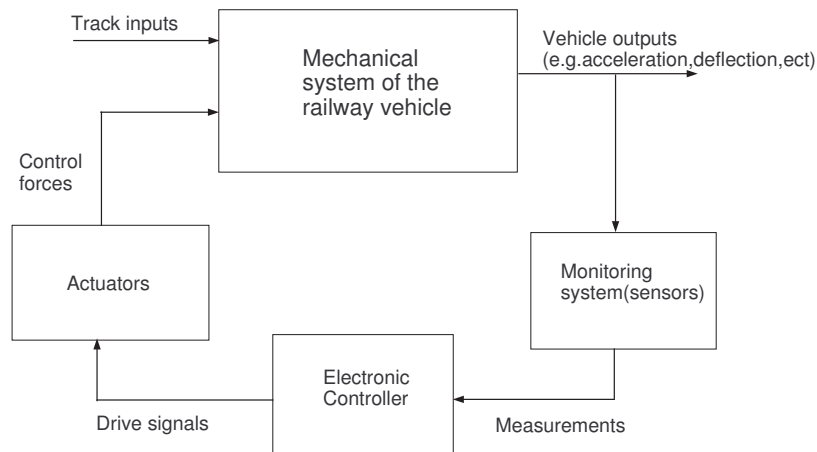


Figure 1.6: General active suspension scheme

1.4 Smart materials and smart structures

Smart materials are materials that have capabilities to respond to environmental stimuli, such as temperature, moisture, PH, or electric and magnetic fields, to compensate for undesired effects or enhance the desired effects. Typical examples of smart materials include piezoelectrics, electrostrictives, magneto-strictives, shape memory alloys (SMA), biomimetic and conductive polymers, electrochromic coatings, and magneto-rheological (MR), and electro-rheological (ER) fluids. In general, they possess the capability of actuating and /or sensing. Smart materials, in scientific literature, are often called intelligent materials or adaptive materials.

Embedding sensors, actuators, logic and control in structures, such as bridge, building, composite wings of aircrafts, vehicle bodies, results in smart structures. In the same way, apart from smart structures, various terms are also used, such as intelligent structures, adaptive structures, active structures. Though these terms are quite similar upon their appearances, they still have great difference in their meanings. Boller [1998] gave his own view by categorizing materials and systems into different levels, which is summarized by Table[1.1].

Materials&System	Sensor	Actuator	Controller	Processor
Intelligent	✓	✓	✓	✓
Adaptive	✓	✓	✓	
Active	✓	✓		
Sensory	✓			
Passive Materials				

Table 1.1: Categorization of materials and systems

Smart materials and structures represent a new rapidly growing interdisciplinary technology that embraces the fields of materials and structures, sensor and actuator systems and information processing and control as shown by figure 1.7. The development of this field is supported by the development in the field of materials and the field of control. New smart materials have been developed for sensing and actuation in more efficient ways. Also a well

designed and implemented controller plays a significant role in achieving the smart structure that is desired.

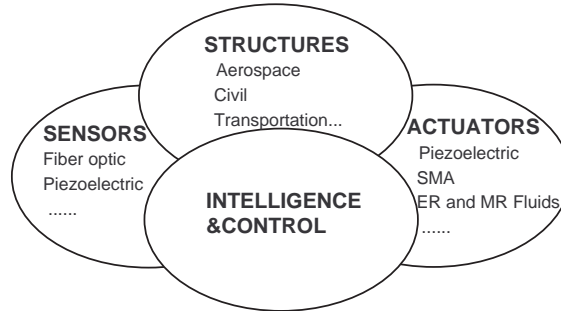


Figure 1.7: Smart materials and structure system

The potential application areas of smart materials and structures are very widespread and include energy conservation, expensive systems with high potential for operational savings, e.g. transportation systems such as aircrafts or automobiles, aerospace structures, civil infrastructure, structural health monitoring, intelligent highways, high-speed railways, active noise suppression, robotics(Jr et al. [1996]). A number of smart materials can be used for vibration control purposes as actuators and sensors such as piezoelectric, shape memory, electrostrictive and magnetostrictive materials. Piezoelectric actuators and sensors have been extensively used in vibration control applications and will be considered in this thesis.

1.5 Motivations of the Research

Smart structures are considered to have the capability to contribute to vibration suppression of flexible structures, hence improving system performance. With integrated sensors and actuator materials, they might eliminate the need for extensive heavy mechanical actuation systems. Therefore, the system will be lighter in weight, consume less energy and achieve higher performance levels through their functionality for suppressing vibrations.

Much research has been done for improving the ride quality of flexible-bodied railway vehicles: 1) by improvements in suspension control design

or 2) by structural damping through the concept of smart structure aiming at reducing the vehicle body structural vibration. In this research, it is motivated to use both of the two approaches, complementary to each other, to improve the ride quality of the railway vehicles. Therefore, the idea of suppressing the vibration of flexible-bodied railway vehicle through smart structure and active secondary suspensions is proposed. Smart actuators are to be incorporated into flexible structures, i.e. flexible bodied railway vehicles, combining with appropriate control strategies, to realize vibration suppression and robust control to improve the performance of the system.

Clearly the need of studying in-depth the flexible railway structure incorporated smart materials from both a theoretical and practical point of view is of great importance. It is to take a rigorous study of the flexible railway structure with smart materials, to investigate the feasibility of the smart material for railway application, and to incorporate control solutions based on selected sensor/actuator configuration.

1.6 Research aims and objectives

The aim of the proposed research is to contribute towards the improvement of the performance of a flexible bodied high-speed railway vehicle via the use of smart materials in addition to active secondary suspension control, thus minimizing vibrations to achieve satisfactory control of both the rigid body modes and flexible modes with certain robustness.

The objectives of this research are

1. Investigate the feasibility of introducing piezoelectric actuators and sensors to the flexible railway structure for effective ride quality enhancement at high-speeds.
2. Rigorous modeling of the flexible-bodied railway vehicle.
3. Placement of actuators and sensors to achieve the required performance with minimum effort of control.

4. Development of appropriate control strategies. Comparison between the application of different control laws (e.g. centralized/desentralized control, classical control method, optimal control method, robust control method etc.)

1.6.1 Thesis structure

The thesis is organized as follows:

- Chapter 2 is a detailed survey of work involving active suspension control of railway vehicles and suppressing of flexible modes of the vehicle body with piezoelectric actuators and sensors.
- Chapter 3 introduces the track profile and the assessment methods used in this thesis, which includes power spectral density analysis, root mean square value assessment by covariance analysis and by time domain analysis.
- Chapter 4 provides a detailed modeling of the side-view model of a typical flexible-bodied railway vehicle with stack piezoelectric actuators mounted on the vehicle body.
- Chapter 5 covers a brief study of the dynamic of the electro-servo hydraulic actuator used for the secondary suspension control, the design of a inner loop PID controller for the hydraulic actuator, brief introduction of the piezoelectric actuators and sensors used in this thesis, and finally the placement of actuators and sensors.
- Chapter 6 is a preliminary control study on active suspension control in order to demonstrate the necessity of controlling of the flexibility of the vehicle body to achieve better ride quality. Classical method of modal control with skyhook damping and advanced control method of LQG control are applied and the results are compared. The effect of dynamics of the electro-servo hydraulic actuator on the performance of the system is finally evaluated.

- Chapter 7 describes the design of the decentralized controller. Active suspension controller aimed to reduce the rigid modes and the controller for active structural damping aimed to reduce the flexible modes of the vehicle body are the two sub controllers. Two control methods, modal controller with skyhook damping and LQG control are applied for control design.
- Chapter 8 describes the design of the centralized controller. Modern control approaches \mathcal{H}_2 control, \mathcal{H}_∞ control are applied and a new technology, model predictive control technology based on mixed $\mathcal{H}_2/\mathcal{H}_\infty$ control approach are applied.
- Chapter 9 contains a conclusion on the work that is done in this thesis and suggestion for future work.

1.7 Summary

This chapter briefly introduced the railway transportation and the tendency of development for future fast speed flexible-bodied railway vehicles. The research problem is defined, the new concept for solving the problem is proposed, the aim of the research is identified. Finally, the objectives for achieving the aim are presented.

Chapter 2

Literature Review

In this chapter, a literature review is provided on relevant work to this research. The first section covers work related to active suspension of railway vehicles, which also covers the suppressing of the flexible motion with active suspension control. The second section is a coverage on work of application of smart materials/structures for vibration control purposes, especially with piezoelectric actuators. The third part is a survey on research on improving the ride quality of flexible-bodied railway vehicles with piezoelectric actuators and sensors. Finally a review is done on the methods for actuator and sensor placement.

2.1 Vibration control of railway vehicles

2.1.1 Active suspension control

Good ride quality of railway vehicles is usually achieved by a careful design of the secondary suspension system. With passive suspensions, the performance limits have been reached due to the inherent trade-offs to be met in the design process (Pratt [1996]). Active suspension provides improved performance in relaxing the many conflicting requirements for suspension system of a railway vehicle. Karnopp [1978] discussed the need for active suspensions. Orvnas [2008] provides a comprehensive literature survey of concepts and previous work on active secondary suspension in trains.

Control methods that are usually used can be categorized into classical control and modern model-based strategies (e.g. optimal control, H-infinity control).

Classical control scheme is simple and believed much easier to apply than advanced control methods (Williams [1986]). Skyhook damping is usually used as the introduction to active suspension control. Besides, it is also a good start point for developing the controller (Foo and Goodall [2000]). It controls the resonance of the suspension without making things worse at high frequencies. However, skyhook damping can create large suspension deflections when gradients and curves are encountered.

Modern control methods are capable of achieving a more complicated multi-objective control and balance well between different or even conflicting performance requirements, but they usually result in very complex controllers and may be difficult to implement (Goodall and Kortum [2002]). For example, the optimal control theory finds its regulator in minimizing a prescribed performance function that may involve various kinds of criteria. The advantages are that it ensures a stable closed-loop system with guaranteed levels of stability robustness (Foo and Goodall [2000]). This control method is good in theory but more difficult to implement. Nevertheless, it has been used by many researchers (Pratt [1996], Paddison [1995] and Foo and Goodall [2000]).

Li and Goodall [1999] compared different control strategies for applying skyhook damping control in active suspension systems for railway vehicles. Williams [1986] compared classical and optimal control methods for active suspension systems. Pratt [1996] conducted a comprehensive study of the active suspension applied to railway trains. Modified skyhook damping method, complementary filter control and optimal control were used for the secondary vertical active suspension control. Foo and Goodall [2000] applied classical control methods using skyhook damping and optimal control method for active suspension control of flexible-bodied railway vehicles. \mathcal{H}_∞ control approach was applied by Tsunashima and Morichika [2004] for ride quality improvement of an AGT vehicle. Ray [1992] studied active suspension control of an one quarter car using the LQG-LTR approach and it proved to be robust

by stochastic robustness analysis.

2.1.2 Vibration suppression of the flexible modes

As recent railway vehicles are manufactured increasingly lighter to achieve high speed, suppression of the motion of flexible modes of vehicle bodies has become essential in improving the ride comfort of railway vehicles. According to Takigami and Tomioka [2008] and Schirrer and Kozek [2008], methods that have already been proposed can be categorized into two complementary approaches: (1) applying active/semi-active suspension control (2) structural damping (passive or active). In this section, the literature survey is focused on the first approach. In the next section, the applications of piezoelectric technology for structural damping will be given.

The problem of suppressing the flexible modes started to be addressed very early for ground vehicles. Nagai and Sawada [1987] designed the active suspension system not only to control the rigid body motions but also to suppress the bending vibrations of a high speed ground vehicle. The characteristics of the actuator (the pneumatic suspension) was taken into consideration. The motion of vehicle body was divided into odd-function mode and even-function mode by modal decomposition. Decentralized optimal modal control that assumes the vertical motions of the body at front and rear are independent was applied. Then centralized optimal modal control was also employed, where odd-function mode and the even-function mode were controlled independently.

Capitani and Tibaldi [1989] studied the active suspension of a flexible vehicle. Firstly, a full LQG regulator was designed based on the full model that includes both the rigid body modes and flexible body modes. Then a reduced controller was designed by only taking account of the rigid body model. The performance of the full controller and reduced controller were compared. It was claimed that whether the reduced controller give satisfactory performance is dependent on the trade-off between the regulation cost and the control energy.

Hac [1986, 1989] studied active suspension control of a half car model

including elastic modes. Optimal control theory was adopted. The performance index included various criteria such as ride comfort, road tracking ability, hardware limitations.

Hac et al. [1996a,b] evaluated the effectiveness of active suspensions and subsequently semi-active suspensions in reducing the structural vibrations of a vehicle body. Their work emphasized on making the controller itself more aware of the flexible modes. Skyhook damping control was found effective for rigid body vehicles, but it did not perform as satisfactorily in reducing structural resonances as a passive system.

Wu et al. [2004] used semi-active suspension for vibration control of the high-speed vehicle. Elastic deformation effect was considered in a multi-body system dynamical model of the car body structure. It was shown that the ride indices on the car body floor in the place of bogie centre between the flexible car body model and rigid car body model had not much difference, but there was a big difference in the place of car body centre.

Foo and Goodall [2000] placed a third actuator in addition to two secondary suspension actuators at the centre of the vehicle for reducing the effects of first flexible mode of the vehicle body. Both classical control method with skyhook damping and Optimal control method were applied.

Sugahara et al. [2007] proposed a method by controlling the damping force of axle dampers installed between bogie frames and wheel sets. Semi-active controller was applied to determine the optimal damping force based on the skyhook control theory.

2.2 Smart materials and structures

Chopra [2002] gives an comprehensive review of state of the art of smart structures and integrated systems. Boller [1998] provides the state of the art and trends in using smart materials and systems in transportation vehicles. Hurlebaus and Gaul [2005] gives an overview of research in several fields of application of smart structure dynamics technologies. Active vibration control through the use of piezoelectric materials is included.

2.2.1 Piezoelectric materials

The piezoelectric effect was discovered by Pierre and Jacques Curie in 1880 , but it was not fully used until 1940s (Ahmadian and DeGuilio [2001]). Now piezoelectric materials have been widely used as sensory and active materials in many applications in the field of smart structures for flexible structure vibration control due to their accuracy in sensing and actuation, light weight, and ability to generate large force without reaction.

Piezoelectric materials can transfer mechanical energy to electrical energy or conversely, electrical energy to mechanical energy. When a piezoelectric material is mechanically stressed it develops an electrical charge across its terminals. This effect is known as the piezoelectric effect. Conversely, an electric field or charge that is applied to the same material will produce mechanical strain. This effect is referred to the converse piezoelectric effect.

Therefore, piezoelectricity is the combined effect of the electrical behavior of the material and Hooke's Law. Consider a typical piezoelectric transducer as in Figure 2.1. The strain-charge form of the constitutive equations of the

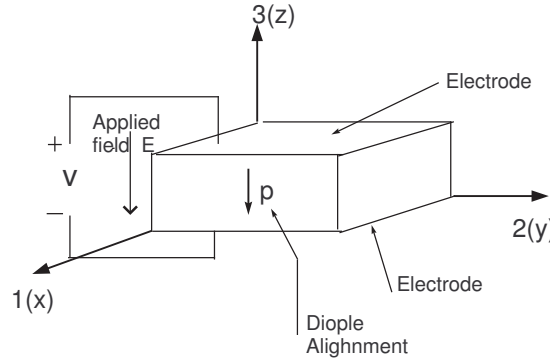


Figure 2.1: Piezoelectric element and notations

piezoelectric transducer are

$$S_i = s_{ij}^E T_j + d_{mi} E_m \quad (2.1)$$

$$D_m = d_{mi} T_i + \xi_{ik}^T E_k \quad (2.2)$$

where the indices $i, j = 1, 2, \dots, 6$ and $m, k = 1, 2, 3$ refer to different directions within the material coordinate system. S, T, D and E are the strain, stress, electrical displacement (charge per unit area) and the electrical field (volts per unit length) respectively. s^E is the elastic compliance (the inverse of elastic modulus), d the piezoelectric strain constant, ξ the permittivity, of the material. The upper script E on s^E means the compliance data was measured under at least a constant, and preferably a zero, electric field. The upper script T on ξ^T means that the permittivity data was measured under at least a constant, and preferably a zero, stress field.

The piezoelectric strain constant, d_{ij} is defined as the ratio of developed free strain to the applied electric field E . d_{33} , d_{31} and d_{32} are of major interest. i - the direction voltage applied or charge is collected; j - the direction of displacement or force. d_{32} and d_{31} constants are related to d_{33} by Poisson effect with a negative sign. The phenomenon when a material is compressed in one direction, it usually tends to expand in the other two directions perpendicular to the direction of compression, is called Poisson effect. By convention, when a electric field, which is relatively small in value compared to the poling field and in the same direction to the poling vector, is applied to the piezoelectric transducer, the element will expand in z direction and contract along the x and y directions due to the Poisson coupling. So d_{33} is positive; d_{31} and d_{32} are negative.

Transform the strain-charge form to the stress-charge form

$$T_j = c_{ij}^E S_i - e_{mi}^t E_m \quad (2.3)$$

$$D_m = e_{mi} S_i + \xi_{ik}^S E_k \quad (2.4)$$

where $c^E = (s^E)^{-1}$, $e = d(s^E)^{-1}$ and $\xi^S = \xi^T - d(s^E)^{-1}d^t$. In this thesis, the stress-charge constitutive equations will be used.

2.2.2 Control with piezoelectric actuators and sensors

Piezoelectric actuators and sensors have been extensively used in vibration control applications. Ahmadian and DeGuilio [2001] gives a good review on the recent developments on piezoceramics for vibration suppression. The review of previous research proves that PZT with different control schemes can be used to significantly reduce structural noise and vibration without adding any significant amount of weight to the structure. Most of the studies of PZT, both experimental and analytical, for noise and vibration suppression are still on relatively simple structures such as beams and plates. Halim and Moheimani [2001] conducted a comprehensive research on vibration analysis and control of smart structures. The research was concentrated on flexible structures and using piezoelectric materials as actuators and sensors. It covered the topic of modeling smart structures, optimal placement of actuators and sensors and spatial $\mathcal{H}_2/\mathcal{H}_\infty$ control of flexible structures.

Two commonly used piezoelectric materials are polyvinylidene fluoride (PVDF), a semicrystalline polymer film, and lead zirconate titanate(PZT), a piezoelectric ceramic material. PVDF is much more compliant and lightweight, thus more attractive for sensing applications. PZT is more favoured as an actuator since PZT has larger electromechanical coupling coefficients than PVDF so PZT can induce larger forces or moments on structures. It is shown that PZT can be effectively used as a transducer for vibration control of flexible structures(Halim [2002]).

The linear electrically equivalent model of a piezoelectric element is a capacitor C_p and a voltage source v_p due to the strain in the element in series, as shown by Fig 2.2. w is the disturbance on the structure. v_s is the voltage the piezoelectric will produce as a sensor when a strain is induced inside the structure. v_a is the voltage applied to the piezoelectric actuator.

There are two main types of piezoelectric actuators: Piezoelectric(PZT) patch actuators (d_{31} effect) and PZT stack actuators (d_{33} effect). The first type is often bonded on thin structures such as beams and plates and provides bending moments to the structure and is limited in the size of moments. Piezoelectric stack actuators make use of the increase of the ceramic thickness

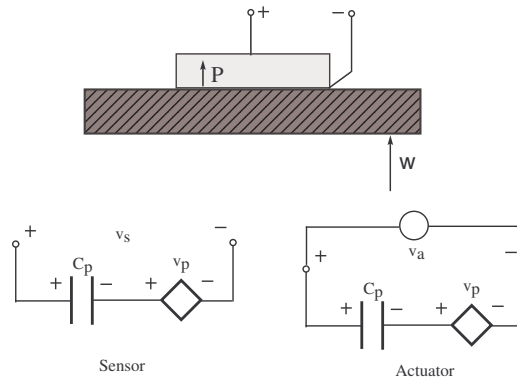


Figure 2.2: Electrical equivalent of a piezoelectric

in direction of the applied electrical field (d_{33} effect) and provide point forces when they are restrained . This type of actuator can produce extremely fine position changes with large forces up to several 10,000N.

There are also different types of actuations such as piezoelectric patch actuation, point forces and pair of moments. Figure 2.3 shows a piezoelectric patch actuator bonded on a beam. Figure 2.4 shows a piezoelectric stack actuator fixed by a stiffening structure and provides point force to the surface. Figure 2.5 shows a piezoelectric stack actuator mounted in mechanical structure and provides a pair of moments to the host structure. In this thesis, piezoelectric stack actuators are used to provide pair moments (as shown by Figure 2.5) for vibration control of the railway vehicle body.



Figure 2.3: PZT patch actuator

Control strategies with piezoelectric materials in literature can be categorized into three categories:

1. **Passive** Methods that use passive electrical elements to shunt the PZT. By Shunting the piezoelectric transducer to an electrical impedance, a

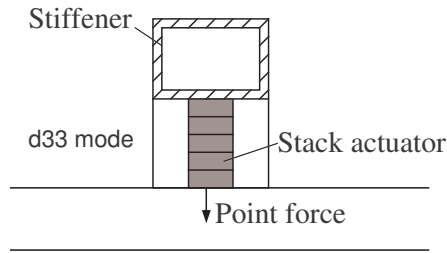


Figure 2.4: PZT stack actuator

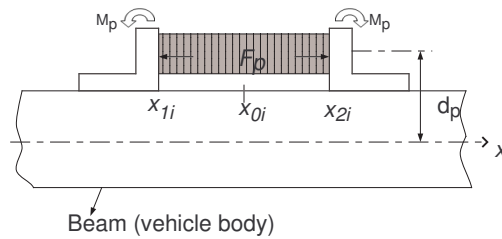


Figure 2.5: Piezoelectric stack actuator

part of the induced electrical energy can be dissipated. Hence the impedance acts as a means of extracting mechanical energy from the base structure (Takigami and Tomioka [2008]; Moheimani [2003]).

2. **Active** Methods with which active control systems are designed to drive PZT. And the control strategies are categorized as

Self-sensing

The piezoelectric transducer is used simultaneously as a sensor and an actuator. The idea is to replace the function of a sensor in the feedback loop by estimating the voltage induced inside the piezoelectric transducer. A self-sensing piezoelectric actuator provides a perfect collocation of sensor and actuator (Law et al. [2003]; Tzou and Hollkamp [1994]).

Active collocated

A pair of piezoelectric transducers, with one as a sensor and the other as an actuator. It has guaranteed stability in presence of out-of-bandwidth

dynamics (Halim and Moheimani [2002]; Moheimani [2005]).

Active non-collocated

Measured signals are used to determine the electric power through a designed controller and feedback to the piezo actuator (Kamada et al. [2005]). A stronger vibration reduction can be achieved with a non-collocated scheme (Benatzky and Kozek [2008])

3. **Hybrid and semiactive** Methods that combine the shunted and active control techniques (Law et al. [2003]; Tzou and Hollkamp [1994]).

2.2.3 Piezoelectric technology for flexible-bodied vehicles

There has been much research on applying piezoelectric for vibration control of flexible-bodied railway vehicles. Both passive (Takigami and Tomioka [2008]; Hansson et al. [2003]) and active (Kamada et al. [2005]; Schandl et al. [2007]) control schemes have been tried. In some of the studies, the model of the railway vehicle is simplified to a flexible beam (Kamada et al. [2005, 2008]), and experiments have been done on scaled vehicle bodies (Takigami and Tomioka [2008]; Kozek et al. [2009]; Benatzky et al. [2007]). However the feasibility of a full-scale implementation is still not very clear.

With passive method, piezoelectric elements are shunted by electric circuits to reduce the bending vibration of railway vehicles. Vibration energy is converted to electrical energy, which is then dissipated in a shunt circuit (Takigami and Tomioka [2008, 2005]; Hansson et al. [2003]). Kamada et al. [2008] introduced two strategies for shunt damping using piezoelectric stack transducers for vibration suppression of railway vehicle to enhance ride quality and good robustness against mass perturbation was confirmed.

An active damping concept was applied to the suppress the structural vibration modes of a car body with piezoelectric actuators by Kamada et al. [2005]. Independent \mathcal{H}_∞ controllers were designed for the first three flexible modes with only one acceleration sensor and five piezoelectric actuators. The

effectiveness of the controller was verified on a 1/6 scaled model experiment setup with piezoelectric actuators embedded to the setup.

In the research by Schandl et al. [2007], piezo-stack actuators were also proposed and studied in improving the ride comfort of light weight railway vehicles. The piezo-stack actuators mounted in consols together with collocated sensor patches were attached to the structure. A centralized control scheme was applied. The output signals of the sensors for measuring the flexible deformation of the car body were used in a feedback control loop, and a bending moment was generated and directly applied to the car body by the actuators. State feedback controller was designed with the method of pole placement and the states were estimated from the sensor signals.

Kozek et al. [2009] extended the work of Schandl et al. [2007]. Collocated strain sensors and piezoelectric actuators were used to introduce force/moments pairs into the car body structure for improving passenger ride comfort. Robust \mathcal{H}_∞ control was applied and the design steps are illustrated, nonlinear actuator dynamics were modeled and compensated, optimal placement of actuators and sensors was addressed and the feasibility of the proposed concept was demonstrated in laboratory experiments.

Benatzky et al. [2007] compared controller design utilizing the μ -synthesis procedure and pole-placement combined with Kalman-filter techniques and their implementation on a 1/10 scaled flexible structure experiment of a metro vehicle car body. A better performance was achieved by μ -synthesis procedure because of the fact that the uncertainty associated with the model of the structure as well as the fact of the performance variables to be controlled are not identical to the measurements. At the same time considerably lower control cost was needed with μ -synthesis controller.

Based on the studies carried by Benatzky et al. [2007], Schirrer and Kozek [2008] proposed the use of co-simulation for effective and efficient verification and validation of the control design for metro rail vehicle car bodies because controller design is usually carried out on order-reduced or simplified models.

2.2.4 Modeling and analysis of smart structures

Modeling of smart structures is not solely about modeling of flexible structures, but also about modeling of the smart actuators and sensors attached to the structure. For basic studies, a good description of general methods of modeling of continuous structures is provided by Bishop and Johnson [1960]. When the complicated shapes and structural patterns make the development and solution of descriptive partial differential equations burdensome, they are considered modeled as either lumped or distributed parameter systems. Various discretization techniques, such as finite element(FE) modeling, modal analysis and lumped parameters have been widely used in literature (Foo and Goodall [2000], Tohtake et al. [2005], Kozek et al. [2009]), which allow the approximation of the partial differential equations.

The system model can be formulated analytically or by system identification. According to Kozek et al. [2009], a suitable model for controller design can be derived from its FE model in the design stage, which is essential for control concept studies and actuator and sensor placement optimization. However, due to limited model accuracy, it is advised to use a more accurate model from an identification procedure for final controller computation and implementation.

The technique of modal analysis allows the vibratory motion to be represented by an infinite series of mode shapes, multiplied by system time dependent coordinates, which govern the participation of each mode shape in the overall motion. The number of modes is necessarily reduced to a finite number in order to achieve a workable mathematical model, while in the other hand the truncation of the number of modes leads to a limitation in the accuracy of the model. Instability can be caused by the unmodeled dynamics. With control design that has sufficient robust properties can overcome the bad effects that may be caused by the truncated models (Gavin [Jan 2001]).

Popprath et al. [July 2006] investigated an approximately 1/10-scaled model of a metro vehicle car body concerning the low structural eigenmodes. In the research by Schandl et al. [2007] and Schirrer and Kozek [2008], a multibody model of the flexible-bodied railway vehicle was developed by

modal approach to represent the flexible deformations and finite-element method is employed for calculating the set of eigenfunctions. Frequency response modes (FRMs) was used for modeling essential local deformations caused by the moment input of the actuators which can not be represented sufficiently by modal approach. Mechatronic damping system was applied by Kamada et al. [2005] and Schandl et al. [2007] for generating the stiffness and structural damping, which are not necessarily provided by the structure itself in the design of extremely light-weight railway vehicles.

2.3 Actuator and sensor placement

The placement of actuators and sensors on a flexible structure for vibration control plays an important role in achieving a good performance.

Criteria for the optimal placement of actuators and sensors are given in Gawronski [1999], Gawronski [2004] and Leleu et al. [2001]. Gawronski [2004] introduced criteria for optimal actuator/sensor placement based on the \mathcal{H}_2 , \mathcal{H}_∞ or the Hankel system norm of the transfer function matrices from the actuators to the sensors. In general the positions with strongest local deformations are to be selected. The placement criterion by Leleu et al. [2001] is based on state controllability/observability. The controllability gramian W_c /observability gramian W_o and the standard deviation of the eigenvalues $\sigma(\lambda_i)$ are used, thus the criterion accounts for model uncertainties.

Hac and Liu [1993] gave a systematic method for solving the problem of optimal sensor and actuator placement in the control of flexible structures. The optimization criteria are chosen based on the energies of the input and the output when the flexible structures is imposed with transient and persistent disturbances.

Aldraihem [1997] formulated an optimization criterion for size and location of piezoelectric actuators/sensors patches bonded a beam. The criterion is based on the degree of modal controllability and practical considerations. The modes are weighed differently according to their importance to the system.

Benatzky and Kozek [2008] investigated the influence of the actuator size

on the closed-loop stability of collocated and non-collocated transfer function models utilized in the structural control of flexible beams.

2.4 Summary

This literature review has covered the work on active suspension control of railway vehicles for improving the ride quality, vibration control with piezoelectric actuators and sensors and the application of the piezoelectric actuators and sensors for improving the ride quality of flexible-bodied railway vehicles. Aspects of modeling of flexible structures, control methods/strategies, and placement of actuators and sensors have been included.

Chapter 3

Assessment Methods

A reliable accurate assessment of the performance is of importance in the development of active suspension controllers of a railway vehicle. Ride quality and suspension deflections are the two important aspects in evaluating suspension performance.

Ride quality is generally characterized by the root mean square (RMS) accelerations of the vehicle body in response to disturbances from the track. The appearance of ride quality differs depending on the choice of weights, statistical approaches or evaluation formulae.

Throughout this thesis, the RMS accelerations of the vehicle body in gravity%, the suspension deflections in millimeteres, the suspension control inputs in Newtons, the control inputs from piezoelectric actuators in Volts and the power spectral density (PSD) of the accelerations and the control inputs are used as measures of the performance of the system. Three methods for analysis, namely frequency response analysis, covariance analysis and time history analysis for measuring ride quality are used. In this chapter, the track inputs subjected to the railway vehicle and these three methods for measuring ride quality are to be introduced.

3.1 Track profile

Railway vehicles are dynamically-complex systems which are subject to a variety inputs from the track, which can be categorized into two categories:

1. Stochastic(random) inputs due to track irregularities, i.e. random changes in the track vertical, lateral, and cross level positions.
2. Deterministic inputs, such as steps, curves and gradients.

The study in this thesis is concerned with the vertical ride quality of a railway vehicle running on a straight track. Track irregularities are the primary cause of ride degradation. Therefore, only the stochastic inputs, i.e. the vertical random track irregularities, are considered.

3.1.1 Track irregularities

The irregularities of a railway track can be represented by a spatial power spectrum, which is normally approximated as a fourth order equation (Pratt [1996])

$$S_S(f_s) = \frac{\Omega_v}{f_s^2 + 5.86f_s^3 + 17.29f_s^4} m^2(\text{cycle}/m)^{-1} \quad (3.1)$$

where Ω_v is the vertical track roughness in m and f_s is the spatial frequency of the track in cycle/m .

It is widely accepted to approximate Equation (3.1) by a simpler expression by neglecting the higher terms.

$$S_S(f_s) = \frac{\Omega_v}{f_s^2} m^2(\text{cycle}/m)^{-1} \quad (3.2)$$

In order to be used in dynamic analysis, the information given in Equation (3.2) needs to be converted into temporal form.

The dynamic modes of a railway vehicle lie between 0.1Hz and 20Hz, it will therefore be excited by track inputs in this frequency range. The relationship between the spatial wavelengths and the temporal excitation is velocity dependent

$$f_s(\text{cycles}/m) = \frac{f_t(\text{cycles}/s)}{v(m/s)} \quad (3.3)$$

3.1. TRACK PROFILE

Substituting (3.3) into (3.2), the track wavelengths in terms of the temporal frequency f_t is given by

$$S_S(f_t) = \frac{\Omega_v v^2}{f_t^2} m^2(\text{cycle}/m)^{-1} \quad (3.4)$$

Expression (3.4) can be converted to a spectrum with a temporal base when divided by the speed $v(m/s)$

$$S_T(f_t) = \frac{S_S(f_t) m^2(\text{cycle}/m)^{-1}}{v (m/s)} \quad (3.5)$$

The wheelsets are connected directly to dampers and this necessitates track velocities as an input if the model of the railway vehicle is to be expressed in a state-space form. Therefore, it is needed to convert the vertical track displacement spectrum given by (3.5) into its derivative. Firstly, convert (3.5) so that $S_T(f_t)$ is expressed in terms of *radians* rather than *cycles*

$$S_T(f_t) = \frac{\Omega_v v}{2\pi f_t^2} m^2(\text{rad}/s)^{-1} \quad (3.6)$$

The derivative of the spectrum is derived by multiplying the spectrum by $(2\pi f_t)^2$

$$\dot{S}_T(f_t) (m/s)^2(\text{rad}/s)^{-1} = S_T(f_t) m^2(\text{rad}/s)^{-1} \times (2\pi f_t)^2 \quad (3.7)$$

which gives

$$\dot{S}_T(\omega_t) = 2\pi\Omega_v v (ms^{-1})^2(\text{rad}/s)^{-1} \quad (3.8)$$

Finally convert the expression back to the representation in terms of *cycles* rather than *radians*

$$\dot{S}_T(f_t) = (2\pi)^2\Omega_v v (ms^{-1})^2(Hz)^{-1} \quad (3.9)$$

The vertical track spectrum is flat over all frequencies, and it is in essence white noise with a Gaussian distribution. The approximations made earlier ignoring the fourth order expression in favor of the simpler inverse-square

relationship give rise to the infinite bandwidth of this white noise, otherwise a high frequency roll-off of the expression given by (3.1) would occur giving rise to a finite bandwidth velocity spectrum. In this research, the random track is generated from (3.9) and a track roughness 2.5×10^{-7} m is used (Foo [2000]), which typically corresponds to a good quality track.

3.2 Frequency domain analysis

The frequency domain technique can be used to evaluate vehicle ride quality and suspension deflections in response to track irregularities and the PSD plots of the signals of interest.

The output power spectrum $S_y(\omega)$ is equal to the square of the modulus of the system transfer function $H(j\omega)$ multiplied by the input power spectrum $S_\omega(\omega)$

$$S_y(\omega) = H(j\omega)H(-j\omega)S_\omega(\omega) = |H(j\omega)|^2 S_\omega(\omega) \quad (3.10)$$

To account for the time delay, t_{delay} , between the front and rear wheelset. $H(j\omega)$ needs to be modified to

$$H(j\omega) = H_f(j\omega) + H_r(j\omega)e^{-j\omega t_{delay}} \quad (3.11)$$

where $H_f(j\omega)$ is the transfer function from the front velocity input to the output, and $H_r(j\omega)$ is the transfer function from the rear velocity input to the output.

The RMS values of the signal can be obtained from

$$\sigma(\omega) = \sqrt{\int_0^\infty |H(j\omega)|^2 S_\omega(\omega)} \quad (3.12)$$

Equation (3.12) requires numerical integration to infinity, which is not practically possible. Hence a finite limit is used instead. This does not pose a problem for railway vehicle application as the higher frequency components are usually attenuated by the suspension dynamics and the effect is negligible.

3.3 Covariance analysis

A summary on covariance analysis will be provided in this section (Foo [2000] and Paddison [1995]). Covariance analysis is based on Lyapunov equation. The system model can be represented by the following state-space formulation

$$\dot{x} = Ax + B_w w \quad (3.13)$$

$$y = Cx + D_w w \quad (3.14)$$

where A is the state matrix, B_w the disturbance input matrix and w the disturbance input.

The RMS values of the outputs are calculated from the solution of Lyapunov equation. It requires all the elements of the feedforward matrix D_w to be zero, i.e. the model is strictly proper. In addition, white noise input is required.

The autocorrelation function of the track input is derived from the track PSD function

$$E\{w(t)w^T(t + \tau)\} = \int_{-\infty}^{\infty} S_T\left(\frac{\omega}{2\pi}\right)e^{j\omega\tau} d\omega \quad (3.15)$$

After performing the integration, the autocorrelation may be stated more simply as

$$E\{w(t)w^T(t + \tau)\} = (2\pi)^2 \Omega_v v \delta(\tau) = q_w \delta(t - \tau) \quad (3.16)$$

The variance is simply the value of the autocorrelation function at zero, $q_w(0)$. The track disturbance input is a Gaussian white noise process. This can be used in Lyapunov equation to provide the stationary state covariance matrix P_x ($\dot{P}_x = 0$) of the system given by (3.14)

$$AP_x + P_x A^T + B_w q_w B_w^T = 0 \quad (3.17)$$

P_x is a positive definite square matrix, and is symmetric if $B_w q_w B_w^T$ is symmetric. It should be noted that the positive definite solution of the

3.3. COVARIANCE ANALYSIS

Lyapunov equation exists only for stable systems and P_x is finite only when the system is strictly proper. Then the covariance of the output vector is given by

$$\sigma^2 = CP_x C^T \quad (3.18)$$

The RMS value is given by

$$\sigma = \sqrt{|\sigma^2|} \quad (3.19)$$

However, the system concerned in this thesis is driven by two random velocity inputs from the track, which are Gaussian white noise processes. For the railway vehicle of length L_v and a traveling speed of v m/s, there will be a time delay between the front and rear input due to the distance between the front and rear bogies. The front and rear velocity are related by

$$\dot{Z}_R(t) = \dot{Z}_L(t - t_{delay}) \quad (3.20)$$

With a constant track variance given by (3.9), the auto-correlation function of the track input in this instance is

$$Q_w = (2\pi)^2 \Omega_v v \begin{bmatrix} \delta(t - \tau) & \delta(t - \tau + t_{delay}) \\ \delta(t - \tau - t_{delay}) & \delta(t - \tau) \end{bmatrix} \quad (3.21)$$

Then

$$B_w Q_w B_w^T = (2\pi)^2 \Omega_v v [B_{wL} B_{wL}^T + B_{wR} B_{wR}^T + B_{wR} B_{wL}^T e^{A^T t_{delay}} + e^{A t_{delay}} B_{wL} B_{wR}^T] \quad (3.22)$$

In equation 3.22, Q_w is the covariance, which is the auto-correlation function at zero. Instead of solving (3.17), solving the following equation for P_x

$$AP_x + P_x A^T + B_w Q_w B_w^T = 0 \quad (3.23)$$

Finally the variance of the system can be calculated by (3.18)

3.4 Time domain analysis

In time domain, it is to find the RMS (root mean square) of a signal by investigating the vehicle model output responses with respect to the track data recordings. The RMS value for a given output can be found using

$$y_{rms} = \sqrt{E[y^2(t)]} = \sqrt{\lim_{T \rightarrow \infty} \int_0^T y^2 dt} \quad (3.24)$$

or approximately

$$y_{rms} \approx \sqrt{\frac{1}{n} \sum_{i=1}^n y_i^2} \quad (3.25)$$

where n is the number of elements in the data sample. It is easily seen that the accuracy of the RMS value depends upon the available duration of track data T , and the number of sample points n (in other words, it depends upon the available number of sample points and the sampling interval). Therefore, a sufficiently long track together with an adequate number of sample points should be selected in order to achieve accurate RMS results

To analyze the frequency information of the signal, fast Fourier transform (FFT) can be performed to the output response of the railway vehicle model by simulating it with the track data. Similarly, a sufficiently long duration of track data and an adequate number of points should be used to reveal accurate information of the signal frequency content.

Though the time history analysis methods are slower and less accurate than covariance and frequency methods. Time analysis is the best solution when the model contains non-linearities or it is difficult to get a linear model of the system because both the covariance and frequency methods can only be used with a linear model.

3.5 Summary

This chapter has described the representation of the track irregularities. Vertical ride quality of a railway vehicle running on a straight track is of

3.5. SUMMARY

main concern of this thesis. Track irregularities are the primary cause of ride degradation. It has introduced the method of frequency response analysis for calculating the PSDs of signals of interest, and method of covariance analysis and time history analysis for calculating r.m.s values.

Chapter 4

Derivation of the Model

4.1 Overview

It is very important to obtain a sufficiently accurate model of the system for control design. In this chapter, the side-view model of a flexible-bodied railway vehicle is derived. Flexibility in the bodies of high-speed railway vehicles creates a number of difficulties which in practice may result in the body structure being heavier than it might otherwise be. When an active suspension is used it becomes particularly important to model the vehicle and its flexibility in an effective manner because: (i) active control might inadvertently excite the flexible modes (ii) there is also the opportunity to control the flexibility.

The vehicle body of the railway vehicles is to be assumed as a flexible free-free beam, which is justified because the secondary suspension is very soft that the vehicle body moves in the manner of a free-free beam. Both the flexible modes and rigid modes will be included in the model. The bogie will be considered rigid and are connected with the vehicle body with various suspension elements (i.e. spring and dampers). The system is subject to three inputs sources: track disturbances, the control forces provided across the secondary suspensions and the control moments provided by the piezoelectric actuators attached to the railway vehicle body.

4.2 Rigid model of a railway vehicle

The dynamics of a real railway vehicle is very complex, which can be non-linear and has high coupling in certain modes. The models developed, however, are almost all linear and time-invariant. The linear time-invariant model justifies itself in representing the real system because the railway suspensions usually operate about a static equilibrium position, and the design and analysis techniques available are all based on linear system theory.

The mathematical model of the system is based on the side-view of a railway vehicle as shown in Figure 4.1 (Foo and Goodall [1998]). It is a simplified model that only two wheel sets are included instead of four because the time delay between the inputs to the two wheel sets on the same bogie can be treated as negligible.

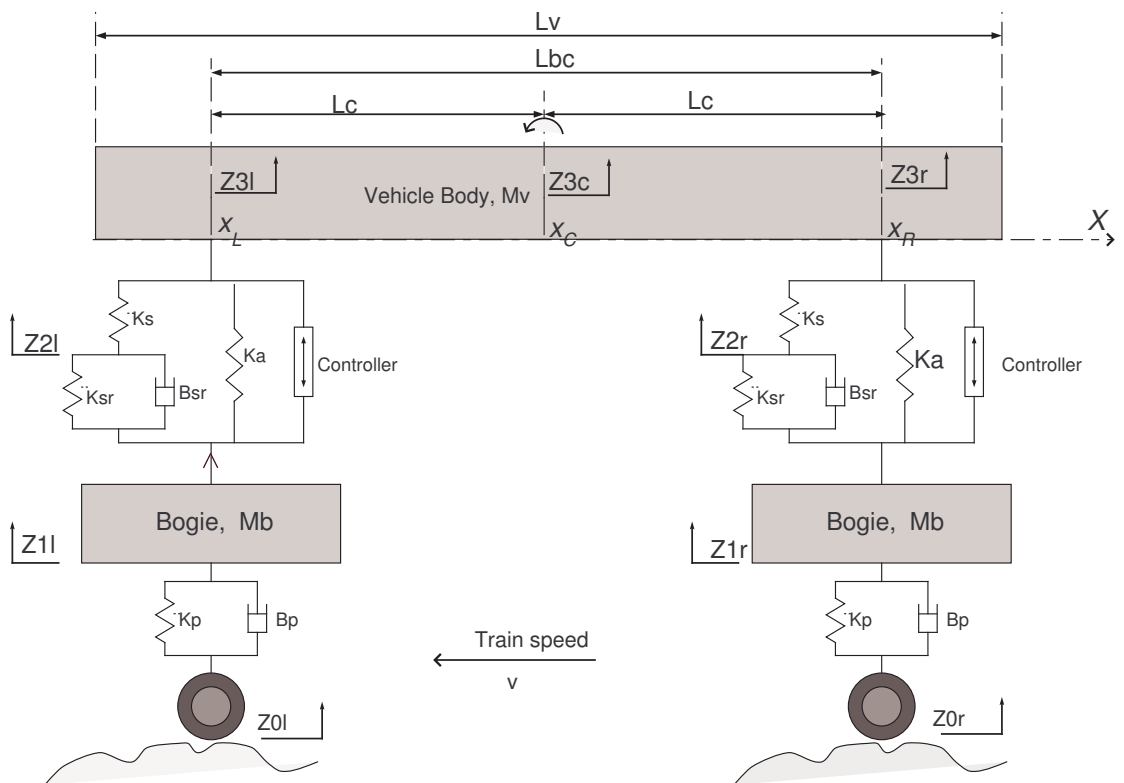


Figure 4.1: Sideview model of a typical high speed passenger railway vehicles

Based on the model shown by Fig 4.1, there are seven degrees of freedom,

4.2. RIGID MODEL OF A RAILWAY VEHICLE

i.e. the vehicle body's bounce mode and pitch mode, the bounce modes of the two bogie masses, and two modes associated with the internal dynamics of the air spring. When flexibility is considered, extra flexible modes of the vehicle body will be added. However, in this section, it is to first derive rigid model of the railway vehicle.

The vehicle body is influenced by the forces generated by the passive secondary suspension components: K_s , K_a , K_{sr} , B_{sr} , and by the active control forces from the actuators across the secondary suspensions on the left and the right : U_L , U_R . The bogie motions are effected by both and primary suspension components, i.e. K_p and B_p , and the passive secondary components as well as the reaction of the active secondary forces. The primary suspension is subjected to the disturbances from the track \dot{Z}_{0L} and \dot{Z}_{0R} .

For a system with more than a few degrees of freedom, it becomes a cumbersome way to derive the equations of motion with Newton's second law of motion. Lagrangian Equation will be used to establish the equations of motions of the railway vehicles. Lagrange's equation provides a systematic unified approach for handling the modeling problems of a wide range of physical systems. The differential equations that describe the system will be readily obtained once the systematic procedure is carried out. It is especially advantageous to use Lagrange's equation to model large complex systems, for it deals with the model from the energy point of view. Lagrange's Equation is given by

$$\frac{d}{dt}\left(\frac{\partial T}{\partial \dot{p}_n}\right) - \frac{\partial T}{\partial p_n} + \frac{\partial D}{\partial \dot{p}_n} + \frac{\partial V}{\partial p_n} = Q_n \quad (4.1)$$

where $n = 1, 2, \dots$ denotes the number of independent coordinates that exist in the system; p_n is the generalized coordinate; \dot{p}_n is the generalized velocity; T is the total kinetic energy of the system; D is the dissipation function of the system; V is the total potential energy of the system; Q_n is the generalized applied force at the coordinate n .

For the convenience of modeling, we assume that there are two small masses, $m_L \rightarrow 0$ and $m_R \rightarrow 0$, locating at where displacements of Z_{2L} and Z_{2R} are measured respectively. The energy expressions for the system given

4.2. RIGID MODEL OF A RAILWAY VEHICLE

by Fig [4.1] are

$$T = \frac{1}{2}Mv\dot{Z}_{3C}^2 + \frac{1}{2}I_{vc}\dot{\Theta}^2 + \frac{1}{2}m_L\dot{Z}_{2L}^2 + \frac{1}{2}m_R\dot{Z}_{2R}^2 + \frac{1}{2}M_b\dot{Z}_{1L}^2 + \frac{1}{2}M_b\dot{Z}_{1R}^2 \quad (4.2)$$

$$D = \frac{1}{2}B_{sr}(\dot{Z}_{2L} - \dot{Z}_{1L})^2 + \frac{1}{2}B_{sr}(\dot{Z}_{2R} - \dot{Z}_{1R})^2 + \frac{1}{2}B_p(\dot{Z}_{1L} - \dot{Z}_{0L})^2 + \frac{1}{2}B_p(\dot{Z}_{1R} - \dot{Z}_{0R})^2 \quad (4.3)$$

$$V = \frac{1}{2}K_a(Z_{3L} - Z_{1L})^2 + \frac{1}{2}K_a(Z_{3R} - Z_{1R})^2 + \frac{1}{2}K_s(Z_{3L} - Z_{2L})^2 + \frac{1}{2}K_s(Z_{3R} - Z_{2R})^2 + \frac{1}{2}K_{sr}(Z_{2L} - Z_{1L})^2 + \frac{1}{2}K_{sr}(Z_{2R} - Z_{1R})^2 + \frac{1}{2}K_p(Z_{1L} - Z_{0L})^2 + \frac{1}{2}K_p(Z_{1R} - Z_{0R})^2 \quad (4.4)$$

The seven generalized coordinates are chosen as Z_{3C} , Θ , Z_{2L} , Z_{2R} , Z_{1L} , Z_{1R} , where Z_{3C} is the bounce position of the vehicle body measured at the vehicle centre x_C , θ is the pitch angle of the vehicle body, Z_{1L} and Z_{1R} are the bounce position of the assumed two small masses, and Z_{2L} and Z_{2R} are the bounce position of the left bogie mass and the right bogie mass. When the pitch angle θ is small, the relationship between the coordinates can be described as

$$Z_{3L} = Z_{3C} + L_c\Theta \quad (4.5)$$

$$Z_{3R} = Z_{3C} - L_c\Theta \quad (4.6)$$

where Z_{3L} and Z_{3R} are the bounce of the vehicle body measured at the positions x_L and x_R respectively.

Apply the Lagrange's equation of equation (4.1) to the system

$$\frac{d}{dt}\left(\frac{\partial T}{\partial \dot{Z}_{3C}}\right) - \frac{\partial T}{\partial Z_{3C}} + \frac{\partial D}{\partial \dot{Z}_{3C}} + \frac{\partial V}{\partial Z_{3C}} = U_r + U_c + U_f \quad (4.7)$$

$$\frac{d}{dt}\left(\frac{\partial T}{\partial \dot{\Theta}}\right) - \frac{\partial T}{\partial \Theta} + \frac{\partial D}{\partial \dot{\Theta}} + \frac{\partial V}{\partial \Theta} = U_r L_c - U_f L_c \quad (4.8)$$

$$\frac{d}{dt}\left(\frac{\partial T}{\partial \dot{Z}_{2L}}\right) - \frac{\partial T}{\partial Z_{2L}} + \frac{\partial D}{\partial \dot{Z}_{2L}} + \frac{\partial V}{\partial Z_{2L}} = 0 \quad (4.9)$$

$$\frac{d}{dt}\left(\frac{\partial T}{\partial \dot{Z}_{2R}}\right) - \frac{\partial T}{\partial Z_{2R}} + \frac{\partial D}{\partial \dot{Z}_{2R}} + \frac{\partial V}{\partial Z_{2R}} = 0 \quad (4.10)$$

$$\frac{d}{dt}\left(\frac{\partial T}{\partial \dot{Z}_{1L}}\right) - \frac{\partial T}{\partial Z_{1L}} + \frac{\partial D}{\partial \dot{Z}_{1L}} + \frac{\partial V}{\partial Z_{1L}} = -U_f \quad (4.11)$$

$$\frac{d}{dt}\left(\frac{\partial T}{\partial \dot{Z}_{1R}}\right) - \frac{\partial T}{\partial Z_{1R}} + \frac{\partial D}{\partial \dot{Z}_{1R}} + \frac{\partial V}{\partial Z_{1R}} = -U_r \quad (4.12)$$

The differential equations obtained from equation (4.9), (4.10) are

$$B_{sr}(\dot{Z}_{2L} - \dot{Z}_{1L}) + K_s(Z_{2L} - Z_{3C} + L_c\theta) - K_{sr}(Z_{1L} - Z_{2L}) = 0 \quad (4.13)$$

$$B_{sr}(\dot{Z}_{2R} - \dot{Z}_{1R}) + K_s(Z_{2R} - Z_{3C} + L_c\theta) - K_{sr}(Z_{1R} - Z_{2R}) = 0 \quad (4.14)$$

It should be noted that the states \dot{Z}_{2R} and \dot{Z}_{2L} can be eliminated from the rest of the differential equations by substituting in their expressions in terms of other states, which are solved out from equations (4.13) and (4.14).

Lagrangian equations use degrees of freedom of the structure to describe the dynamic of the system. If represented in state-space form, the dynamic of the system is described by system states. The number of system states are usually equal or larger than twice the number of degrees of freedom of freedom. The state-space representation of the model is formed as

$$\dot{\mathbf{x}}_r = \mathbf{A}_r \mathbf{x} + \mathbf{B}_r \mathbf{u} + \mathbf{G} \mathbf{w} \quad (4.15)$$

where matrices \mathbf{A}_r , \mathbf{B}_r , and \mathbf{G} the system matrix, force input matrix, disturbance input matrix, and \mathbf{x}_r the states of the system are set as

$$\mathbf{x}_r = [\dot{Z}_{3C} \quad Z_{3C} \quad \dot{Z}_{1L} \quad Z_{1L} \quad \dot{Z}_{1R} \quad Z_{1R} \quad Z_{2L} \quad Z_{2R} \quad \dot{\Theta} \quad \Theta] \quad (4.16)$$

4.2. RIGID MODEL OF A RAILWAY VEHICLE

$\mathbf{u} = [U_L \ U_R]$ is the control input vector across the secondary suspension; $\mathbf{w} = [\dot{Z}_{0L} \ \dot{Z}_{0R}]$ is the track (disturbance) input vector. \mathbf{A}_r is the system matrix, \mathbf{B}_r is the control input matrix, and \mathbf{G} is the disturbance input matrix and they are obtained from as follows. The calculations were done in MATHEMATICA.

Find the state-space representation by relative states, which are defined as

$$\begin{aligned} R_1 &= Z_{3L} - Z_{1L} & R_2 &= Z_{3R} - Z_{1R} & R_3 &= Z_{2L} - Z_{1L} \\ R_4 &= Z_{2R} - Z_{1R} & R_5 &= Z_{1L} - Z_{0L} & R_6 &= Z_{1R} - Z_{0R} \end{aligned} \quad (4.17)$$

If the new state vector is chosen as

$$\mathbf{x}_r = \left[\dot{Z}_{3C} \ \dot{\theta} \ \dot{Z}_{1L} \ \dot{Z}_{1R} \ R_1 \ R_2 \ R_3 \ R_4 \ R_5 \ R_6 \right] \quad (4.18)$$

Then the appearance of energy expressions given by equation (4.3) and (4.4) can be written as

$$D = \frac{1}{2}B_{sr}\dot{R}_3^2 + \frac{1}{2}B_{sr}\dot{R}_4^2 + \frac{1}{2}B_p\dot{R}_5^2 + \frac{1}{2}B_p\dot{R}_6^2 \quad (4.19)$$

$$\begin{aligned} V &= \frac{1}{2}K_a R_1^2 + \frac{1}{2}K_a R_2^2 + \frac{1}{2}K_s(R_1 - R_3)^2 + \frac{1}{2}K_s(R_2 - R_4)^2 \\ &\quad + \frac{1}{2}K_{sr}R_3^2 + \frac{1}{2}K_{sr}R_4^2 + \frac{1}{2}K_p R_5^2 + \frac{1}{2}K_p R_6^2 \end{aligned} \quad (4.20)$$

and equation (4.2) remains the same. The state-space model by the new state is obtained as

$$\mathbf{A}_r = \begin{bmatrix} 0 & 0 & 0 & 0 & -\frac{K_s+K_a}{M_v} & -\frac{K_s+K_a}{M_v} & \frac{K_s}{M_v} & \frac{K_s}{M_v} & 0 & 0 \\ 0 & 0 & 0 & 0 & \frac{L_c(K_s+K_a)}{I_{vc}} & -\frac{L_c(K_s+K_a)}{I_{vc}} & -\frac{L_c}{I_{vc}}K_s & \frac{L_c}{I_{vc}}K_s & 0 & 0 \\ 0 & 0 & -\frac{B_p}{M_b} & 0 & \frac{K_a+K_s}{M_b} & 0 & -\frac{K_s}{M_b} & 0 & -\frac{K_p}{M_b} & 0 \\ 0 & 0 & 0 & -\frac{B_p}{M_b} & 0 & \frac{K_a+K_s}{M_b} & 0 & -\frac{K_s}{M_b} & 0 & -\frac{K_p}{M_b} \\ 1 & L_c & -1 & 0 & 0 & 0 & 0 & 0 & 0 & 0 \\ 1 & -L_c & 0 & -1 & 0 & 0 & 0 & 0 & 0 & 0 \\ 0 & 0 & 0 & 0 & \frac{K_s}{B_{sr}} & 0 & -\frac{K_s+K_{sr}}{B_{sr}} & 0 & 0 & 0 \\ 0 & 0 & 0 & 0 & 0 & \frac{K_s}{B_{sr}} & 0 & -\frac{K_s+K_{sr}}{B_{sr}} & 0 & 0 \\ 0 & 0 & 1 & 0 & 0 & 0 & 0 & 0 & 0 & 0 \\ 0 & 0 & 0 & 1 & 0 & 0 & 0 & 0 & 0 & 0 \end{bmatrix} \quad (4.21)$$

$$\mathbf{B}_r = \begin{bmatrix} \frac{1}{M_v} & \frac{1}{M_v} \\ -\frac{L_c}{I_{vc}} & \frac{L_c}{I_{vc}} \\ -\frac{1}{M_b} & 0 \\ 0 & -\frac{1}{M_b} \\ 0 & 0 \\ 0 & 0 \\ 0 & 0 \\ 0 & 0 \\ 0 & 0 \end{bmatrix} \quad (4.22)$$

$$\mathbf{G} = \begin{bmatrix} 0 & 0 \\ 0 & 0 \\ \frac{E_p}{M_b} & 0 \\ 0 & \frac{E_p}{M_b} \\ 0 & 0 \\ 0 & 0 \\ 0 & 0 \\ 0 & 0 \\ -1 & 0 \\ 0 & -1 \end{bmatrix} \quad (4.23)$$

4.3 Model of the flexible structure

The flexible body of the railway vehicle is assumed as a free-free Euler-Bernoulli beam of length, l , cross section area, A_b , material density, ρ_b and flexural rigidity, EI , which depends on the Young's modulus of elasticity E and the second moment of area I . The flexural vibration of the beam is induced by the excitations transmitted through the suspensions from the track disturbances. Here it is assumed that there are n_p stack piezoelectric actuators attached to the surface of the beam to suppress the flexure vibration of the beam.

These are the main assumptions about the flexible structure

- Bernoulli-Euler theory is used as the method of analysis, it assumes that plane cross-sections of the beam remain plane during flexure and the radius of curvature of a bent beam is large compared with the beam's depth (Bishop and Johnson [1960]).

4.3. MODEL OF THE FLEXIBLE STRUCTURE

- The mass and stiffness contributions of the piezoelectric elements are considerably smaller than those of the beam so they can be ignored.

The transverse deflection at point x of the beam and time t is denoted by $v(x, t)$, assuming the beam is one-dimension only. The governing PDE (Partial differential equation) that describes the dynamics of the structure of the flexible beam is given as follows (Halim et al(2002)).

$$EI \frac{\partial^4 v(x, t)}{\partial x^4} + \rho_b A_b \frac{\partial^2 v(x, t)}{\partial t^2} = \sum_{i=1}^{n_p} \frac{\partial^2 M_{px}(x, t)}{\partial x^2} + F_{x_L}(t) \delta(x-l_1) + F_{x_R}(t) \delta(x-l_2) \quad (4.24)$$

where F_{x_L} and F_{x_R} are the forces from the left and right suspensions. $i=1, 2, \dots, n_p$ denote the number of piezoelectric actuators, M_{px} the moment acting on the beam by the piezoelectric actuators, which is given by (Halim et al(2001))

$$M_{px}^i(x, t) = K_a V_{ai} [H(x - x_{1i}) - H(x - x_{2i})] \quad (4.25)$$

where V_{ai} is the voltage applied to the i th actuator. $H(\cdot)$ is the step function. x_{1i} and x_{2i} denote the location of the two ends of the i th piezoelectric actuator along the X axis. And K_a is a constant based on the properties of the beam and the piezoelectric actuators. The first forcing term in PDE equation (4.24) can be determined from equation (4.25), using the property of Dirac's delta function

$$\int_{-\infty}^{\infty} \delta^{(n)}(t - \theta) \phi(t) dt = (-1)^n \phi^{(n)}(\theta) \quad (4.26)$$

where $\delta^{(n)}$ is the n th derivative of δ and ϕ is continuous at θ .

The beam equation contains a fourth-order derivation in x , so four boundary conditions are needed to find a unique solution $z(x, t)$. Since no external bending moment and no external force are applied at the free ends of the beam, the bending moment and the shear force at the free ends are

4.3. MODEL OF THE FLEXIBLE STRUCTURE

zero. Therefore, the end conditions for both free ends of the beam are

$$\frac{\partial^2 z(x, t)}{\partial x^2} \Big|_{x=0} = \frac{\partial^3 z(x, t)}{\partial x^3} \Big|_{x=0} = 0 \quad (4.27)$$

$$\frac{\partial^2 z(x, t)}{\partial x^2} \Big|_{x=L_v} = \frac{\partial^3 z(x, t)}{\partial x^3} \Big|_{x=L_v} = 0 \quad (4.28)$$

where the x coordinate of the left end and the right end of the beam are 0 and L_v respectively.

By the modal analysis technique, the solution of the transverse deflection $v(x, t)$ is assumed to be in the form

$$v(x, t) = z_{3c}(t) + \theta(t)(x - L_b/2) + \sum_{r=1}^{\infty} q_r(t)\phi_r(x) \quad (4.29)$$

where $q_r(t)$ is the r th flexible mode in generalized coordinate and $\phi_r(x)$ is the corresponding mode shape(eigenfunction), which is determined from the eigenvalue problem

$$\phi_r(x) = \frac{\cosh \lambda_r x + \cos \lambda_r x - \frac{\cosh(\lambda_r l) - \cos(\lambda_r l)}{\sinh(\lambda_r l) - \sin(\lambda_r l)}}{(\sinh(\lambda_r x) + \sin(\lambda_r x))} \quad (4.30)$$

The frequency equation of an undamped free-free beam is

$$\cos(\lambda_r l) \cosh(\lambda_r l) - 1 = 0 \quad (4.31)$$

Through equation (4.31), a series of λ_r can be determined, and the corresponding natural frequencies ω_r determined by

$$\lambda^4 = \frac{\omega^2 A_b \rho_b}{EI} \quad (4.32)$$

4.3. MODEL OF THE FLEXIBLE STRUCTURE

The eigenfunction mode shapes have orthogonality properties

$$\int_0^L \phi_r(x)\phi_p(x)dx = \delta_{rp} \quad (4.33)$$

$$\int_0^L \frac{EI}{\rho_b A_b} \frac{d^4 \phi_r(x)}{dx^4} \phi_p(x) dx = \omega_r^2 \delta_{rp} \quad (4.34)$$

where δ_{rp} is the Kronecker delta function.

The flexible motions can be denoted by a set of uncoupled ordinary differential equations, which can be obtained by integrating equation (4.24) over the beam length, using the orthogonality properties of equation (4.33) and (4.34) and Dirac's delta function property of equation (4.26) as well as the solution in 4.29.

$$\ddot{q}_r(t) + 2\zeta_r \omega_r \dot{q}_r(t) + \omega_r^2 q_r(t) = \frac{K_a \sum_{i=1}^{n_p} \Psi_{ri} V_{ai}(t) + F_{x_L} \phi_r(l_1) + F_{x_R} \phi_r(l_2)}{M_b} \quad (4.35)$$

where ω_r is the natural frequency of the r^{th} flexible mode. Structural damping is added and ζ_r is the damping ratio of the r^{th} flexible mode. M_b is the mass of the beam, and Ψ_{ri} is given by

$$\Psi_{ri} = \frac{d\phi_r}{dx}(x_{2i}) - \frac{d\phi_r}{dx}(x_{1i}) \quad (4.36)$$

Ψ_{ri} is for the i th piezoelectric actuator, and is a function of the position of the piezoelectric actuator, x_{0i} , and the length of the actuator L_p .

The multi-input-infinite-output transfer function from the applied actuator voltages $\mathbf{V}_a(s)$ to the beam deflection $Z(x, s)$ at location x , is written as

$$G(x, s) = \frac{K_a}{M_b} \sum_{r=1}^{\infty} \frac{\phi_r(x) \Psi_r^T}{s^2 + 2\zeta_r \omega_r s + \omega_r^2} \quad (4.37)$$

where

$$\mathbf{V}_a(s) = [V_{a1}(s), \dots, V_{an_p}(s)]^T \quad (4.38)$$

$$\Psi_r^T = [\Psi_{r1} \Psi_{r2} \cdots \Psi_{rn_p}] \quad (4.39)$$

4.3. MODEL OF THE FLEXIBLE STRUCTURE

Although there is an infinite number of flexible modes, we can only consider a finite number for practical purposes. The first flexible mode has shown the most significant influence on ride quality of the railway vehicle (Foo and Goodall [2000]). Therefore, only the first two flexible modes, i.e. the first symmetrical flexible mode and the first asymmetrical flexible mode, of the body of the railway vehicle have so far been taken in account in this thesis. The mode shapes of the first two flexible modes are shown in Figure 4.2.

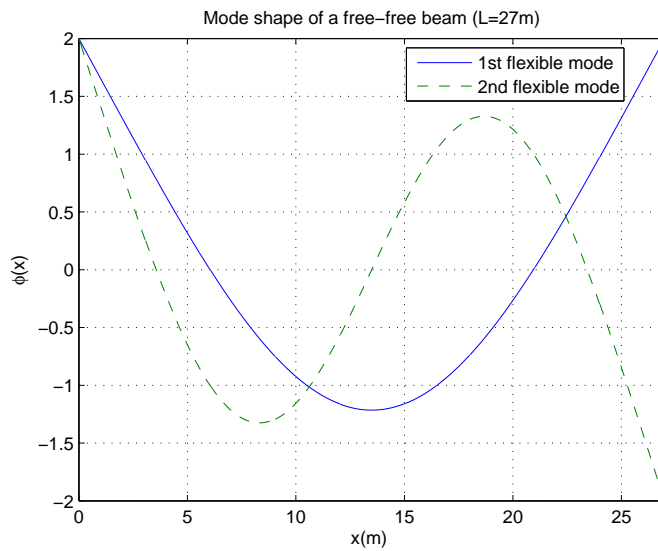


Figure 4.2: Mode shapes of the free-free beam of a railway vehicle

The excitation of each mode is a result of the contribution of all the external forces acting on the beam and the moments from all piezoelectric actuators. While a control law needs to be designed to determine the moments from the piezoelectric actuators so that the excitation of the modes are reduced.

4.4 Flexible model of the railway vehicle

According to the ODE equation (4.35), the ordinary differential equations of the first two flexible motions can be written as

$$\ddot{q}_1(t) + 2\zeta_1\omega_1\dot{q}_1(t) + \omega_1^2q_1(t) = \frac{F_{x_L}\phi_1(x_L) + F_{x_R}\phi_1(x_R)}{M_v} + \frac{K_a}{M_v} \sum_{i=1}^{n_p} \Psi_{1i}V_{ai}(t) \quad (4.40)$$

$$\ddot{q}_2(t) + 2\zeta_2\omega_2\dot{q}_2(t) + \omega_2^2q_2(t) = \frac{F_{x_L}\phi_2(x_L) + F_{x_R}\phi_2(x_R)}{M_v} + \frac{K_a}{M_v} \sum_{i=1}^{n_p} \Psi_{2i}V_{ai}(t) \quad (4.41)$$

where F_{3L} and F_{3R} are given by

$$F_{x_L} = F_{K_s}(x_L) + F_{K_a}(x_L) + U_L \quad (4.42)$$

$$F_{x_R} = F_{K_s}(x_R) + F_{K_a}(x_R) + U_R \quad (4.43)$$

where F_{K_s} and F_{K_a} are forces generated by springs K_s and K_a

$$F_{K_s}(x_L) = -K_s(Z_{x_L} - Z_{2L}) \quad (4.44)$$

$$F_{K_a}(x_L) = -K_a(Z_{x_L} - Z_{1L}) \quad (4.45)$$

$$F_{K_s}(x_R) = -K_s(Z_{x_R} - Z_{2R}) \quad (4.46)$$

$$F_{K_a}(x_R) = -K_a(Z_{x_R} - Z_{1R}) \quad (4.47)$$

where Z_{x_L} and Z_{x_R} are the vertical displacement of vehicle body at position x_L and x_R

$$Z_{x_L} = Z_{3L} + q_1(t)\phi_1(x_L) + q_2(t)\phi_2(x_L) \quad (4.48)$$

$$Z_{x_R} = Z_{3R} + q_1(t)\phi_1(x_R) + q_2(t)\phi_2(x_R) \quad (4.49)$$

Substituting equations (4.42) and (4.43) into equations (4.40) and (4.41), and by using equations (4.44)- (4.47), (4.48) and (4.49), it is found the matrix

4.4. FLEXIBLE MODEL OF THE RAILWAY VEHICLE

representation of equation (4.40)-(4.41) in terms of all the states of the system

$$\dot{\mathbf{x}}_{flex} = \mathbf{A}_{rf}\mathbf{x}_{rigid} + \mathbf{A}_f\mathbf{x}_{flex} + \mathbf{B}_{f1}\mathbf{u} + \mathbf{B}_{f2}\mathbf{V}_a \quad (4.50)$$

where

$$\mathbf{x} = [\mathbf{x}_{rigid} \quad \mathbf{x}_{flex}] \quad (4.51)$$

where

$$\begin{aligned} \mathbf{x}_{rigid} &= [\dot{Z}_{3C} \quad \dot{\theta} \quad \dot{Z}_{1L} \quad \dot{Z}_{1R} \quad R_1 \quad R_2 \quad R_3 \quad R_4 \quad R_5 \quad R_6] \\ \mathbf{x}_{flex} &= [\dot{q}_1 \quad q_1 \quad \dot{q}_2 \quad q_2] \\ \mathbf{u} &= [U_l \quad U_R] \\ \mathbf{V}_a &= [V_{a1}(s) \dots V_{an_p}(s)] \end{aligned} \quad (4.52)$$

and

$$\mathbf{A}_{rf} = \begin{bmatrix} 0 & 0 & 0 & 0 & -\frac{(K_s+K_a)\phi_1(x_L)}{M_v} & -\frac{(K_a+K_s)\phi_1(x_R)}{M_v} & \frac{K_s\phi_s(x_L)}{M_v} & \frac{K_s\phi_s(x_R)}{M_v} & 0 & 0 \\ 0 & 0 & 0 & 0 & 0 & 0 & 0 & 0 & 0 & 0 \\ 0 & 0 & 0 & 0 & -\frac{(K_a+K_s)\phi_2(x_L)}{M_v} & -\frac{(K_a+K_s)\phi_2(x_R)}{M_v} & \frac{K_s\phi_a(x_L)}{M_v} & \frac{K_s\phi_a(x_R)}{M_v} & 0 & 0 \\ 0 & 0 & 0 & 0 & 0 & 0 & 0 & 0 & 0 & 0 \end{bmatrix} \quad (4.53)$$

$$\mathbf{A}_f = \begin{bmatrix} -2\zeta_1\omega_1 & -\omega_1^2 - \frac{2(K_a+K_s)\phi_1^2(x_L)}{M_v} & 0 & 0 \\ 1 & 0 & 0 & 0 \\ 0 & 0 & -2\zeta_2\omega_2 & -\omega_2^2 - \frac{2(K_a+K_s)\phi_2^2(x_L)}{M_v} \\ 0 & 0 & 1 & 0 \end{bmatrix} \quad (4.54)$$

$$\mathbf{B}_{f1} = \begin{bmatrix} \frac{\phi_1(x_L)}{M_v} & \frac{\phi_1(x_R)}{M_v} \\ 0 & 0 \\ \frac{\phi_2(x_L)}{M_v} & \frac{\phi_2(x_R)}{M_v} \\ 0 & 0 \end{bmatrix} \quad (4.55)$$

$$\mathbf{B}_{f2} = \frac{K_a}{M_v} \begin{bmatrix} \Psi_{11} & \Psi_{12} & \cdots & \Psi_{1n_p} \\ 0 & 0 & \cdots & 0 \\ \Psi_{21} & \Psi_{22} & \cdots & \Psi_{2n_p} \\ 0 & 0 & \cdots & 0 \end{bmatrix} \quad (4.56)$$

Modify the differential equations of (4.7)- (4.12) for rigid model by changing the force terms generated by K_s and K_a using equations (4.44)-(4.47), which is realized by directly substituting Z_{x_L} for Z_{3L} and Z_{x_R} for Z_{3R} in equations (4.7)- (4.12). Then the new differential equations for the flexible model are achieved. The state-space representation is given by

$$\dot{\mathbf{x}}_{rigid} = \mathbf{A}_r \mathbf{x}_{rigid} + \mathbf{A}_{fr} \mathbf{x}_{flex} + \mathbf{B}_r \mathbf{u} + \mathbf{G} \mathbf{w} \quad (4.57)$$

where matrices \mathbf{A}_r , \mathbf{B}_r , and \mathbf{G} are the same as given in equation (4.15), matrix \mathbf{A}_{fr} is given by

$$\mathbf{A}_{fr} = \begin{bmatrix} 0 & -\frac{2(K_s+K_a)}{M_v} \phi_1(x_L) & 0 & 0 \\ 0 & 0 & 0 & \frac{2(K_s+K_a)L_c}{I_{vc}} \phi_2(x_L) \\ 0 & \frac{K_a+K_s}{M_b} \phi_1(x_L) & 0 & \frac{K_s+K_a}{M_b} \phi_2(x_L) \\ 0 & \frac{K_a+K_s}{M_b} \phi_1(x_R) & 0 & \frac{K_a+K_s}{M_b} \phi_2(x_R) \\ 0 & 0 & 0 & 0 \\ 0 & 0 & 0 & 0 \\ 0 & \frac{K_s}{B_{sr}} \phi_1(x_L) & 0 & \frac{K_s}{B_{sr}} \phi_1(x_L) \\ 0 & \frac{K_s}{B_{sr}} \phi_1(x_R) & 0 & \frac{K_s}{B_{sr}} \phi_1(x_R) \\ 0 & 0 & 0 & 0 \\ 0 & 0 & 0 & 0 \end{bmatrix} \quad (4.58)$$

Combining equations (4.50) and (4.57) the state-space representation of

the model of a flexible-railway vehicle is given by

$$\dot{\mathbf{x}} = \begin{bmatrix} \mathbf{A}_r(12 \times 12) & \mathbf{A}_{\text{fr}}(12 \times 4) \\ \mathbf{A}_{\text{rf}}(4 \times 12) & \mathbf{A}_f(4 \times 4) \end{bmatrix} \mathbf{x} + \begin{bmatrix} \mathbf{B}_r \\ \mathbf{B}_{\text{fl}} \end{bmatrix} \mathbf{u} + \begin{bmatrix} \mathbf{0} \\ \mathbf{B}_{\text{f2}} \end{bmatrix} \mathbf{V}_a + \begin{bmatrix} \mathbf{G} \\ \mathbf{0} \end{bmatrix} \mathbf{w} \quad (4.59)$$

where \mathbf{A}_{fr} and \mathbf{A}_{rf} are called (flexible-rigid) and (rigid-flexible) coupling matrices respectively.

4.5 Coupling between rigid motion and flexible motion

According to the explanation by Gevarter [1970], the coupling between the rigid motion and the flexible motion, as we imagine, is introduced by control and takes places in two ways, i.e. actuation and sensing. In the way of actuation, the forces and moments that are applied to control the rigid body motion will also excite the flexible motions, q_r . The rigid body control, e.g. F_c , is converted to the generalized force, F_n , by a factor, i.e. $\phi_r(h)$

$$F_n = \phi_r(h)F_c \quad (4.60)$$

In the way of sensing, the sensors that were designed to sense the rigid body motion for feedback control purpose will also sense the flexible motion, e.g. q_r . The factor(mode shape), i.e. $\phi_r(x)$, is used to convert the r^{th} generalized coordinate, q_r , into the quantity, v_r , sensed by the sensors.

$$v_r = q_r\phi_r(x) \quad (4.61)$$

Besides active control using real actuators and sensors, the passive control elements springs K_s and K_a can be also viewed as collocated sensor and actuators. The vertical displacement that are sensed by springs (K_s and K_a) in the secondary suspension consists of the rigid modes as well as the flexible modes, which in turn changed the forces that are produced by the springs when they are functioning as actuators.

4.6 Model analysis and simulations

In this section, it is to verify the modeled flexible-bodied railway vehicle. The following tests are performed

- Eigenvalue analysis
- Step responses
- Power spectrum analysis
- Ride quality analysis

The eigenvalues of the modeled flexible-bodied railway vehicle based on the parameter values given in the Appendix A are:

Mode	Eigenvalue	Damping	Freq.(Hz)
Body Bounce	$-0.67 \pm 4.13i$	0.16	0.67
Body Pitch	$-1.09 \pm 5.21i$	0.2	0.85
First flexible	$-2.73 \pm 53.03i$	0.0513	8.45
Second flexible	$-7.44 \pm 146i$	0.051	23.2
Front bogie bounce	$-21.08 \pm 62.8i$	0.318	10.55
Rear bogie bounce	$-21.10 \pm 62.8i$	0.318	10.55

The structural damping values of the free-free beam which represents the flexible body of a railway vehicle may vary in practice, and are difficult to determine. A 5% modal damping is assumed for the two flexible modes of the model considered here, which is usually considered a reasonable value for a vehicle fitted with seats, trims, etc.

Sample step responses of the modeled railway vehicle are shown by Figure 4.4, Figure 4.5, Figure 4.6 and Figure 4.7. The step track velocity input, $[\dot{Z}_{0L} \ \dot{Z}_{0R}]$, as shown by Figure 4.3, is a unit pulse of 0.3 second duration to the front wheelset with a 0.35 sec time delay to the rear wheelset. The time delay is given by L_{bc}/v , where v is the speed of the vehicle.

High frequency oscillations are shown by the step response of the flexible model. It shows that the magnitude of the high frequency oscillation is the biggest in the centre acceleration.

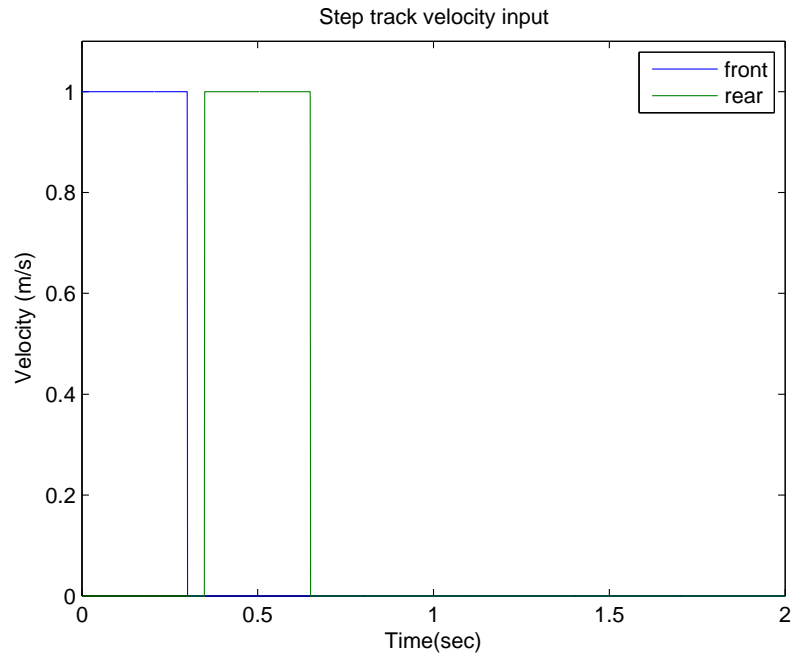


Figure 4.3: Step track inputs

Root mean square (RMS) values of the vertical accelerations of the vehicle body are used to evaluate the ride quality. The railway vehicle is subjected to random track inputs with a track roughness of 2.5×10^{-7} as discussed in section 3.1.1. The ride quality of a passive railway vehicle model are given in Table 4.1. It shows a degradation of the ride quality when flexibility is included in the model. The ride quality at the centre has the biggest percentage of degradation.

Table 4.1: RMS results for a passive system

	Acce.(%g)			Defle.(mm)	
	Left	Centre	Right	Left	Right
Rigid	2.66	1.66	3.41	7.78	11.00
Flexible	3.04	3.04	3.75	7.8	11.35

PSDs (Power spectral densities) of the vertical accelerations are given in Figures 4.8, 4.9 and 4.10. The resonances of the first two flexible modes are shown in the PSD plots. The first flexible mode is around 8.3Hz and

4.6. MODEL ANALYSIS AND SIMULATIONS

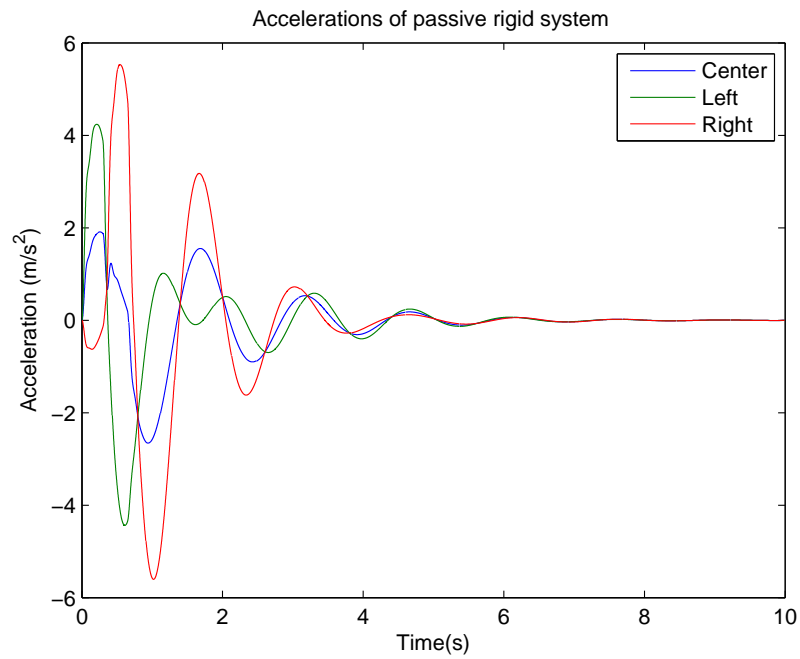


Figure 4.4: Step responses of passive rigid system: vertical accelerations

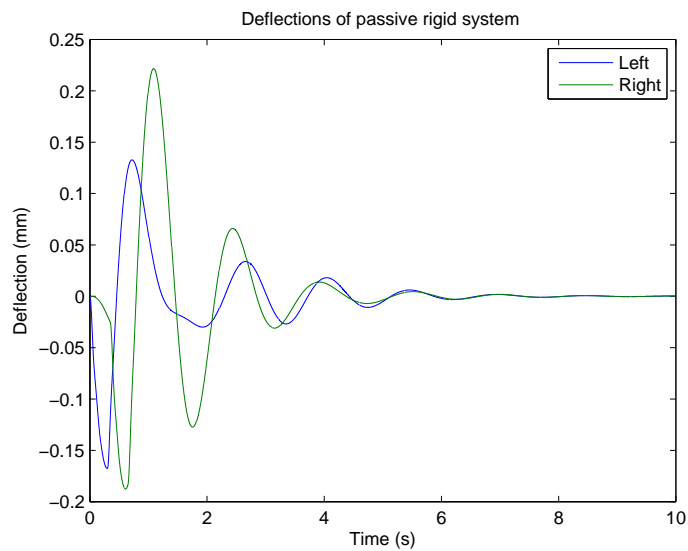


Figure 4.5: Step responses of passive rigid system: deflections

4.6. MODEL ANALYSIS AND SIMULATIONS

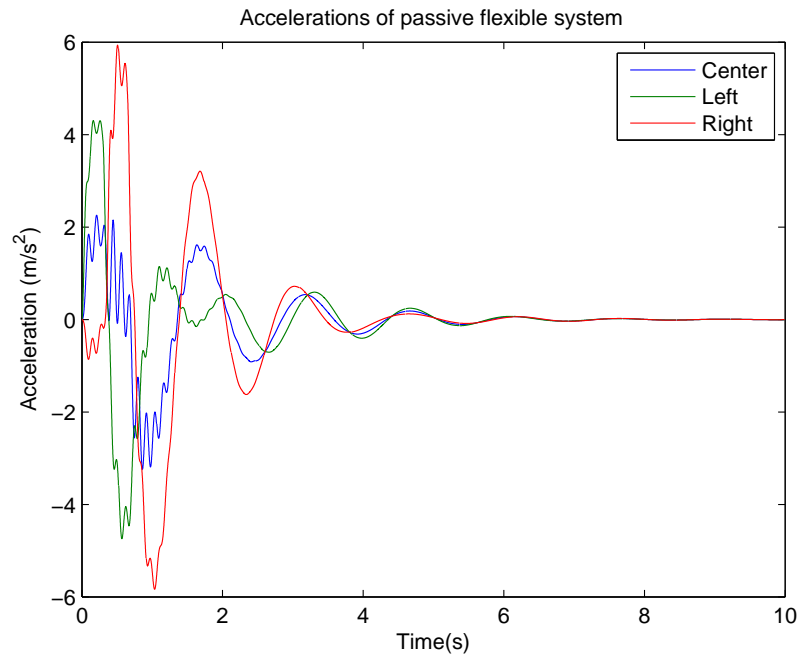


Figure 4.6: Step responses of passive flexible system: vertical accelerations

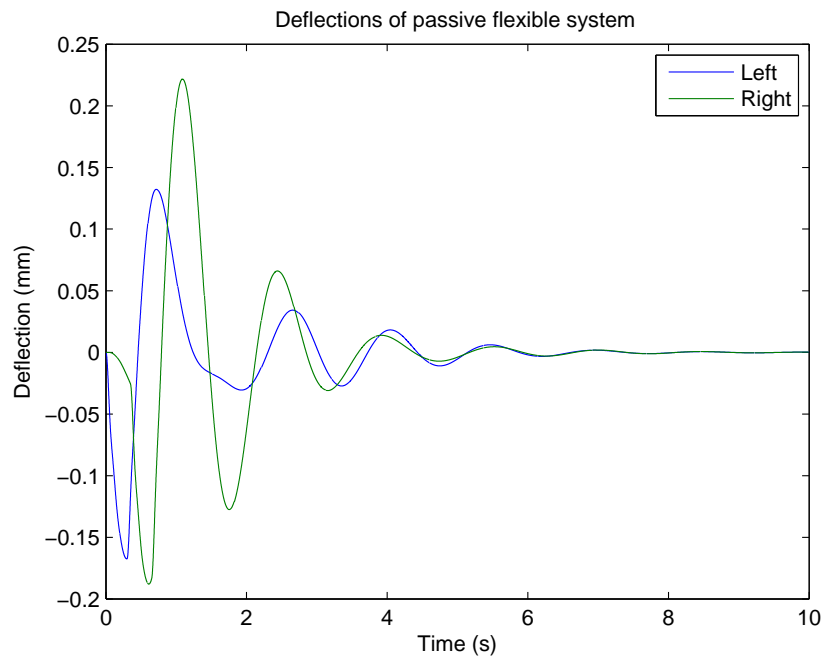


Figure 4.7: Step responses of passive flexible system: deflections

4.7. SUMMARY

is the main cause of vertical bending. The second mode which is around 23Hz has become very small. This shows that it is reasonable to just include the first two flexible modes in the model for control design. The dips shown in centre acceleration PSD in Figure 4.8 are caused by geometric filtering. However, it is not an effect in the left and right accelerations because they are combinations of bounce and pitch modes.

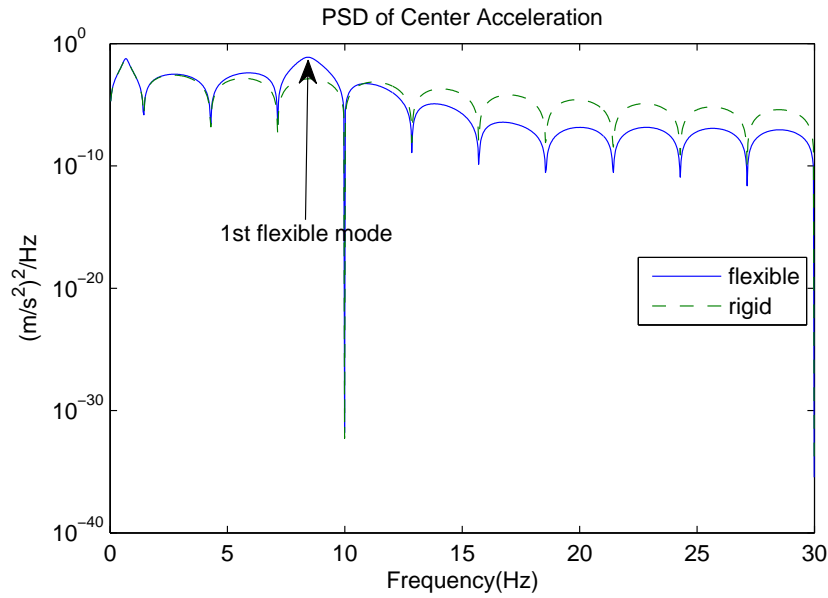


Figure 4.8: PSD of centre acceleration for passive system

The analysis above shows that the light body of high speed railway vehicles regarded as flexible structures becomes an important issue, and suppression of the vibration of flexible modes is needed in order to maintain an acceptable ride comfort or further improved ride quality for future trains.

4.7 Summary

The model of a typical flexible-bodied railway vehicle is derived. Modal analysis technique has been used to model the flexibility of the vehicle body, which is assumed as a free-free beam. Couplings terms between the rigid motion and flexible motion are included in the model. The models are finally

4.7. SUMMARY

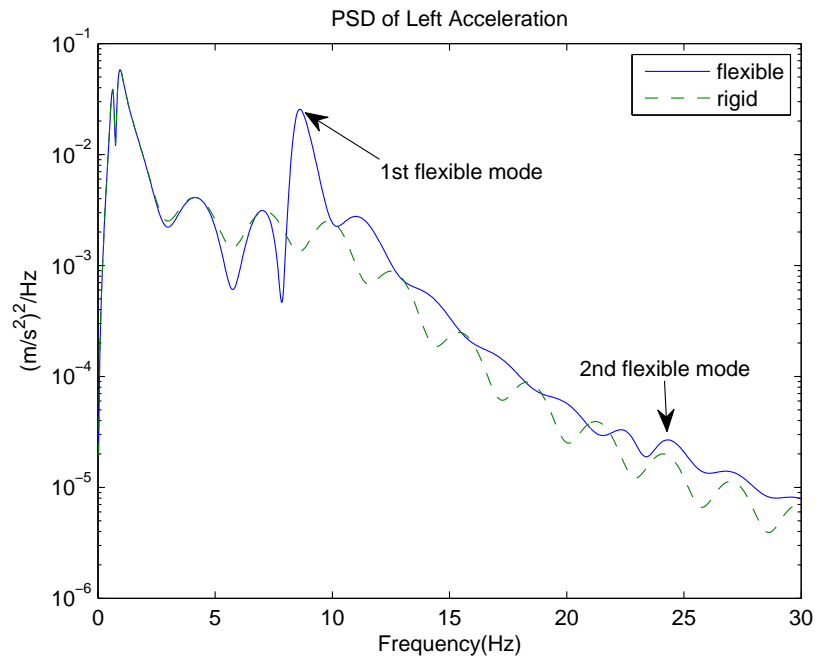


Figure 4.9: PSD of left acceleration for passive system

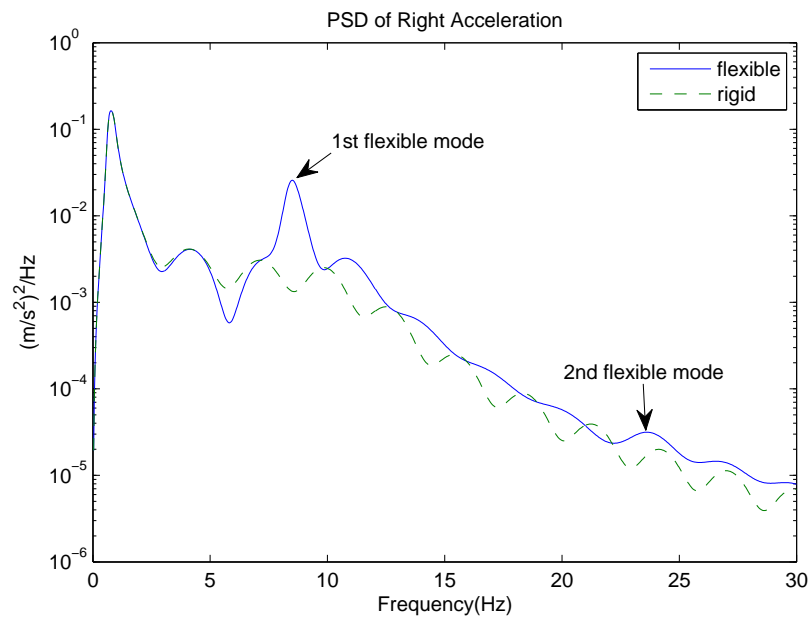


Figure 4.10: PSD of right acceleration for passive system

4.7. SUMMARY

presented in state-space form with relative states. Finally, the developed model is tested and analyzed. It shows the effect flexibility brings to the performance of the system.

Chapter 5

Actuators and Sensors

This chapter includes introduction to actuators and sensors that are used in this research and the placement of actuators and sensors for suppressing the flexible modes. Electro-servo hydraulic actuator is firstly introduced and its linearized model is presented. A lead-lag compensator is designed for the electro-servo hydraulic actuator and the dynamics of the compensated actuator are analyzed. Then the piezoelectric stack actuator and piezoelectric patch sensors are introduced and their working principles are briefly described. Finally locations of piezoelectric sensors/actuators for the railway vehicle body (assumed a free-free beam) are presented using placement indices based on structural \mathcal{H}_2 and \mathcal{H}_∞ norms.

5.1 Electro-servo Hydraulic Actuator

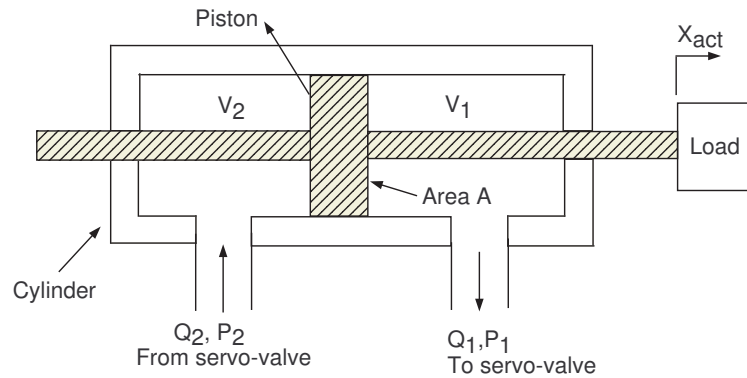
As railway vehicles are designed to be compact, the type of an actuator in a railway vehicle depends on its location. Electro-servo hydraulic actuators and electromagnetic actuators are usually among the considerations (Foo and Goodall [1998]). For active secondary suspension control in this research, the limited space between the secondary suspension and the body allows only an electro-servo hydraulic actuator to be installed.

In control design, actuators are usually assumed ideal and are able to produce the commanded force accurately. In reality, actuator dynamics can

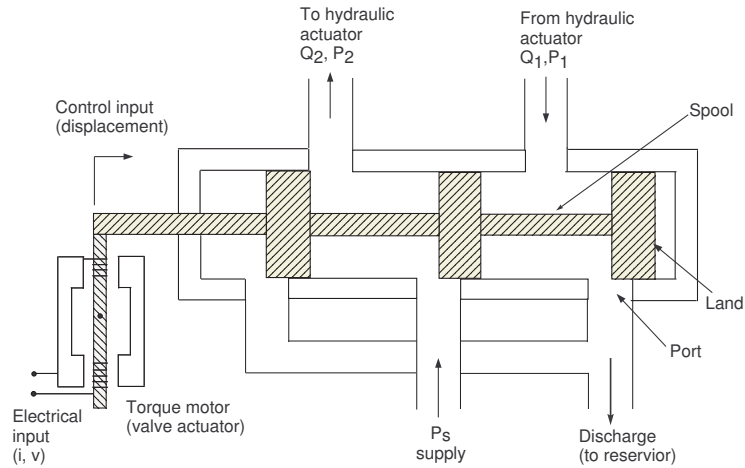
5.1. ELECTRO-SERVO HYDRAULIC ACTUATOR

be very complicated and interaction exists between the actuator and the vehicle system. Thus, it is important to look into the effects of the dynamics of the real actuators on the performance of the system.

The structure of an electro-hydraulic actuator is shown in Figure 5.1(a). This is a double acting actuator because the fluid pressure acts on both sides of the piston. Only a brief description of the derivation of the model is presented here, detailed analysis can be found in the work by Pratt [1996] and Sam and K.Hudha [2006]



(a) Double acting hydraulic actuator



(b) Servo-valve

Figure 5.1: Servo-valve electro-hydraulic actuator

5.1.1 Spool valve

The fluid flow Q_1 and Q_2 are controlled by the spool-valve as is shown in Figure 5.1(b).

$$Q_2 = x_v b c_d \sqrt{\frac{2(P_s - P_2)}{\rho}} \quad (5.1)$$

$$Q_1 = x_v b c_d \sqrt{\frac{2P_1}{\rho}} \quad (5.2)$$

where x_v is the spool valve displacement. b is the land width, c_d is the discharge coefficient at each port, ρ is the density of the hydraulic fluid, and P_s is the supply pressure of the hydraulic fluid. The pressure at the discharge end is taken to be zero.

For small displacement about the operating point, the following linearized equations (5.1) and (5.2) can be given

$$\delta Q_1 = k_{q1} \delta x_v - k_{c1} \delta P_1 \quad (5.3)$$

$$\delta Q_2 = k_{q2} \delta x_v + k_{c2} \delta P_2 \quad (5.4)$$

where k_{q1} and k_{q2} are the flow gains

$$k_{q1} = \left(\frac{\partial Q_1}{\partial x_v} \right) \Big|_{P_1}$$

$$k_{q2} = \left(\frac{\partial Q_2}{\partial x_v} \right) \Big|_{P_2}$$

and k_{c1} and k_{c2} are the flow pressure coefficients

$$k_{c1} = \left(\frac{\partial Q_1}{\partial P_1} \right) \Big|_{x_v}$$

$$k_{c2} = \left(\frac{\partial Q_2}{\partial P_2} \right) \Big|_{x_v}$$

5.1.2 Hydraulic primary actuator

The flow rate at the ports of a hydraulic actuator is regulated typically by a spool valve. The flow rate of Q into a chamber depends primarily on two factors:

1. Increase in chamber volume
2. Increase in pressure. Assuming that there is no leakage in the flow

the fluid conservation (i.e flow continuity) equations can be written as

$$Q_1 = A \frac{dx_{act}}{dt} - \frac{V_1}{\beta} \frac{dP_1}{dt} \quad (5.5)$$

$$Q_2 = A \frac{dx_{act}}{dt} + \frac{V_2}{\beta} \frac{dP_2}{dt} \quad (5.6)$$

Equation (5.5) and (5.6) are associated with the annulus side and the bore side of the cylinder respectively. Q_1 and Q_2 are the flow rates. P_1 and P_2 are the oil pressures. V_1 and V_2 are the oil volumes. x_{act} is the extension of the actuator. β is the bulk modulus.

For incremental changes about the operating point, equation (5.5) and (5.6) can be written as

$$\delta Q_1 = A \frac{d\delta x_{act}}{dt} - \frac{\bar{V}_1}{\beta} \frac{d\delta P_1}{dt} \quad (5.7)$$

$$\delta Q_2 = A \frac{d\delta x_{act}}{dt} + \frac{\bar{V}_2}{\beta} \frac{d\delta P_2}{dt} \quad (5.8)$$

where \bar{V}_1 and \bar{V}_2 are the oil volumes about the operating point.

In a linear model, the incremental-value given by equations 5.7 and 5.8 are used instead of the total-value equations 5.5 and 5.6. Equating cylinder oil flows given by equations (5.7) and (5.8) with the spool-valve flows given by equations (5.3) and (5.4) gives

$$A \frac{d\delta x_{act}}{dt} - \frac{\bar{V}_1}{\beta} \frac{d\delta P_1}{dt} = k_q \delta x_v - k_c \delta P_1 \quad (5.9)$$

$$A \frac{d\delta x_{act}}{dt} + \frac{\bar{V}_2}{\beta} \frac{d\delta P_2}{dt} = k_q \delta x_v + k_c \delta P_2 \quad (5.10)$$

5.1.3 Simplified model of spool valve and torque motor

As the spool valve is not the main component, the mechanical dynamics of the spool-valve and its centering spring is represented by a simple second order mass-damper-stiffness arrangement. Assume that the torque motor has current, i , as its input. The torque motor develops a torque proportional to the input current, and this torque is converted into a linear force and drives the spool valve, which gives the spool displacement x_v . The transfer function is given by

$$x_v = \frac{k_i}{m_s s^2 + c_s s + k_s} i \quad (5.11)$$

5.1.4 Load equation

To evaluate the force developed by the cylinder, F_{act} , assume c_{act} the ram damping associated with the energy dissipation effects for all moving part of the hydraulic actuator. According to Newton's law, F_{act} is given by

$$F_{act} = A(P_2 - P_1) - c_{act}\dot{x}_{act} \quad (5.12)$$

5.1.5 State-space model of hydraulic actuator

According to equations 5.9,5.10 and 5.11, the state-space representation of the linear model of the hydraulic actuator is given as

$$\begin{bmatrix} \delta\dot{x}_v \\ \delta\ddot{x}_v \\ \delta\dot{P}_1 \\ \delta\dot{P}_2 \end{bmatrix} = \begin{bmatrix} 0 & 1 & 0 & 0 \\ -\frac{k_s}{m_s} & -\frac{c_s}{m_s} & 0 & 0 \\ -\frac{\beta}{V_1}k_{q1} & 0 & \frac{\beta}{V_1}k_{c1} & 0 \\ \frac{\beta}{V_2}k_{q2} & 0 & \frac{\beta}{V_2}k_{c2} & 0 \end{bmatrix} \begin{bmatrix} \delta x_v \\ \delta\dot{x}_v \\ \delta P_1 \\ \delta P_2 \end{bmatrix} + \begin{bmatrix} 0 \\ \frac{k_i}{m_s} \\ 0 \\ 0 \end{bmatrix} i + \begin{bmatrix} 0 \\ 0 \\ \frac{\beta}{V_1}A \\ -\frac{\beta}{V_2}A \end{bmatrix} \delta\dot{x}_{act}$$

$$F_{act} = [0 \quad 0 \quad -A \quad A] \begin{bmatrix} \delta x_v \\ \delta\dot{x}_v \\ \delta P_1 \\ \delta P_2 \end{bmatrix} + [0]i + [-c_{act}]\delta\dot{x}_{act} \quad (5.13)$$

5.1.6 Control of the hydraulic actuator

The active suspension system of the railway vehicle is composed of two loops, namely outer loop and inner loop. The outer loop controller is used to calculate the target force to reject the track disturbances, and the inner loop controller is used to keep actual force generated by the actuator to the desired force.

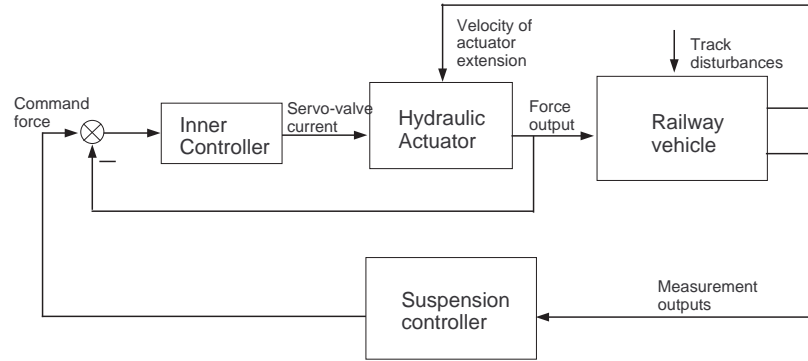


Figure 5.2: Controller Structure of a railway suspension system

Here the inner loop controller is designed without connecting to the railway vehicle suspension. The Nichols chart of open loop of the hydraulic actuator from current input to force output is plotted in Figure 5.3 and shows that the system is unstable.

Lead-lag compensator is to be designed for the inner controller. Phase lead is firstly designed to increase the phrase margin by 80° . Then phase lag is added at frequency 178Hz in order to achieve a phase margin of about 80° for the final compensated actuator. Hence the transfer function of the lead-lag compensator is given as

$$H(s) = \frac{(3282.1 \times 3.3311 \times 10^{-7})s + 1}{(3.3311 \times 10^{-7})s + 1} \frac{0.0089s + 1}{(0.0089 \times 462.38)s + 1} \quad (5.14)$$

The lead-lag compensation allows the introduction of phase lead to stabilize a system, while providing attenuation at higher frequencies. Figure 5.4 shows the Bode diagram of the controller, the uncontrolled hydraulic actuator and the open-loop of the controlled hydraulic actuator. Figure 5.5 is the Nichols

5.1. ELECTRO-SERVO HYDRAULIC ACTUATOR

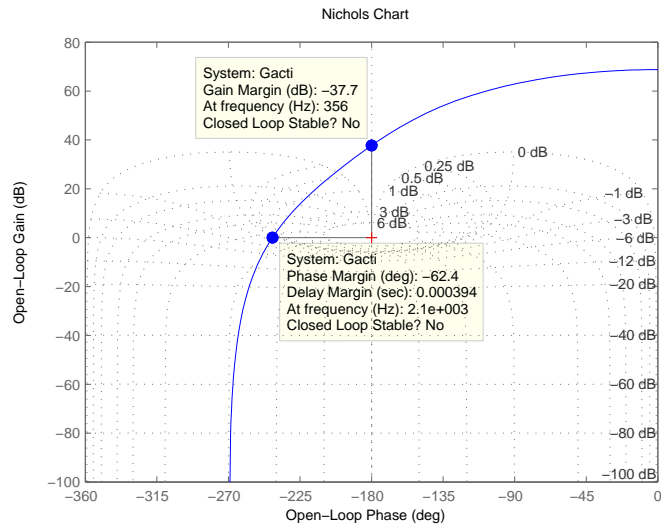


Figure 5.3: Open loop uncompensated hydraulic actuator

chart of the open-loop compensated hydraulic actuator and it shows that gain margin of 69dB and phase margin of 74° have been achieved. The closed-loop bandwidth is 230Hz as shown by the Bode diagram of the closed-loop compensated hydraulic actuator in Figure 5.6.

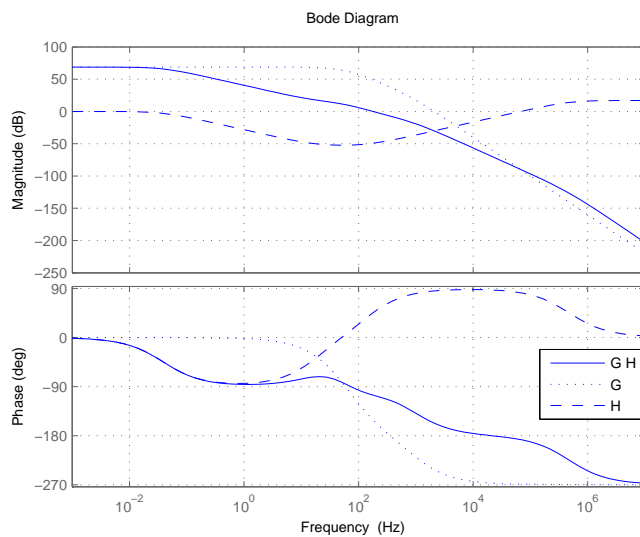


Figure 5.4: Controller design for hydraulic actuator

5.1. ELECTRO-SERVO HYDRAULIC ACTUATOR

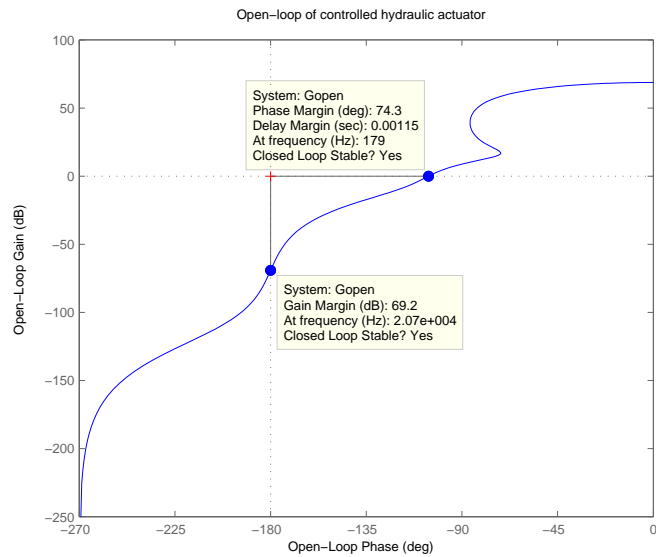


Figure 5.5: Open loop of controlled hydraulic actuator

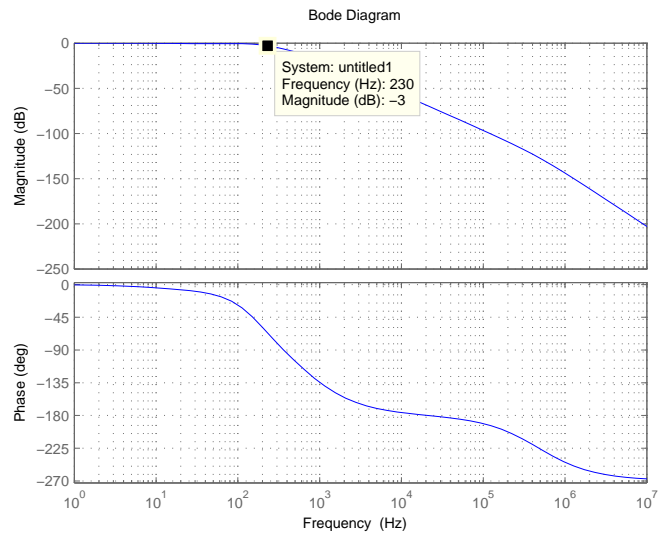


Figure 5.6: Closed-loop of controlled hydraulic actuator

5.1. ELECTRO-SERVO HYDRAULIC ACTUATOR

Figure 5.7 shows the time response of the closed-loop hydraulic actuator to a square-wave force demand of 1kN at 10Hz. Figure 5.8 shows the ability of the closed-loop system to reject a unit 1Hz square-wave disturbance placed on the extension of the actuator given a zero force demand.

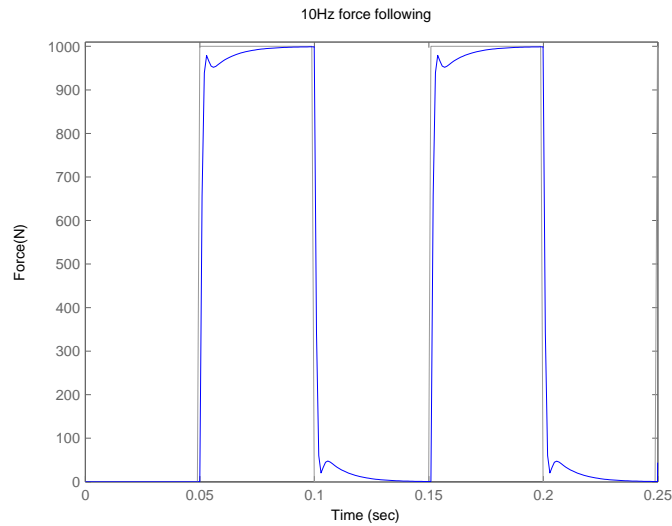


Figure 5.7: Closed-loop hydraulic actuator force following

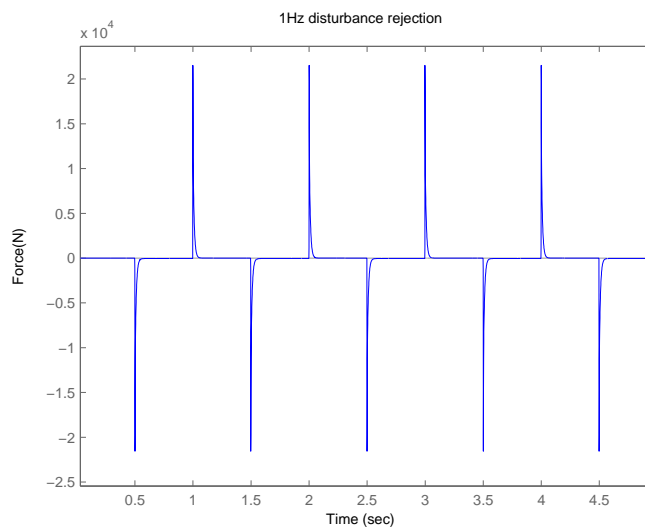


Figure 5.8: Closed-loop hydraulic actuator disturbance rejection

It is important to note that the above controller was designed without connecting the actuator to the suspension system and the velocity input is assumed to be zero. Thus, a very high bandwidth is obtained. However, the actuator in practice is connected to the secondary suspension, and the velocity input at the extension of the actuator affects the overall performance of the system: to cause the bandwidth of the overall actuator to decrease and the stability margin of the loop to reduce. The limited bandwidth of the actuator will make it difficult to control the flexible modes of the vehicle body. The effect of actuator dynamics on vibration control of railway vehicles will be discussed in section 6.3.

5.2 Piezoelectric actuators and sensors

5.2.1 Piezoelectric actuators

Piezoelectric stack actuators have been found the most suitable to control the present flexible structure of the railway vehicle. Due to the size, mass and stiffness of the structure, considerable moments have to be applied by the actuator. Stack piezoelectric actuators are capable of introducing the necessary moments (Schirrer and Kozek [2008]). Figure 5.9 shows the stack piezoelectric actuator that is used in this thesis.

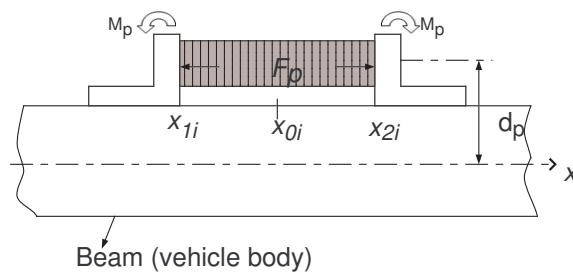


Figure 5.9: Piezoelectric actuator

Piezoelectric stack actuator expands when an voltage is applied to it. The actuation force is generated when this expansion is constrained by mounting the actuator in a mechanical structure (Figure 5.9). In this thesis, the

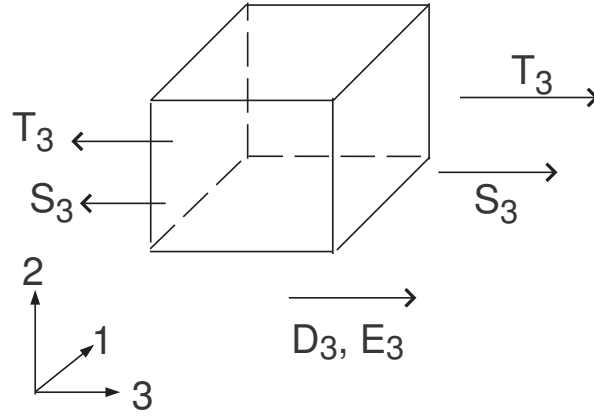


Figure 5.10: Piezoelectric element

piezoelectric stack actuators are assumed to be linear, which means that the force generated by the actuator is proportional to the voltage applied to the actuator.

According to equation (2.3), the piezoelectric constitutive equation is written as

$$T_3 = c_{33}^E S_3 - e_{33}^t E_3 \quad (5.15)$$

where e is the piezoelectric coupling matrix and

$$E_3 = V_p / h_{St} \quad (5.16)$$

where V_a is the applied voltage in 3 direction, h_{St} is the thickness of one disk.

The first term of equation (5.15) gives the usual influence of the stiffness (as by any material). The second term when multiplied with the cross section A_p of the actuator gives the force F_p generated by the piezoelectric actuator.

$$F_p = A_p T_3 = A_p e_{33} \frac{V_a}{h_{St}} \quad (5.17)$$

The moment M_p which works on the beam is given by

$$M_p = F_p d_p = A_p e_{33} d_p \frac{V_a}{h_{St}} \quad (5.18)$$

where d_p is the vertical distance from the neutral axis of the carbody to

the vertical centre of the piezoelectric actuator. Hence the coefficient K_a in equation (4.35) is given as

$$K_a = A_p e_{33} d_p / h_{St} \quad (5.19)$$

Detailed working principle of the piezoelectric actuator was not included above. In this thesis, it is concentrated on the active vibration control of the flexible vehicle body with active damping by piezoelectric actuators, so it is only important to use an actuator with a linear input/output relation and sufficient dynamics.

5.2.2 Piezoelectric sensors

Piezoelectric patches are used as sensors. They are bonded to the structure and produce a voltage signal that is proportional to the average curvature. The measurements by piezoelectric sensors, in comparison to position, velocity and acceleration measurements, is advantageous when only the vibrations of the flexible modes have to be measured and the signal part of the rigid body modes has to be eliminated (Benatzky et al.).

The vibration of the beam will induce strain inside the beam element. This strain will then induce an electric charge inside the piezoelectric sensor due to the piezoelectric effect. The charge Q and the voltage v_{pj} generated across the sensor electrodes, are related by the capacitance of the sensor, C_p

$$v_{pj} = Q / C_p \quad (5.20)$$

The induced voltage v_{pj} by the j^{th} piezoelectric sensor is given by (Halim [2002])

$$v_{pj}(t) = \frac{K_s}{C_p} \sum_{r=1}^{\infty} \Psi_{rj} q_r(t) \quad (5.21)$$

where

$$\Psi_{rj} = \frac{d\phi_r}{dx}(x_{2j}) - \frac{d\phi_r}{dx}(x_{1j}) \quad (5.22)$$

Equation (5.21) implies that the j^{th} sensor output consists of the

contribution of each bending mode, where the contribution of each mode is proportional to Ψ_{rj} (Halim and Moheimani [2001]).

5.3 Placement of actuators and sensors

The placement of piezoelectric actuators and sensors on a flexible structure for active vibration suppression is a crucial issue because it has a direct effect on the achievable performance. The controllability and observability of the flexible modes vary as the positions of the actuators and sensors change. A flexible mode cannot be controlled by the actuator placed at the node point of the mode. Moreover, if the sensor is placed at one of the nodes, then no control of the mode is possible, even if the actuator is not co-located. In this thesis, the placement of actuators and sensors are determined based on the \mathcal{H}_2 and \mathcal{H}_∞ norms of the flexible structures (Gawronski [1998]).

5.3.1 Norms of a flexible structure

For a continuous-time system $G(\omega)$, the \mathcal{H}_2 norm of the system is defined as

$$\|G\|_2^2 = \frac{1}{2\pi} \int_{-\infty}^{\infty} \text{tr}(G^*(\omega)G(\omega))d\omega \quad (5.23)$$

where $\text{tr}(G^*(\omega)G(\omega))$ is the sum of the squared magnitudes of all the elements of $G(\omega)$. Thus the \mathcal{H}_2 norm can be interpreted as an average gain of the system, performed over all the elements of the matrix transfer function and over all frequencies.

The \mathcal{H}_∞ norm is defined as

$$\|G\|_\infty = \max_{\omega} \sigma_{max}(G(\omega)) \quad (5.24)$$

where $\sigma_{max}(G(\omega))$ is the largest singular value of $G(\omega)$. \mathcal{H}_∞ norm is the worst case gain for sinusoidal inputs at any frequency.

The equations of a flexible structure are uncoupled in modal coordinates and the system norms can be decomposed to a combination of single-input-

single-output norms. The norms of the r^{th} mode and i^{th} actuator and j^{th} sensor can be approximately determined from

$$\|G_{rij}\|_2 \cong \frac{\|b_{ri}\|_2 \|c_{rj}\|_2}{2\sqrt{\zeta_r}\omega_r} \quad (5.25)$$

$$\|G_{rij}\|_\infty \cong \frac{\|b_{ri}\|_2 \|c_{rj}\|_2}{2\zeta_r\omega_r} \quad (5.26)$$

where $2\zeta_r\omega_r$ is defined as a half-power frequency at the r th resonance (Clough and Penzien [1975] and Ewins [2000]). (The interested audience can refer to Gawronski [1998] for the proof of equation (5.25) and (5.26)). The entries of input matrix b_{ri} and output matrix c_{rj} are dependent on the locations of actuators and sensors, respectively.

For a flexible structure with a set of n_p actuators and m_p sensors, the \mathcal{H}_2 (or \mathcal{H}_∞) norm of the r^{th} mode is the root-mean-square sum over all actuators and sensors, which are the additive properties for the \mathcal{H}_2 and \mathcal{H}_∞ norms with a set of actuators and sensors for a mode:

The \mathcal{H}_2 norm of the r^{th} mode can be approximately determined by

$$\|G_r\|_2 \cong \sum_{i=1}^{n_p} \sum_{j=1}^{m_p} \|G_{rij}\|_2 \quad (5.27)$$

And the \mathcal{H}_∞ norm of the r^{th} mode can be approximately determined by

$$\|G_r\|_\infty \cong \sum_{i=1}^{n_p} \sum_{j=1}^{m_p} \|G_{rij}\|_\infty \quad (5.28)$$

The \mathcal{H}_2 norm of the total system is approximately the root-mean-square sum over all its modal norms, that is

$$\|G\|_2 \cong \sum_{r=1}^n \|G_r\|_2 \quad (5.29)$$

where n is the number of modes taken under consideration.

The \mathcal{H}_∞ norm of the total system is approximately the largest of its modal

norms

$$\|G\|_\infty \cong \max_r \|G_r\|_\infty \quad (5.30)$$

The properties presented by equations 5.25 to 5.30 are very useful for evaluating the importance of an arbitrary combination of sensors and actuators and are applicable to structures only, because in general case, system norms cannot be decomposed into a combination of single-input-single-output norms.

5.3.2 Placement indices

The placement indices are defined as

$$\sigma_{2rij} = \frac{\|G_{rij}\|_2}{\|G_r\|_2} \quad (5.31)$$

$$\sigma_{\infty rij} = \frac{\|G_{rij}\|_\infty}{\|G_r\|_\infty} \quad (5.32)$$

Placement indices $\sigma_{2rij} / \sigma_{\infty rij}$ is a measure of the contribution of the i^{th} actuator and j^{th} sensor in the impulse response of the r^{th} mode.

Based on the definition for the placement indices by equation (5.31) and (5.32), the actuator/sensor placement problem is stated as: given a larger set of sensors and actuator (which are the possible mounting positions for actuators and sensors), determine the locations of a smaller subset of sensors or actuators such that the \mathcal{H}_2 or \mathcal{H}_∞ norms of the subset are as close as possible to the norms of the original set.

5.3.3 Placement of actuators and sensors for flexible body of a railway vehicle

Modal model

n_p piezoelectric actuators and m_p piezoelectric sensors are to be attached onto the vehicle body. For the placement of the actuators and sensors, the modal model of the railway vehicle body given by equations (4.40) and (4.41) is used. This model considers only the first two flexible modes and disregards

the coupling between the flexible motion with the rigid motion. The state-space representation of the modal model is written as

$$\dot{\mathbf{x}}_f = \mathbf{A}_f \mathbf{x}_f + \mathbf{B}_{f1} \mathbf{u}_1 + \mathbf{B}_{f2} \mathbf{d} \quad (5.33)$$

$$\mathbf{y} = \mathbf{C}_v \mathbf{x}_f \quad (5.34)$$

where \mathbf{u}_1 is the $(n_p \times 1)$ vector of voltage inputs to the piezoelectric actuators, $\mathbf{d} = [F_{x_L} \ F_{x_R}]$ is the vector of force inputs from suspensions \mathbf{y} is the $(m_p \times 1)$ vector of measured variables by piezoelectric sensors, and \mathbf{x}_f is the state vector

$$\mathbf{x}_f(t) = \begin{bmatrix} \dot{q}_1(t) & q_1(t) & \dot{q}_2(t) & q_2(t) \end{bmatrix} \quad (5.35)$$

The modal description of the system matrix, the input matrices and the output matrices are given as following

$$\mathbf{A}_f = \begin{bmatrix} -2\zeta_1 w_1 & -w_1^2 & 0 & 0 \\ 1 & 0 & 0 & 0 \\ 0 & 0 & -2\zeta_2 w_2 & -w_2^2 \\ 0 & 0 & 1 & 0 \end{bmatrix} \quad (5.36)$$

$$\mathbf{B}_{f1} = \frac{K_a}{M_v} \begin{bmatrix} \Psi_{a11} & \Psi_{a12} & \cdots & \Psi_{a1n_p} \\ 0 & 0 & \cdots & 0 \\ \Psi_{a21} & \Psi_{a22} & \cdots & \Psi_{a2n_p} \\ 0 & 0 & \cdots & 0 \end{bmatrix} \quad (5.37)$$

$$\mathbf{B}_{\mathbf{r}2} = \begin{bmatrix} \frac{\phi_1(x_L)}{M_v} & \frac{\phi_1(x_R)}{M_v} \\ 0 & 0 \\ \frac{\phi_2(x_L)}{M_v} & \frac{\phi_2(x_R)}{M_v} \\ 0 & 0 \end{bmatrix} \quad (5.38)$$

$$\mathbf{C}_{\mathbf{v}} = \frac{K_s}{C_p} \begin{bmatrix} 0 & \Psi_{s11} & 0 & \Psi_{s21} \\ 0 & \Psi_{s12} & 0 & \Psi_{s22} \\ 0 & \vdots & 0 & \vdots \\ 0 & \Psi_{s1m_p} & 0 & \Psi_{s2m_p} \end{bmatrix} \quad (5.39)$$

where Ψ_{ari} is the coefficient of the i^{th} actuator for the r^{th} mode, and Ψ_{srj} is the coefficient of the j^{th} sensors for the r^{th} mode. They are functions of the position of the actuator/sensor (denoted by the centre of the actuator/sensor, x) and the length of the actuator/sensor, L_p .

Candidate positions

According to the definition of the structural norms, placement indices and the input and output matrices given by equations (5.38) to (5.39), the placement of the piezoelectric actuators and sensors is closely related to the absolute values of Ψ_a and Ψ_s , i.e. at the position where Ψ_{ari} and Ψ_{srj} have high absolute values, the placement indices will also have high values and vice versa.

With the length of the piezoelectric actuator and sensor fixed, the plot of $\Psi_a(x)$ of a single actuator is shown in Figure 5.11. The absolute value of $\Psi_a(x)$ reaches its maxima at abdominal positions of the plot: $x = (13.5)$ for the 1st flexible mode, and $x = (7.84)$ and $x = (19.16)$ for the 2nd flexible mode, where x is the coordinate. It is found $\Psi_{a2}(13.5) = 0$, which means centre of the vehicle body is the node point for the second flexible mode, and the second flexible mode can not controlled by piezoelectric actuators placed at $x = (13.5)$.

With the location of sensors fixed, the plot of normalized \mathcal{H}_2 indices and \mathcal{H}_∞ indices as a function of actuator locations, x , are shown in Figures 5.12 and 5.13. It is not surprising to find that the maxima positions in $\mathcal{H}_\infty/\mathcal{H}_2$

5.3. PLACEMENT OF ACTUATORS AND SENSORS

indices plots coincides with the abdominal positions in $\Psi_a(x)$ plot. Therefore, positions $x = (13.5)$, $x = (7.84)$ and $x = (19.16)$ are chosen as candidate positions for actuators. The same candidate positions can also be determined for sensors.

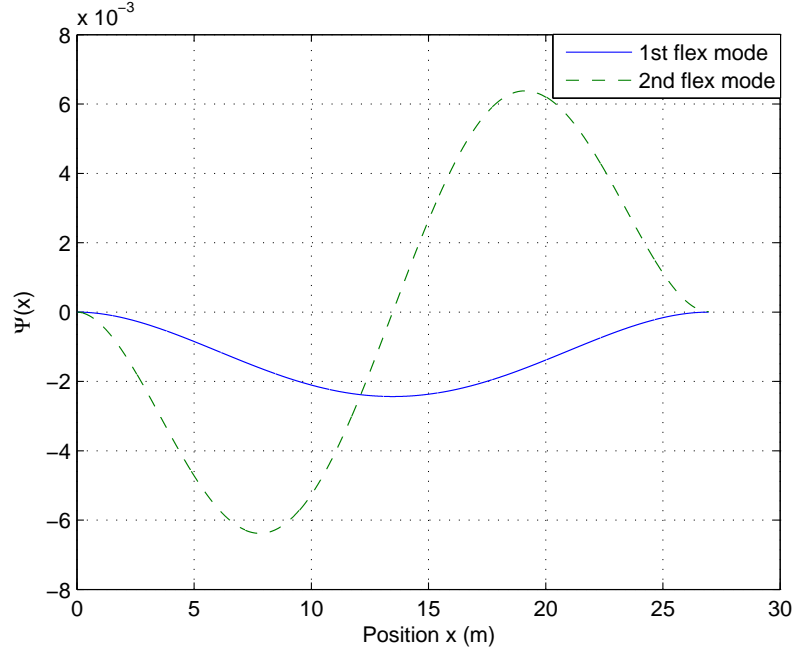


Figure 5.11: Relation between Ψ_r and actuator position with $L_p = 0.194m$

Placement configurations

Based on the candidate positions for actuators and sensors, four different actuator and sensor placement configurations are chosen for investigation (Figure 5.14): For configuration 1, one pair of piezoelectric actuator and sensor are collocated at $x = (13.5)$ for suppressing the 1st flexible mode, and two pairs of actuators and sensors placed at $x = (7.84)$ and $x = (19.16)$ respectively for suppressing the 2nd flexible mode. Configurations 2,3 and 4 are concentrated on the 1st flexible mode. For configuration 2, one pair of actuator and sensor is placed at $x = (13.5)$. For configuration 3 three actuators and one sensor are placed around $x = (13.5)$. For configuration 4, three pairs of actuator and sensors are placed around $x = (13.5)$.

5.3. PLACEMENT OF ACTUATORS AND SENSORS

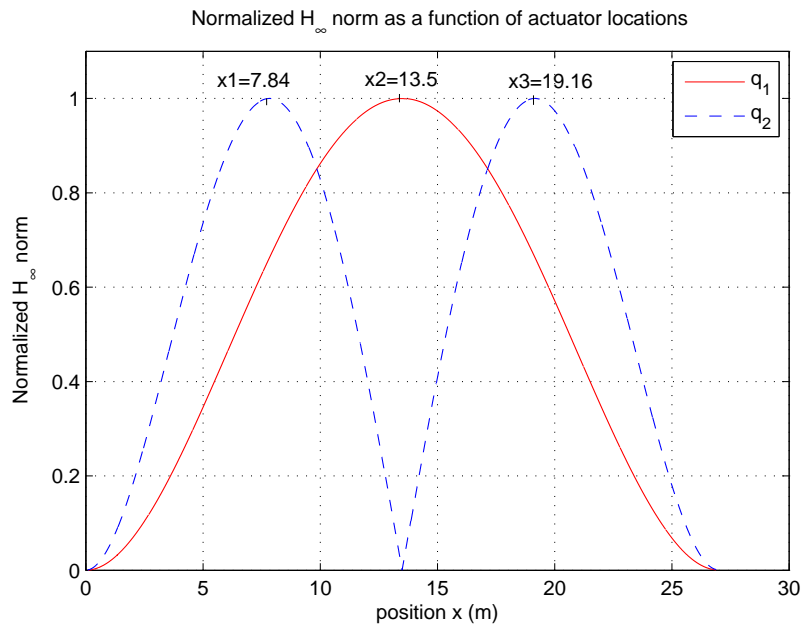


Figure 5.12: Normalized \mathcal{H}_∞ indices as a function of actuator location with fixed sensor

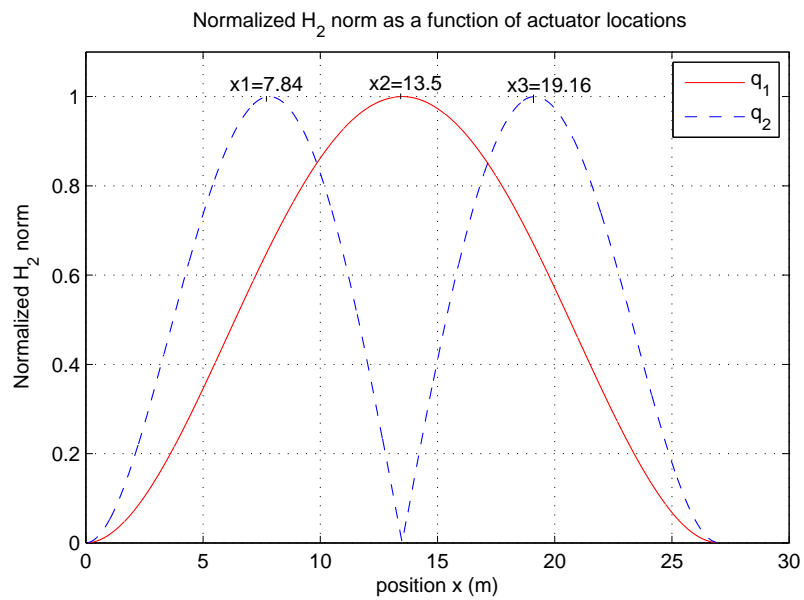


Figure 5.13: Normalized \mathcal{H}_2 indices as a function of actuator location with fixed sensor

5.3. PLACEMENT OF ACTUATORS AND SENSORS

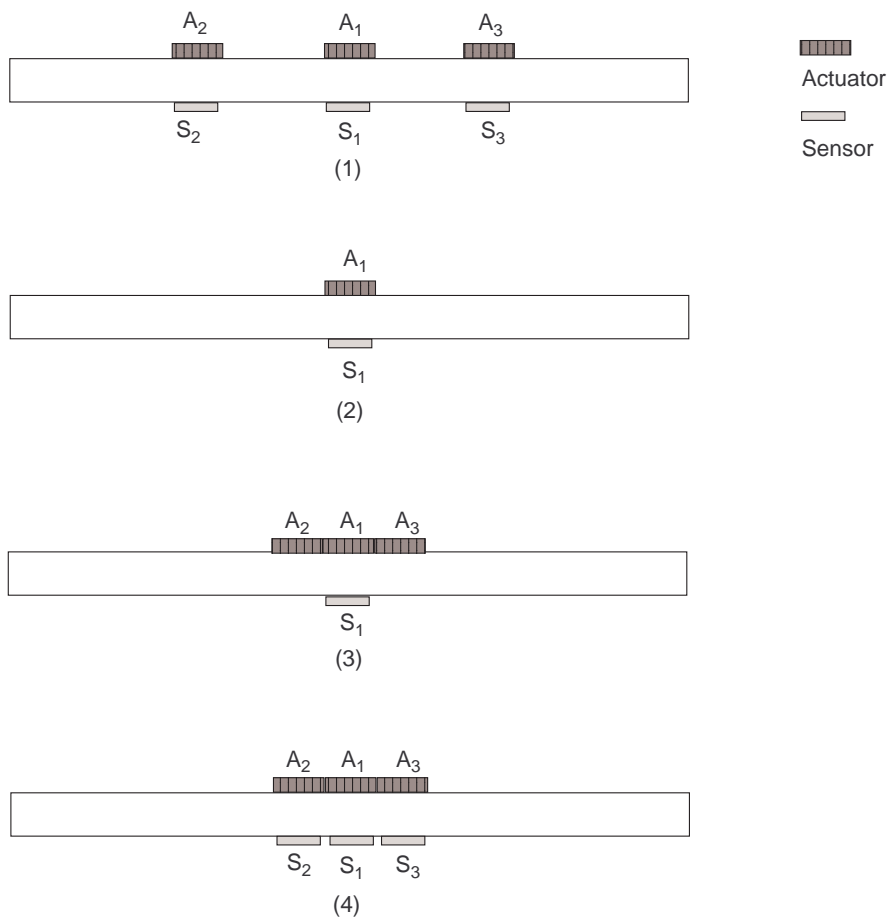


Figure 5.14: Acuator and sensor placement configurations

The \mathcal{H}_2 and \mathcal{H}_∞ norms of the four placement configurations are given in Table 5.1. It is found that config. 4 has the highest \mathcal{H}_2 and \mathcal{H}_∞ norms for the first flexible mode because it has the most actuators and sensors placed at the centre. The norms of Config. 2,3 and 4 for the second flexible mode q_2 is very small. The four configurations will be used for control design and their performance will be compared in Chapter 7 and Chapter 8.

Table 5.1: \mathcal{H}_2 and \mathcal{H}_∞ norms of individual modes of investigated actuator and sensor configurations

config.	\mathcal{H}_2 norm		\mathcal{H}_∞ norm	
	q_1	q_2	q_1	q_2
1	1.9×10^{-6}	3.0×10^{-6}	6.18×10^{-5}	1.61×10^{-4}
2	1.0×10^{-6}	7.48×10^{-18}	3.29×10^{-5}	3.98×10^{-16}
3	1.75×10^{-6}	1.28×10^{-13}	5.69×10^{-5}	6.87×10^{-12}
4	3.03×10^{-6}	2×10^{-9}	9.86×10^{-5}	1.2×10^{-7}

5.4 Summary

A brief description of the dynamics of hydraulic actuator is presented. A lead-lag compensator is designed for the actuator and satisfying stability margins and time-domain performances are achieved. Although an adequate bandwidth of the closed-loop actuator is achieved, in the environment of the railway vehicle system, the bandwidth of the hydraulic actuator will be substantially reduced. The effect of hydraulic actuators on suspension control will be demonstrated in the next chapter.

Piezoelectric stack actuators and piezoelectric patch sensors are introduced. They are assumed to be linear. The procedure for placement of actuators and sensors based on placement indices and $\mathcal{H}_2/\mathcal{H}_\infty$ norms is presented. The candidate positions for piezoelectric actuators and sensors are determined and four placement configurations are chosen.

Chapter 6

Preliminary Studies with Active Suspension Control

This chapter describes the design of active suspension control for improving the ride quality of railway vehicles. Two control approaches, modal control with skyhook damping and LQG control, are applied. It is aimed to investigate the influences of flexibility of the vehicle body on the performance of the designed controllers. For the model based approach of the LQG control, both the rigid model and the flexible model are used as design models for control design and the performance of the resulting controllers are compared. Finally the effect of actuator dynamics upon the ride quality of the railway vehicle with the designed controller is examined. Structural damping via piezoelectric actuation is excluded in this chapter and will be added to control design in Chapter 7 and Chapter 8.

6.1 Modal control with skyhook damping

The classical control method of skyhook damping is advantageous over passive damping because the trade-off between resonance attenuation and high frequency transmissibility has been eased. It is a simple method known to give excellent improvements in ride quality of railway vehicles.

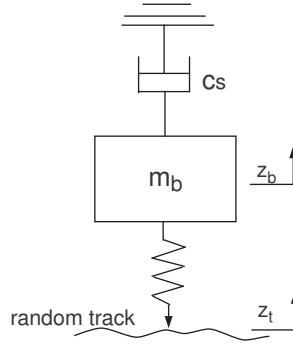


Figure 6.1: Skyhook damping system

6.1.1 Control method

Skyhook damping

Control with skyhook damping (e.g. Figure 6.1) is a simple suspension control method. The control action of an ideal skyhook damper is dependent upon the absolute velocity of a vehicle body.

$$f_{act} = -C_{sky}\dot{z}_b \quad (6.1)$$

where f_{act} is the control force, C_{sky} the skyhook damping gain, and \dot{z}_b is the absolute velocity of the vehicle body.

The implementation of such a control strategy of skyhook damping is virtually impossible as the absolute velocity is difficult to measure directly. In practice, the acceleration of the vehicle body is measured and then the signal is integrated to get the absolute velocity.

A high pass filter is used along with an integrator (Figure 6.2) in order to eliminate the long-term drift caused by offset effect of the transducer due to environmental reasons. A second order Butterworth high-pass filter (HPF) is chosen.

$$H_{hp} = \frac{s^2/\omega^2}{s^2/\omega^2 + s2\zeta/\omega + 1} \quad (6.2)$$

where the cut-off frequency ω is chosen to be significantly less than the main suspension frequency, i.e.

$$\omega = 0.1Hz \quad (6.3)$$

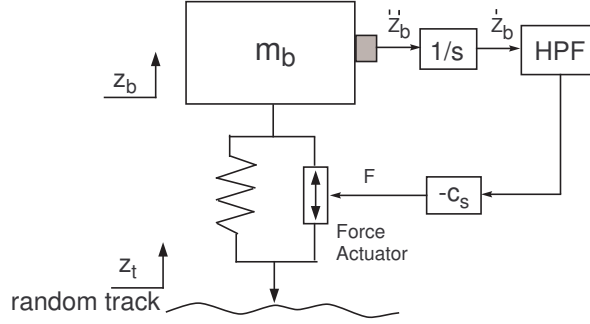


Figure 6.2: Intuitive control configuration: skyhook damping

and the damping ratio ζ and is chosen as

$$\zeta = 70\% \quad (6.4)$$

Then the combined transfer function of the integrator and the HPF is given by

$$G_{int} = \frac{2.533s}{2.533s^2 + 2.228s + 1} \quad (6.5)$$

Hence

$$\hat{z}_b = G_{int}\ddot{z}_b \quad (6.6)$$

It provides the estimation of a velocity from the measured acceleration.

Modal control

Modal control attempts to manage individual modes of the system. The measurement signals are decomposed into modal components, then the modal components are processed individually, and finally they are recombined and feed to the actuators. Figure 6.3 illustrates the structure of modal control for the railway vehicle.

6.1.2 Control design

The structure of the control system is shown in Figure 6.4 Two linear accelerometers are placed above the secondary suspensions at the left (x_L) and right (x_R) of the vehicle for measuring the body accelerations: \ddot{Z}_{x_L} and

6.1. MODAL CONTROL WITH SKYHOOK DAMPING

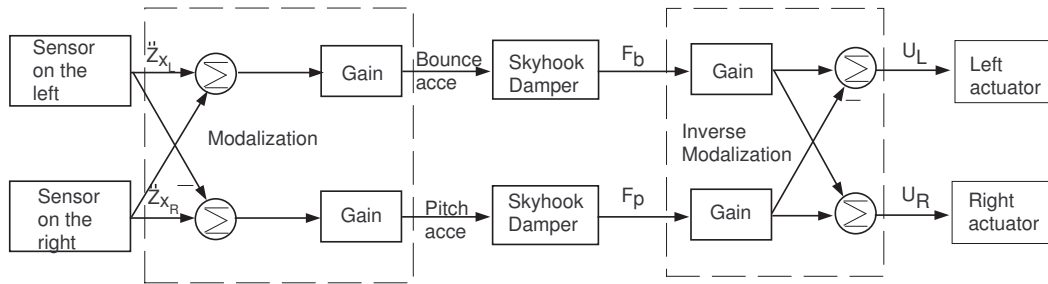


Figure 6.3: Structure of modal control

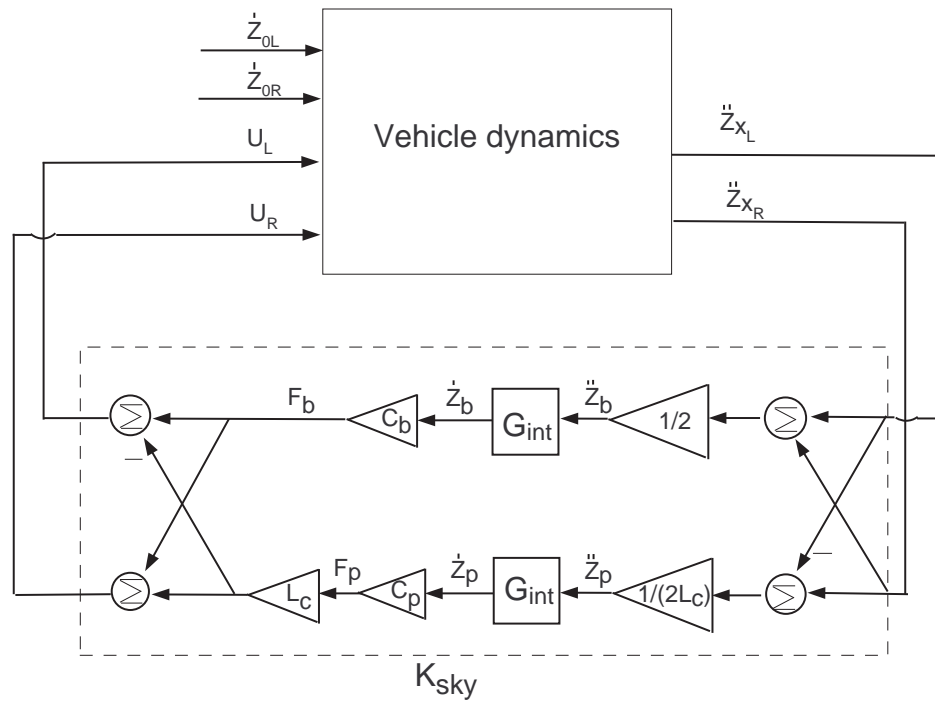


Figure 6.4: Control system of modal control with skyhook damping

\ddot{Z}_{x_R} . U_L and U_R are control forces from the secondary suspension. \dot{Z}_{0L} and \dot{Z}_{0R} are the two disturbance inputs from the track.

By using the relationship between the bounce/pitch accelerations and the left/right accelerations according to equations (4.5) and (4.6), the bounce and pitch modes of the vehicle body can be obtained

$$\ddot{Z}_b = \frac{\ddot{Z}_{x_L}}{2} + \frac{\ddot{Z}_{x_R}}{2} \quad (6.7)$$

$$\ddot{Z}_p = \frac{\ddot{Z}_{x_R}}{2L_c} - \frac{\ddot{Z}_{x_L}}{2L_c} \quad (6.8)$$

Then the bounce and pitch modes are controlled separately by applying different amount of skyhook damping

$$F_b = -c_b \dot{Z}_b \quad (6.9)$$

$$F_p = -c_p \dot{Z}_p \quad (6.10)$$

The skyhook damping gains c_b and c_p are tuned by trial and error to achieve an satisfying performance-typically the damping gain in pitch can be higher than in bounce. For convenience of tuning, the gain matrix is expressed in the form

$$\mathbf{C}_{\text{sky}} = -c_b \begin{bmatrix} 1 & 0 \\ 0 & c_1 \end{bmatrix} \quad (6.11)$$

where $c_1 = c_p/c_b$

Finally the control outputs from individual modes are recombined to drive the actuators across the left and right secondary suspensions.

$$U_L = F_b - L_c F_p \quad (6.12)$$

$$U_R = F_b + L_c F_p \quad (6.13)$$

6.1.3 Results and discussion

Comparisons are made between the results of the controller simulated with rigid model and the controller simulated with flexible model. Results of RMS acceleration levels in %g at the centre(x_C), left(x_L) and right(x_R) of the

6.1. MODAL CONTROL WITH SKYHOOK DAMPING

vehicle, RMS values of suspension deflection at left(x_L) and right(x_R) of the vehicle and RMS values of control forces from the left and right suspension are tabulated in Table 6.1. Results with different skyhook damping gains are included.

Table 6.1: RMS results: modal control with skyhook damping

Para.		System	Acceleration (%g)			Susp. Def. (mm)		Act. forces (kN)	
c_b	c_1		centre	left	right	left	right	left	right
-	-	G_r	2.68	1.66	3.41	7.81	11.34	-	-
-	-	G	3.04	3.04	3.75	7.8	11.35	-	-
6×10^4	2	$G_r + K_{sky}$	1.14	1.86	1.85	8.19	6.64	1.94	1.88
		$G + K_{sky}$	2.47	2.21	2.29	8.19	6.64	1.94	1.89
6×10^4	4	$G_r + K_{sky}$	1.15	1.69	1.65	9.11	5.71	2.42	1.97
		$G + K_{sky}$	2.47	2.07	2.14	9.11	5.71	2.42	1.98
12×10^4	4	$G_r + K_{sky}$	1.03	1.41	1.39	11.09	6.77	3.52	2.54
		$G + K_{sky}$	2.19	1.76	1.83	11.09	6.76	3.52	2.56

In this table, G denotes the flexible model of the plant, G_r denotes rigid model of the plant, K_{sky} denotes the designed controller. It shows that ride quality of the vehicle has been improved by the controller. The step responses of accelerations are shown in Figure 6.5. It shows high frequency oscillations when the controller is applied to the flexible model.

The results with $c_b = 12 \times 10^4$ and $c_1 = 4$ achieve the best ride quality. However there is a degradation in the ride quality when the controller is applied to flexible model, particularly at the centre of the vehicle.

Figure 6.6, 6.7 and 6.8 give power spectral densities (PSDs) of the centre(x_C), left(x_L) and right(x_R) accelerations of the railway vehicle with respect to random track disturbances. The controller is found effective for rigid body, but it does not perform as satisfactorily in reducing structural resonances. Figure 6.9 shows PSDs of the suspension control forces.

6.1. MODAL CONTROL WITH SKYHOOK DAMPING

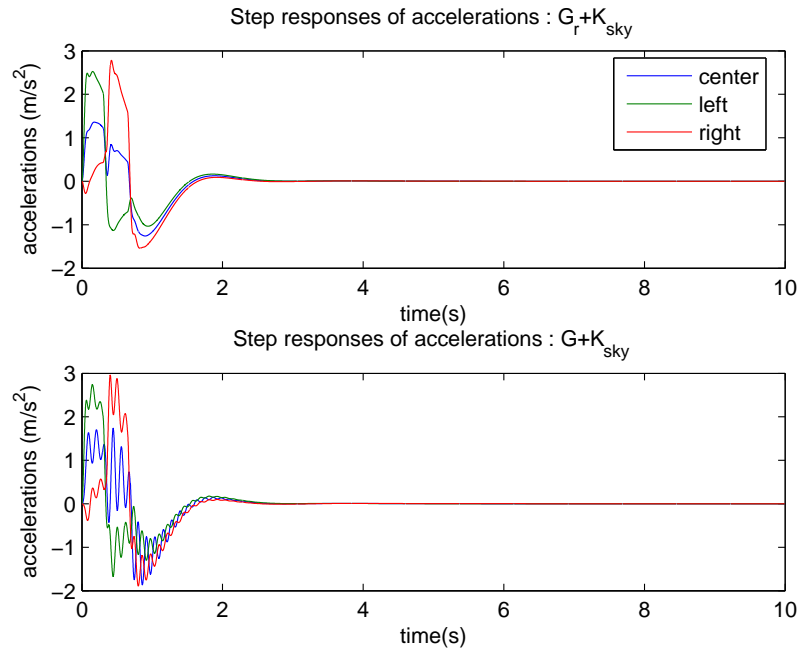


Figure 6.5: Modal control with skyhook damping with $c_b = 12 \times 10^4$ and $c_1 = 4$: Step responses

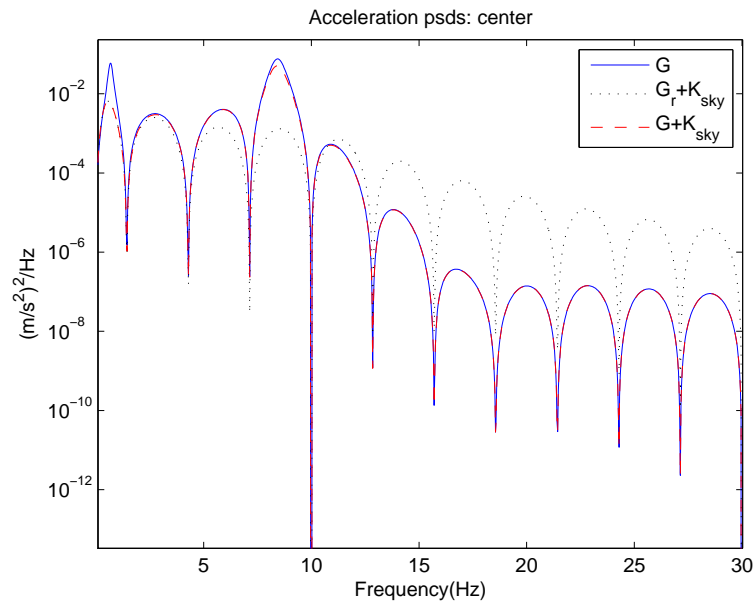


Figure 6.6: Modal control with skyhook damping with $c_b = 12 \times 10^4$ and $c_1 = 4$: Center acceleration PSDs

6.1. MODAL CONTROL WITH SKYHOOK DAMPING

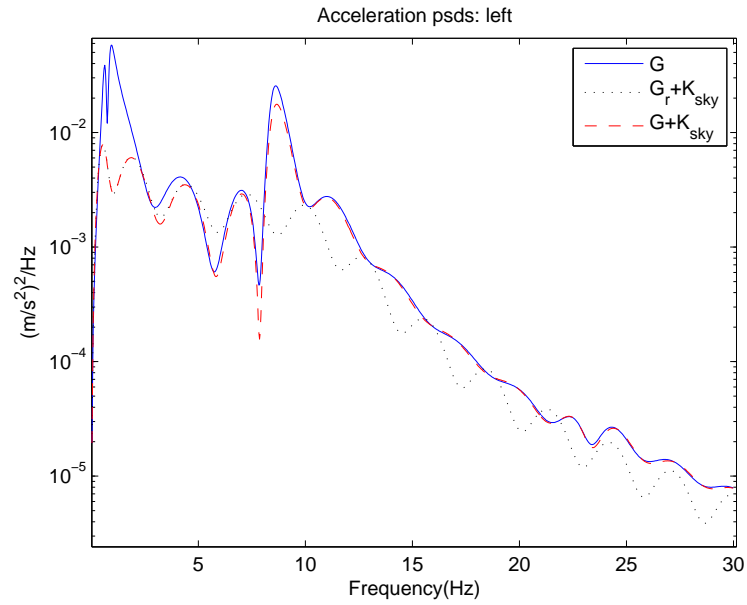


Figure 6.7: Modal control with skyhook damping with $c_b = 12 \times 10^4$ and $c_1 = 4$: Left acceleration PSDs

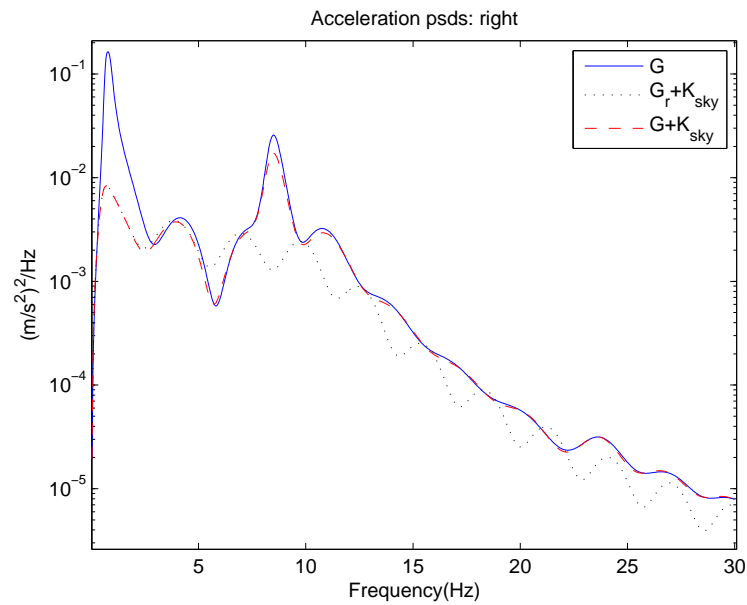


Figure 6.8: Modal control with skyhook damping with $c_b = 12 \times 10^4$ and $c_1 = 4$: Right acceleration PSDs

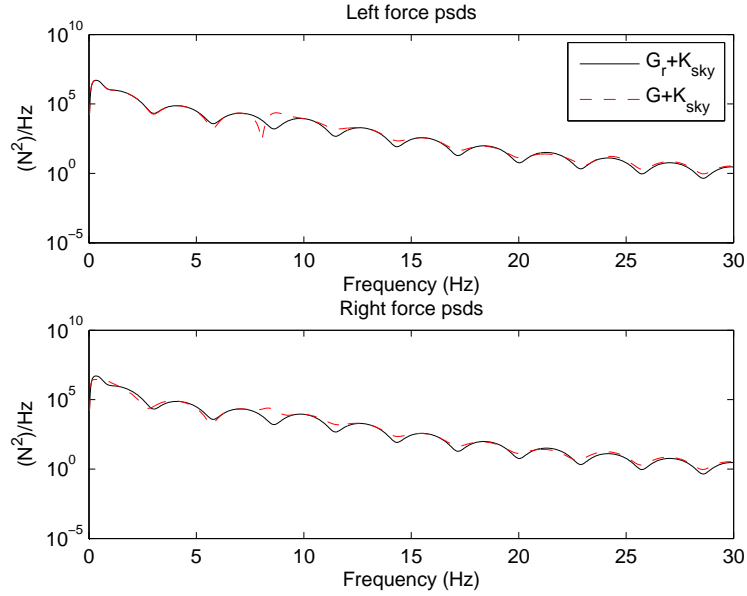


Figure 6.9: Modal control with skyhook damping with $c_b = 12 \times 10^4$ and $c_1 = 4$: Control Force PSDs

6.2 LQG Control

As we are concerned with minimizing the accelerations of the vehicle body in response to persistent stochastic inputs due to the irregularities of the track, LQG control in which the exogenous signals are assumed to be stochastic is clearly the first modern control approach to be considered.

6.2.1 LQG Preliminaries

Linear Quadratic Gaussian namely LQG control is a special type of optimal control. The plant is assumed linear and the controller to be designed is constrained to be of a linear form. The problems of LQG control are solved by minimizing quadratic performance indices, in terms of the control, regulation and/or tracking error variables.

The problem addressed by the theory of LQG control is as the following.

Given a plant model in state-space form,

$$\dot{\mathbf{x}} = \mathbf{A}\mathbf{x} + \mathbf{B}\mathbf{u} + \mathbf{G}\mathbf{w}_d \quad (6.14)$$

$$\mathbf{y} = \mathbf{C}\mathbf{x} + \mathbf{D}\mathbf{u} + \mathbf{H}\mathbf{w}_d + \mathbf{w}_n \quad (6.15)$$

where \mathbf{w}_d and \mathbf{w}_n are vectors of the disturbance (process noise) and measurement noise respectively, which are usually assumed to be white noises, namely zero-mean Gaussian stochastic processes which are uncorrelated in time, having the covariance,

$$E\{\mathbf{w}_d\mathbf{w}_d^T\} = \mathbf{W} \geq 0, \quad E\{\mathbf{w}_n\mathbf{w}_n^T\} = \mathbf{V} \geq 0 \quad (6.16)$$

Here it is assumed that \mathbf{w}_d and \mathbf{w}_n are uncorrelated with each other

$$E\{\mathbf{w}_d\mathbf{w}_n^T\} = 0 \quad (6.17)$$

\mathbf{u} is the vector of control signals, \mathbf{y} is the vector of measured outputs which is corrupted by \mathbf{w}_n . The problem is to devise a feedback-control law which minimizes the cost

$$J = \lim_{T \rightarrow \infty} E \left\{ \int_0^T [\mathbf{z}(t)^T \mathbf{Q} \mathbf{z}(t) + \mathbf{u}^T(t) \mathbf{R} \mathbf{u}(t)] \right\} \quad (6.18)$$

where $\mathbf{z}(t)$ could be the state vector $\mathbf{x}(t)$ or some linear combination of the states

$$\mathbf{z}(t) = \mathbf{M}\mathbf{x}(t) \quad (6.19)$$

\mathbf{Q} and \mathbf{R} are weighting matrices, which are symmetrical and definite

$$\mathbf{Q} = \mathbf{Q}^T \geq 0, \quad \mathbf{R} = \mathbf{R}^T > 0 \quad (6.20)$$

The LQG problem includes the optimal estimation problem and linear quadratic control problem. The solution to the LQG problem is based on the separation principle, illustrated in Figure 6.10. Firstly determine the optimal control for a deterministic linear quadratic regulator (LQR) problem. The

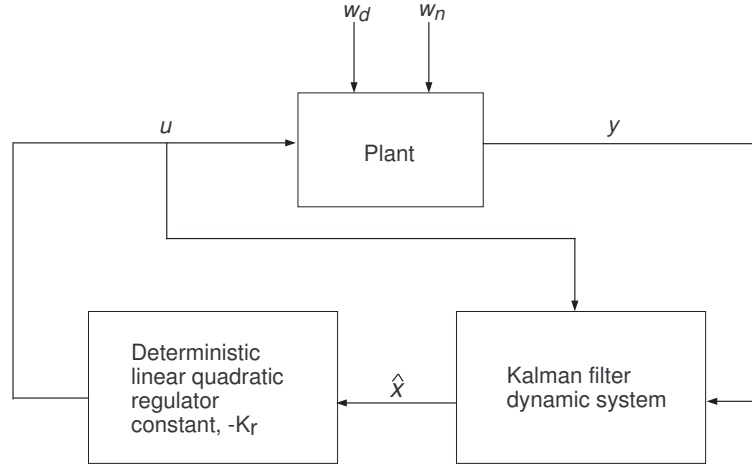


Figure 6.10: The separation principle

solution to this problem can be written in terms of the simple state feedback

$$\mathbf{u}(t) = -\mathbf{K}_r \mathbf{x}(t) \quad (6.21)$$

where \mathbf{K}_r is the gain matrix, which minimizes the performance index given by equation (6.35) and is given by

$$\mathbf{K}_r = \mathbf{R}^{-1} \mathbf{B}^T \mathbf{X} \quad (6.22)$$

and \mathbf{X} is the unique positive semi-definite solution of the algebraic Riccati equation

$$\mathbf{A}^T \mathbf{X} + \mathbf{X} \mathbf{A} - \mathbf{X} \mathbf{B} \mathbf{R}^{-1} \mathbf{B}^T \mathbf{X} + \mathbf{Q} = \mathbf{0} \quad (6.23)$$

It requires that the states \mathbf{x} is measured and available for feedback. In practice, however, the states are not always measurable. Then an optimal estimate $\hat{\mathbf{x}}$ of the state \mathbf{x} by designing the optimal estimator gain \mathbf{K}_f is given by Kalman Filter so that $E \{ (\mathbf{x} - \hat{\mathbf{x}})^T (\mathbf{x} - \hat{\mathbf{x}}) \}$ is minimized. Then $\hat{\mathbf{x}}$ is used as if it were an exact measure of the state \mathbf{x} to solve the linear quadratic control problem. The Kalman filter as the structure of an ordinary observer

is given by

$$\dot{\hat{\mathbf{x}}} = \mathbf{A}\hat{\mathbf{x}} + \mathbf{B}\mathbf{u} + \mathbf{K}_f(\mathbf{y} - \hat{\mathbf{y}}) \quad (6.24)$$

$$\hat{\mathbf{y}} = \mathbf{C}\hat{\mathbf{x}} + \mathbf{D}\mathbf{u} \quad (6.25)$$

where \mathbf{K}_f is the observer gain matrix optimally chosen, which minimizes $E\{[\mathbf{x} - \hat{\mathbf{x}}]^T[\mathbf{x} - \hat{\mathbf{x}}]\}$, and given by

$$\mathbf{K}_f = \mathbf{P}_f \mathbf{C}^T \mathbf{V}^{-1} \quad (6.26)$$

where $\mathbf{P}_f = \mathbf{P}_f^T \geq \mathbf{0}$ is the unique positive semi-definite solution of the algebraic Riccati equation

$$\mathbf{P}_f \mathbf{A}^T + \mathbf{A} \mathbf{P}_f - \mathbf{P}_f \mathbf{C}^T \mathbf{V}^{-1} \mathbf{C} \mathbf{P}_f + \mathbf{W} = \mathbf{0} \quad (6.27)$$

6.2.2 Control design

The structure of the LQG controller is shown by Figure 6.11.

LQR design

The plant is described by the following state-space expression

$$\dot{\mathbf{x}} = \mathbf{A}\mathbf{x} + \mathbf{B}\mathbf{u} \quad (6.28)$$

$$\mathbf{y} = \mathbf{C}\mathbf{x} + \mathbf{D}\mathbf{u} \quad (6.29)$$

where the \mathbf{x} is the state vector

$$\mathbf{x} = [\dot{Z}_{3C} \quad \dot{\theta} \quad \dot{Z}_{1L} \quad \dot{Z}_{1R} \quad Z_{3L} - Z_{1L} \quad Z_{3R} - Z_{1R} \quad Z_{2L} - Z_{1L} \quad Z_{2R} - Z_{1R} \\ Z_{1L} - Z_{0L} \quad Z_{1R} - Z_{0R} \quad \dot{q}_1 \quad \dot{q}_1 \quad \dot{q}_2 \quad \dot{q}_2] \quad (6.30)$$

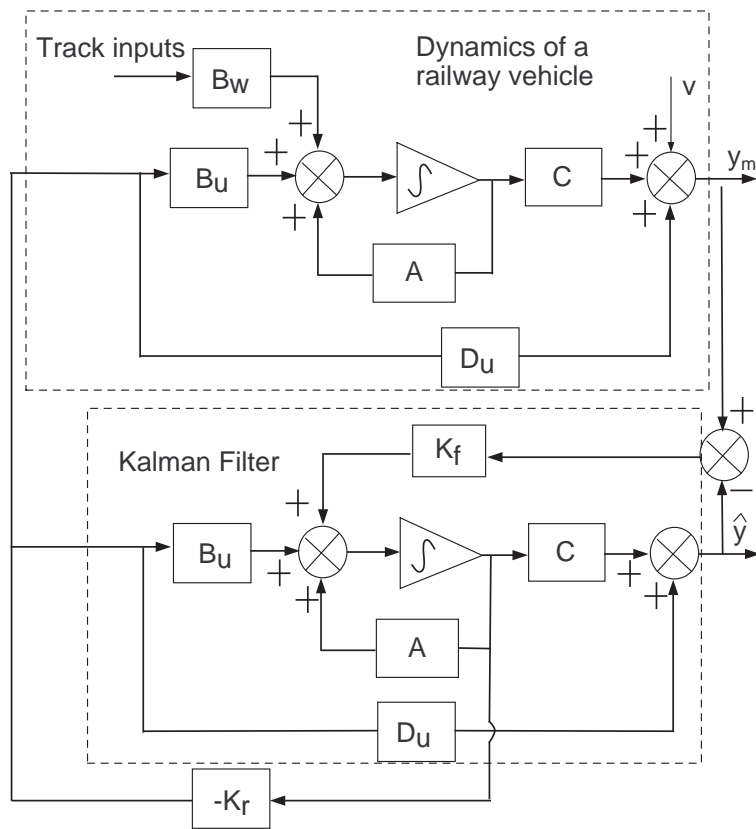


Figure 6.11: Linear quadratic control structure for the railway vehicle

6.2. LQG CONTROL

$\mathbf{u} = [U_L \ U_R]$, and the matrices \mathbf{A} and \mathbf{B} have been given in Chapter 4. If a rigid model is used for control design, the state vector is given by

$$\mathbf{x} = \begin{bmatrix} \dot{Z}_{3C} & \dot{\theta} & \dot{Z}_{1L} & \dot{Z}_{1R} & Z_{3L} - Z_{1L} & Z_{3R} - Z_{1R} & Z_{2L} - Z_{1L} & Z_{2R} - Z_{1R} \\ Z_{1L} - Z_{0L} & Z_{1R} - Z_{0R} & & & & & & \end{bmatrix} \quad (6.31)$$

and the matrices \mathbf{A} and \mathbf{B} change accordingly.

The regulated output vector is chosen as three accelerations of the vehicle body and two suspension deflections

$$\mathbf{y} = [\ddot{Z}_{x_L} \ \ddot{Z}_{x_C} \ \ddot{Z}_{x_R} \ Z_{3L} - Z_{1L} \ Z_{3R} - Z_{1R}] \quad (6.32)$$

The control objective is to minimize the accelerations while maintaining the suspension deflection at an acceptable level and keeping the control inputs small. Output weighting is used instead of state weighting because not all the regulated variables (e.g the accelerations of the vehicle body) can be found in the state variables.

$$\begin{aligned} \mathbf{y}(t)^T \mathbf{Q}_y \mathbf{y}(t) &= (\mathbf{C}\mathbf{x}(t) + \mathbf{D}\mathbf{u}(t))^T \mathbf{Q}_y (\mathbf{C}\mathbf{x}(t) + \mathbf{D}\mathbf{u}(t)) \\ &= \mathbf{x}(t)^T \mathbf{C}^T \mathbf{Q}_y \mathbf{C} \mathbf{x}(t) + 2\mathbf{x}(t)^T \mathbf{C}^T \mathbf{Q}_y \mathbf{D} \mathbf{u}(t) + \mathbf{u}(t)^T \mathbf{D}^T \mathbf{Q}_y \mathbf{D} \mathbf{u}(t) \end{aligned} \quad (6.33)$$

where and \mathbf{Q}_y is the output weighting matrix written as

$$\mathbf{Q}_y = \begin{bmatrix} q_1 & 0 & 0 & 0 & 0 \\ 0 & q_1 & 0 & 0 & 0 \\ 0 & 0 & q_1 & 0 & 0 \\ 0 & 0 & 0 & q_2 & 0 \\ 0 & 0 & 0 & 0 & q_2 \end{bmatrix} \quad (6.34)$$

where q_1 is the weight for the accelerations and q_2 is the weight for suspension

deflections. The quadratic cost function is rewritten into

$$\begin{aligned} J &= \lim_{T \rightarrow \infty} E \left\{ \int_0^T [\mathbf{y}(t)^T \mathbf{Q}_y \mathbf{y}(t)] \right\} \\ &= \lim_{T \rightarrow \infty} E \left\{ \int_0^T [\mathbf{x}(t)^T \mathbf{Q} \mathbf{x}(t) + \mathbf{u}^T(t) \mathbf{R} \mathbf{u}(t) + 2\mathbf{x}(t)^T \mathbf{N} \mathbf{u}(t)] \right\} \end{aligned} \quad (6.35)$$

Hence $\mathbf{Q} = \mathbf{C}^T \mathbf{Q}_y \mathbf{C}$, $\mathbf{R} = \mathbf{D}^T \mathbf{D}$ and $\mathbf{N} = \mathbf{C}^T \mathbf{Q}_y \mathbf{D}$. With the selection of output weight of \mathbf{Q}_y , the values for weights of \mathbf{Q} , \mathbf{R} and \mathbf{N} are determined.

The selection of quadratic weights is difficult and mainly depends on the experience of the designer. Here elements in \mathbf{Q}_y are initially chosen to be square of the inverse of the expected values, $\frac{1}{(\text{expected value})^2}$, then they are tuned based on the physical constraints (e.g. deflection $\leq 12\text{mm}$, control force $\leq 4\text{kN}$). There is a trade-off between the accelerations and suspension deflections. Increasing q_1 leads to smaller accelerations, larger deflections and bigger force inputs and vice versa. Increasing q_2 leads to smaller deflections, larger accelerations and smaller force inputs and vice versa. The optimal state-feedback gain \mathbf{K} is given by equation (6.21). In MATLAB, the following command is used

$$[\mathbf{K}, \mathbf{S}, \mathbf{e}] = \text{lqr}(\mathbf{A}, \mathbf{B}, \mathbf{Q}, \mathbf{R}, \mathbf{N})$$

Kalman filter

Kalman-Bucy filter, the continuous time version of the Kalman filter, is designed to estimate the states of the system. Recall the model of the plant

$$\dot{\mathbf{x}} = \mathbf{A} \mathbf{x} + \mathbf{B}_u \mathbf{u} + \mathbf{B}_w \mathbf{w} \quad (6.36)$$

$$\mathbf{y}_m = \mathbf{C}_m \mathbf{x} + \mathbf{D}_m \mathbf{u} + \mathbf{D}_w \mathbf{w} + \mathbf{v} \quad (6.37)$$

The system is subject to random track disturbances $\mathbf{w} = [\dot{Z}_{0L} \ \dot{Z}_{0R}]$. The measurements feeding to the estimator are chosen as the three accelerations of the vehicle body

$$\mathbf{y}_m = [\ddot{Z}_{xL} \ \ddot{Z}_{xC} \ \ddot{Z}_{xR}] \quad (6.38)$$

\mathbf{y}_m is corrupted by the sensor noises \mathbf{v}

For selection of \mathbf{W} and \mathbf{V} , they are considered more as representations of aspects of the real problem than as tuning parameters, which are to be adjusted until a satisfactory design is obtained. \mathbf{W} is given by the track variance and the measurement noise is normally assumed to have an RMS value of one percent of the maximum acceleration. Based on the above principles, \mathbf{W} and \mathbf{V} are chosen as

$$\mathbf{W} = \begin{bmatrix} 5.4283 \times 10^{-4} & 0 \\ 0 & 5.4283 \times 10^{-4} \end{bmatrix} \quad (6.39)$$

$$\mathbf{V} = \begin{bmatrix} (0.01 \times 0.365)^2 & 0 & 0 \\ 0 & (0.01 \times 0.365)^2 & 0 \\ 0 & 0 & (0.01 \times 0.365)^2 \end{bmatrix} \quad (6.40)$$

It is very important to choose the correct track variance for the process noise and the correct level of sensor noise because they will affect the ride quality of the vehicle (Foo and Goodall [2000]). Then the best \mathbf{K}_f is given by equation (6.26). In MATLAB \mathbf{K}_f and the LQG controller are found with the following commands

```
sys_kf=ss(Ar, [Br Bw], Cm, [Dm Dw]);
[Kf, L, P]=kalman(sys_kf, W, V);
K_lqg=lqgreg(Kf, Kr);
```

6.2.3 Results and discussion

The LQG controller has been designed using the rigid model (G_r) and the flexible model (G), and the resulting controllers are denoted by K_{rLQG} and K_{LQG} respectively.

Results with controller K_{rLQG}

Controller K_{rLQG} is designed with the rigid model G_r of the railway vehicle. Results tabulated in Table 6.2 are RMS acceleration levels in %g, RMS values of suspension deflections and RMS values of control forces. Step responses of

6.2. LQG CONTROL

Table 6.2: RMS results: LQG control design with rigid model with $q_1 = 1/(0.1)^2$ and $q_2 = 1/(0.012)^2$

Sys.	Vertical Acc.(%g)			Susp. Def.(mm)		Act. Force(kN)	
	Center	Left	Right	Left	Right	Left	Right
$K_{rLQG} + G_r$	0.35	0.51	0.53	10.27	10.69	3.82	3.97
$K_{rLQG} + G$	0.46	0.53	0.57	10.27	10.70	3.82	3.97

the accelerations are shown in Figure 6.12. High frequency oscillations appear in the step responses when the controller is simulated with the flexible model.

Figure 6.13, 6.14 and 6.15 give power spectral densities (PSDs) for the centre (x_C), left (x_L) and right (x_R) accelerations of the railway vehicle in response to random track disturbances.

LQG controller gives significantly bigger improvement in ride quality than classical control approach with skyhook damping and the forces are generally increased with LQG controller. However, comparing the results, it also shows that the flexibility of the vehicle body worsens the ride quality when the controller is designed without considering the effect of the flexible modes, even though the accelerations of the rigid motions of the vehicle body are well reduced and the RMS levels of the accelerations are considerably small.

The plots in Figure 6.16 shows that the PSDs of the control forces of system ($G_r + K_{rLQG}$) and system ($G + K_{rLQG}$) are almost the same.

Results with controller K_{LQG}

Controller K_{LQG} is designed with the flexible model, G , of the railway vehicle. Results tabulated in Table 6.3 are RMS acceleration levels in %g, RMS values of suspension deflections and RMS values of control forces with different values for weight q_1 . The RMS results show excellent improvement in ride quality.

Step responses of the accelerations are shown in Figure 6.17. It shows that the high frequency vibrations caused by the flexibility of the vehicle body have been suppressed.

Figure 6.18, 6.19, 6.20 and 6.21 give PSDs for the centre (x_C), left (x_L) and right (x_R) accelerations and PSDs for the suspension control forces of

6.2. LQG CONTROL

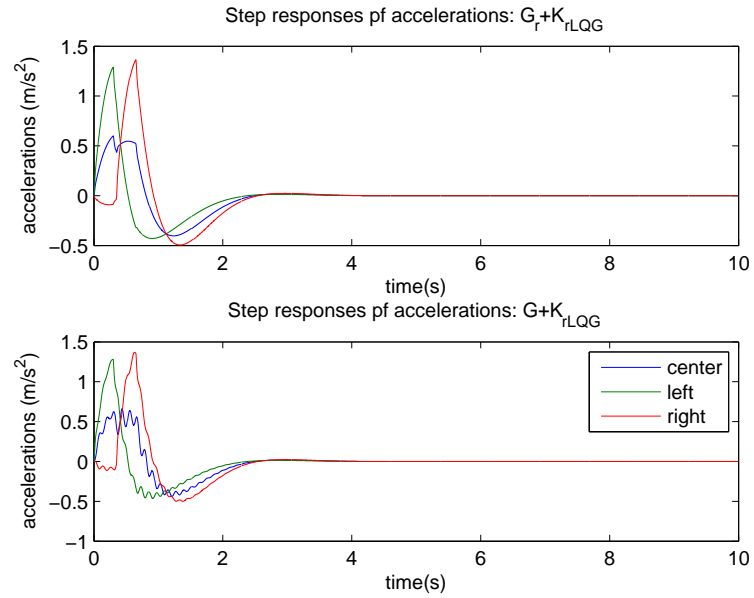


Figure 6.12: LQG control designed with rigid model, with $q_1 = 1/(0.1)^2$ and $q_2 = 1/(0.012)^2$: closed-loop step response

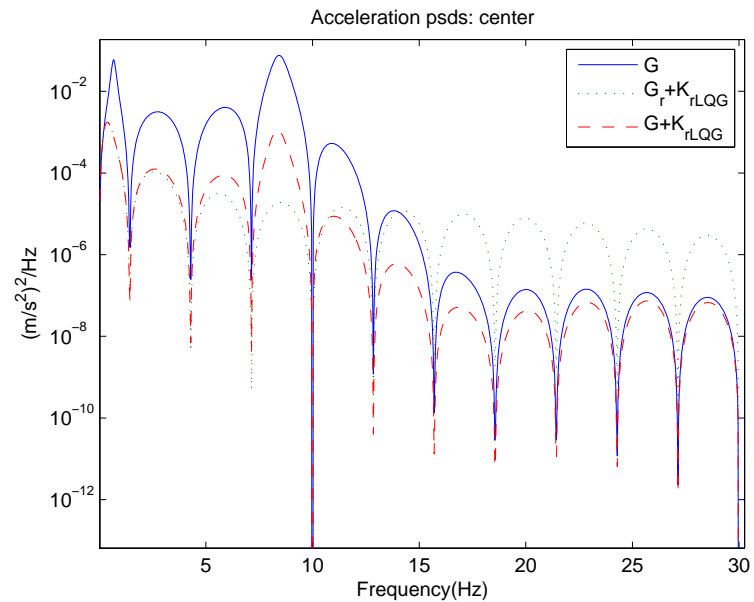


Figure 6.13: LQG control designed with rigid model, with $q_1 = 1/(0.1)^2$ and $q_2 = 1/(0.012)^2$: Center acceleration PSDs

6.2. LQG CONTROL

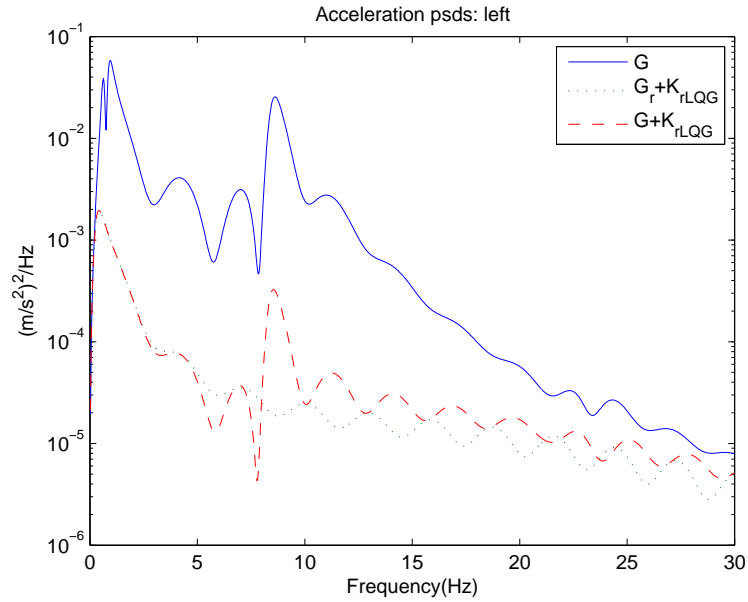


Figure 6.14: LQG control designed with rigid model, with $q_1 = 1/(0.1)^2$ and $q_2 = 1/(0.012)^2$: Left accelerations PSDs

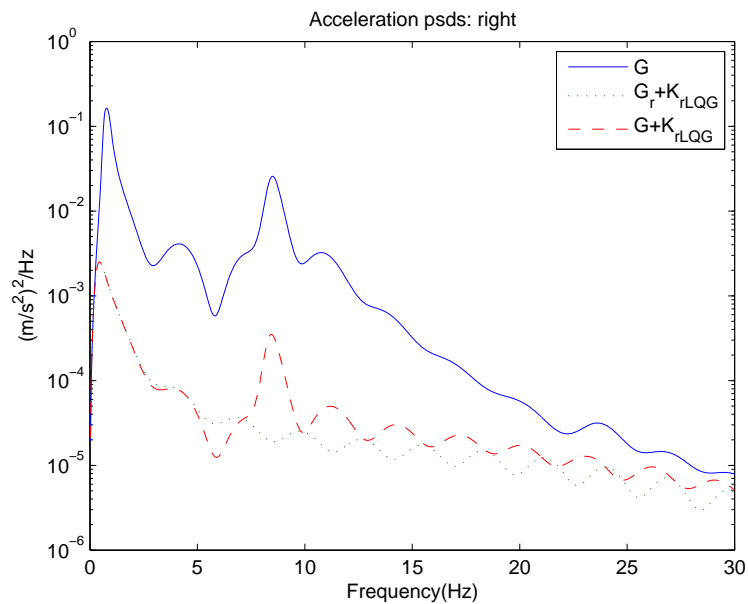


Figure 6.15: LQG control designed with rigid model, with $q_1 = 1/(0.1)^2$ and $q_2 = 1/(0.012)^2$: Right acceleration PSDs

6.2. LQG CONTROL

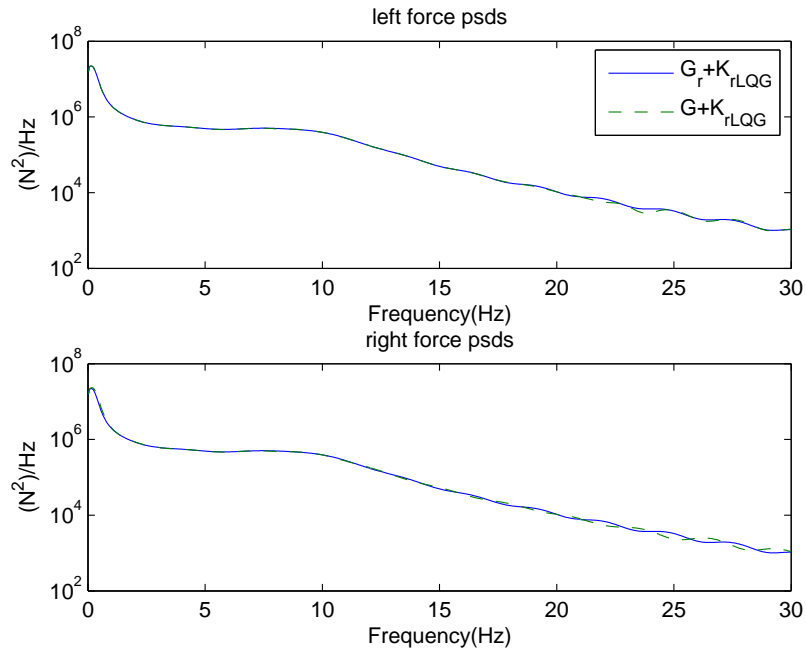


Figure 6.16: LQG control designed with rigid model, with $q_1 = 1/(0.1)^2$ and $q_2 = 1/(0.012)^2$: Control force PSDs

Table 6.3: RMS results: LQG control designed with flexible model with $q_2 = 1/(0.012)^2$

Para.	Vertical Acc. (%g)			Susp. Def. (mm)		Act. Force (kN)	
	Center	Left	Right	Left	Right	Left	Right
$1/(0.20)^2$	0.53	0.81	0.86	8.78	9.20	3.16	3.33
$1/(0.15)^2$	0.45	0.66	0.71	9.40	9.84	3.46	3.62
$1/(0.10)^2$	0.36	0.50	0.54	10.33	10.79	3.87	4.02

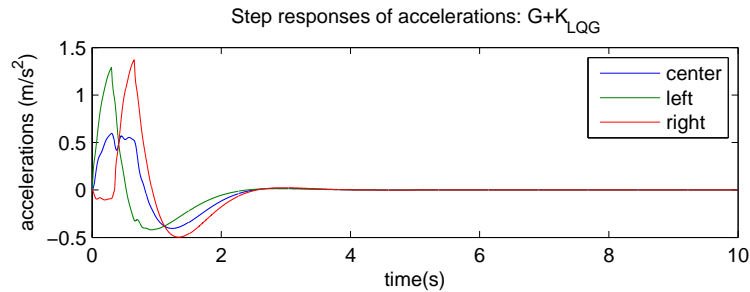


Figure 6.17: LQG control designed with flexible model, with $q_1 = 1/(0.1)^2$ and $q_2 = 1/(0.012)^2$:closed-loop step response

6.3. EFFECT OF ACTUATOR DYNAMICS

the railway vehicle in responses to random track disturbances. The PSDs also prove that flexible modes are well suppressed by the LQG controller designed with the flexible model.

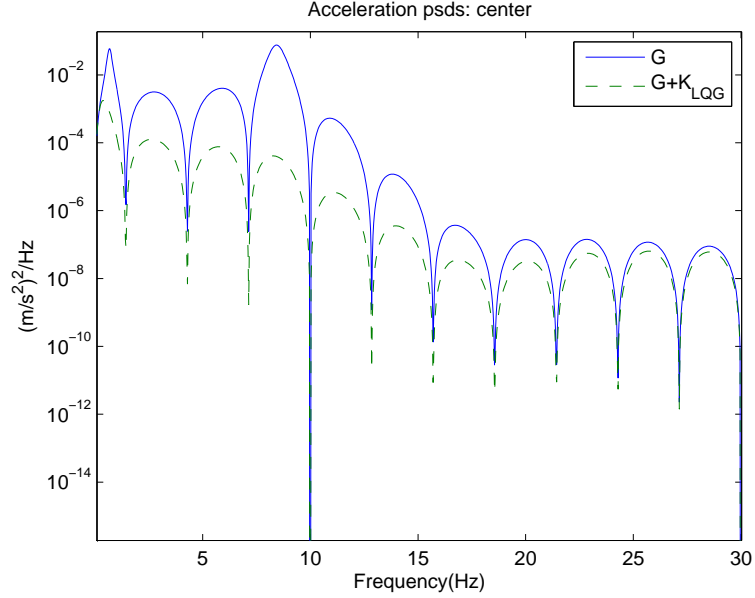


Figure 6.18: LQG control designed with flexible model, with $q_1 = 1/(0.1)^2$ and $q_2 = 1/(0.012)^2$: Center acceleration PSDs

6.3 Effect of actuator dynamics

Table 6.4 and 6.5 tabulates results for the closed-loop systems $G + K_{sky}$ and $G + K_{LQG}$ with actuator dynamics and with ideal actuators. It shows that degradation in ride quality is caused by the inclusion of actuator dynamics.

Table 6.4: RMS results with actuator dynamics: $G + K_{sky}$

Sys.	Vertical Acc.(%g)			Susp. Def.(mm)		Act. Force(kN)	
	Center	Left	Right	Left	Right	Left	Right
with ideal act.	2.19	1.76	1.83	11.09	6.76	3.52	2.56
with real act.	2.26	1.85	1.93	11.04	6.77	3.51	2.57

6.3. EFFECT OF ACTUATOR DYNAMICS

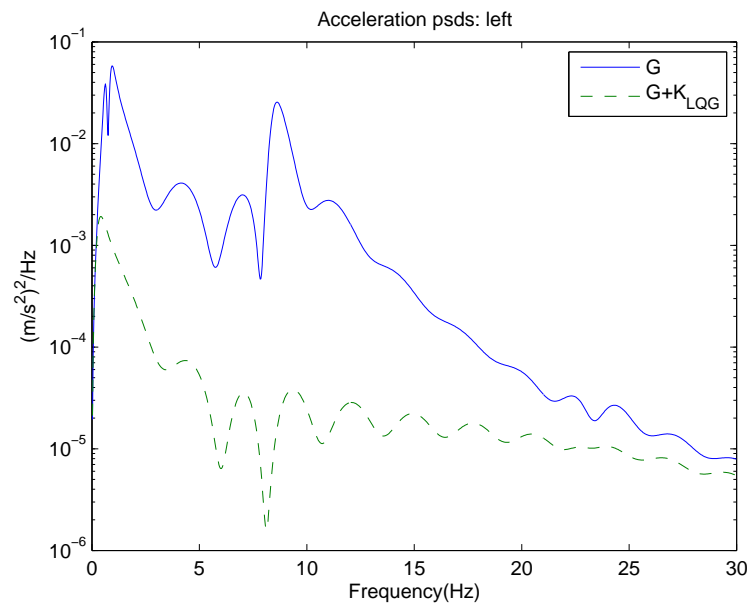


Figure 6.19: LQG control designed with flexible model, with $q_1 = 1/(0.1)^2$ and $q_2 = 1/(0.012)^2$: Left accelerations PSDs

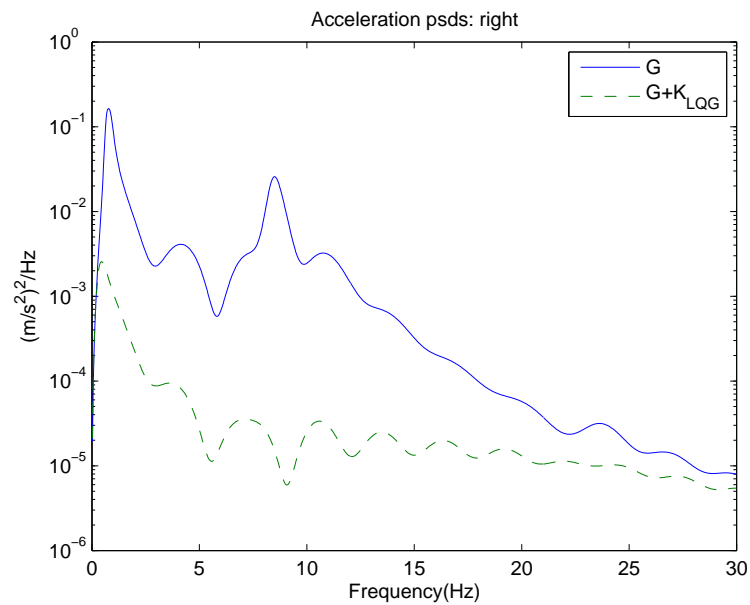


Figure 6.20: LQG control designed with flexible model, with $q_1 = 1/(0.1)^2$ and $q_2 = 1/(0.012)^2$: Right acceleration PSDs

6.3. EFFECT OF ACTUATOR DYNAMICS

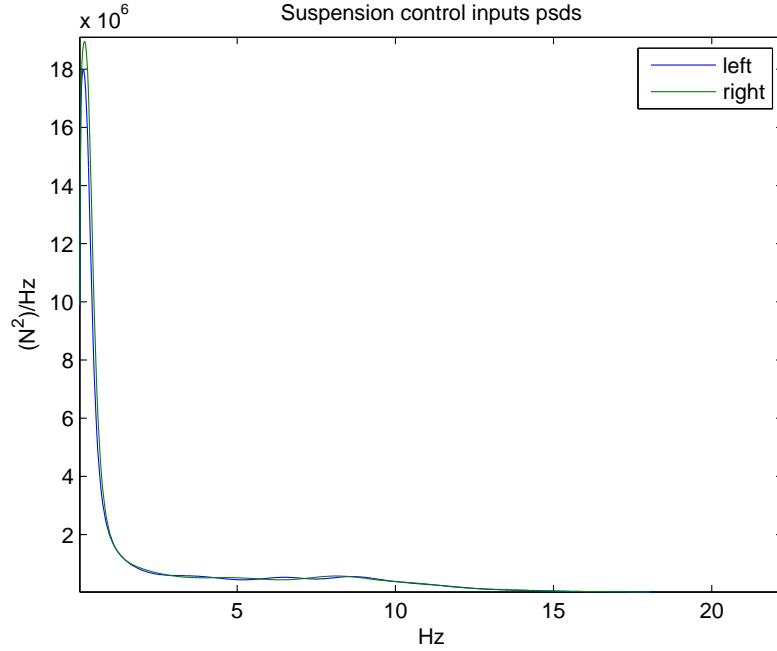


Figure 6.21: LQG control designed with flexible model, with $q_1 = 1/(0.1)^2$ and $q_2 = 1/(0.012)^2$:Control force PSDs

Table 6.5: RMS results with actuator dynamics: $G + K_{LQG}$

Sys.	Vertical Acc.(%g)			Susp. Def.(mm)		Act. Force(kN)	
	Center	Left	Right	Left	Right	Left	Right
with ideal act.	0.36	0.50	0.54	10.33	10.79	3.87	4.02
with real act.	0.36	0.55	0.58	10.33	10.79	3.87	4.02

Figure 6.22,6.23 and 6.24 are the acceleration PSDs for closed-loop system $G+K_{sky}$ with ideal and real actuators.It is shown that ride degradation occurs from 5Hz due to the inclusion of the actuator dynamics.

Figure 6.25 shows the ratios of the force response of a real actuator with the force generated by an ideal actuator with respect to the track inputs. It tells the closed-loop bandwidth of the hydraulic actuator operating with the railway vehicle with controller K_{sky} .

The ratio is equal to unity for 0 to 4Hz. This means that the 'real' actuator is able to track the the low frequency demands. At higher frequencies, unsatisfactory actuator performance begin to emerge in the force

6.3. EFFECT OF ACTUATOR DYNAMICS

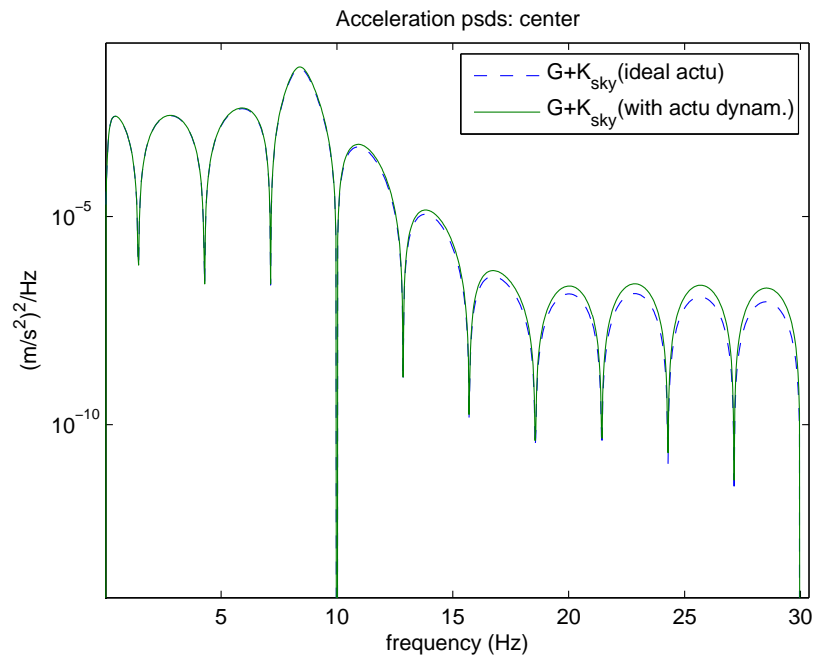


Figure 6.22: Effect of actuator dynamics ($G + K_{sky}$): Center acceleration PSDs

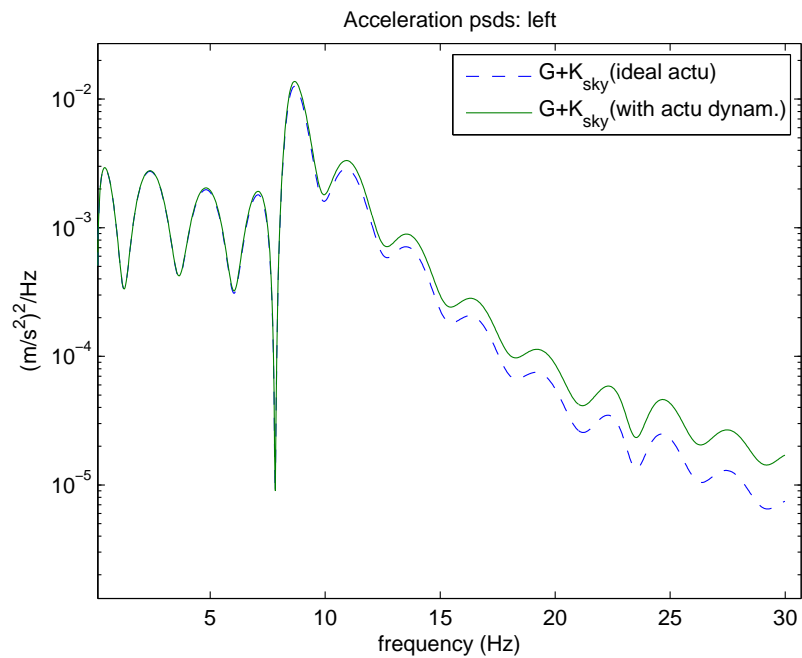


Figure 6.23: Effect of actuator dynamics ($G + K_{sky}$): Left accelerations PSDs

6.3. EFFECT OF ACTUATOR DYNAMICS

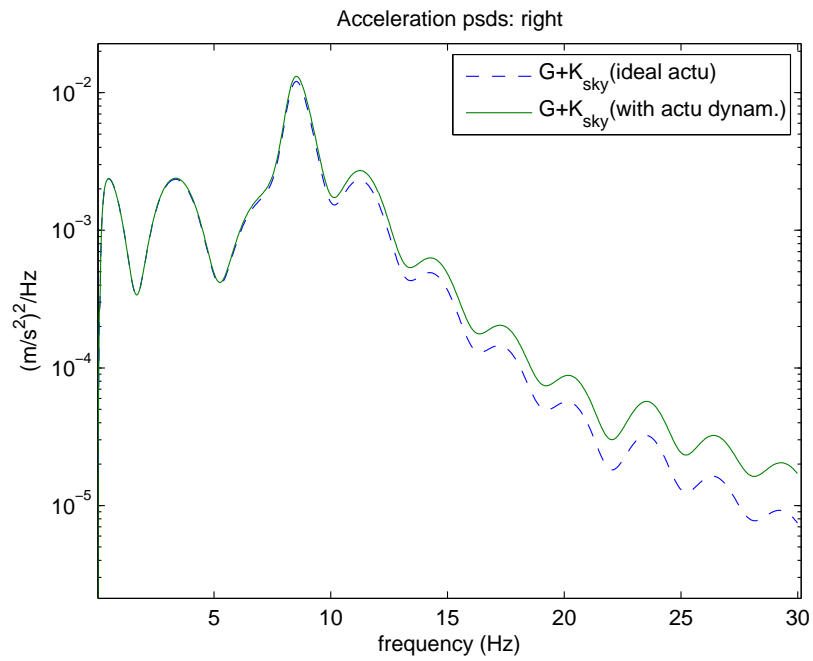


Figure 6.24: Effect of actuator dynamics ($G+K_{sky}$): Right acceleration PSDs

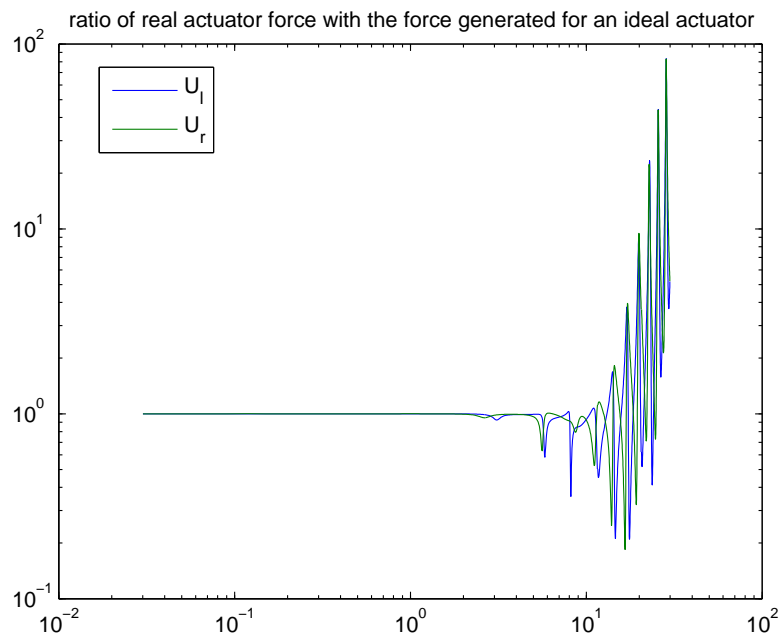


Figure 6.25: Ratio of real force/ideal force of hydraulic actuator

response. This is because the actuators can not respond fast enough to isolate the high frequency vibrations due to the limited bandwidth of the hydraulic actuator. As the real actuator begins to lose control at these frequencies, it is unable to produce the correct amount of force. This results in higher body velocities, hence higher actuator force demand. Therefore, the 'real' actuator force is higher than the ideal force. These effects are a consequence of the track input as a disturbance into the system. High frequency vibrations are transmitted from the bogie and bring a degradation in the ride quality.

6.4 Concluding remarks

The preliminary study described two control approaches, i.e modal control with skyhook damping and LQG control, for the active suspension control of railway vehicles for improving the passenger ride quality.

With the approach of modal control with skyhook damping, the acceleration of the vehicle body in response to random track disturbances are effectively reduced, but the flexibility of the vehicle body brings a big degradation in the ride quality especially at the centre of the vehicle. This indicates the necessity of introducing extra control for suppressing the flexibility of the vehicle body.

Significantly bigger improvements in ride quality are achieved by the LQG controller than the controller designed with classical approach, which is at the cost of increased complexity of the controller and somewhat higher actuator forces. The results show it important to include the flexible modes in the design model so that the flexible modes are effectively suppressed by the controller.

Finally, the effect of the dynamics of the conventional hydraulic actuators was studied. The bandwidth of the hydraulic actuator in operation with the closed-loop system of the railway vehicle is limited. Inclusion of the dynamics of the actuator brings degradation in ride quality of the railway vehicle.

Chapter 7

Control Design I: Decentralized Control

This chapter describes the decentralized control strategy for vibration control of the railway vehicle considering the flexible modes of the vehicle body with the combined conventional active suspension control and active structural damping. It includes the controller design for active damping of the flexible structure of the vehicle with piezoelectric stack actuators and piezoelectric patch sensors, and the controller design for the secondary active suspension control. The two sub controllers are designed independently with decoupled parts of the overall model. In contrast, centralized controller designed with the full model will be considered in chapter 8.

Two combinations of control methods will be considered in this chapter: 1) modal control with skyhook damping for suspension control and LQG control for structural damping. 2) Two individual LQG controllers for structural damping and suspension control respectively.

7.1 Introduction of active structural damping

For active structural damping, piezoelectric actuators and sensors are integrated onto the flexible structure of the railway vehicle body. The signals

from the sensors are feedback to the controller, and the control signal is produced to drive the actuator to produce the necessary moments/force acting on the flexible structure. The structure integrated with actuators, sensors and control is viewed as a smart structure.

Structural damping is necessary for flexible-bodied railway vehicles, although active suspension control is able to improve the ride quality by suppressing both the rigid modes and flexible modes with careful control design. According to the state-space representation of the system model given by equation 4.59, the flexible motion and the rigid motion are coupled (the coupling is discussed in detail in section 4.5). Briefly speaking, coupling is introduced by actuation (e.g. forces from the secondary suspension) that affects both the flexible modes and rigid modes and sensing (e.g. by the conventional accelerometers) that measures both the flexible modes and rigid modes. However, the performance of active suspension control for suppressing the flexible modes using the actuators alone is limited due to several reasons

- The positions of the suspension control x_L and x_R are near the node points of the 1st vertical bending mode, which is the critical flexible mode for ride quality under consideration.
- The limited bandwidth of the conventional actuators (e.g hydraulic actuator) for suspension control.
- The real vehicle body structure is much more complex than a simple beam. The elastic modes include vertical, horizontal bending mode, torsional and diagonal distortion mode (Popprath et al. [July 2006]).

7.2 Structure of decentralized control

The structure of a decentralized control for a regulation problem is shown in Figure 7.1 (Skogestad and Postletwaite [2005]). $G(s)$ is the plant model, which includes the rigid modes and the first two flexible vertical modes of the vehicle body. $G(s)$ is also called the full model in the following

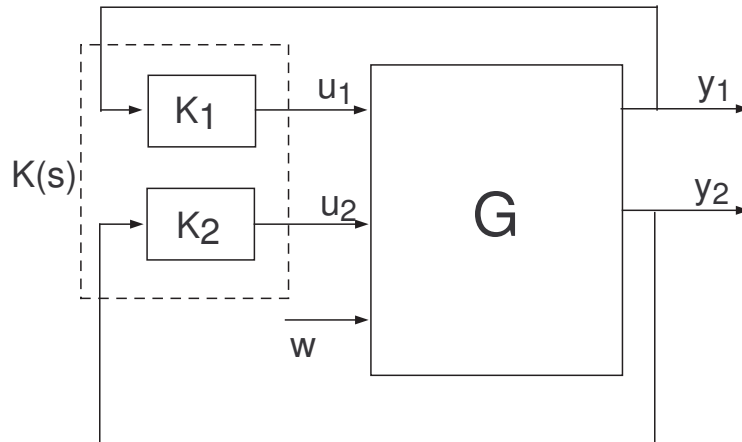


Figure 7.1: Structure of the decentralized control

sections. \mathbf{w} is the vector of exogenous inputs. $K_1(s)$ and $K_2(s)$ are two independent feedback controllers. \mathbf{y}_1 and \mathbf{u}_1 , and \mathbf{y}_2 and \mathbf{u}_2 are the two pairs of measurement outputs and control inputs for $K_1(s)$ and $K_2(s)$ respectively.

The control inputs of the system are chosen as :

\mathbf{u}_1 -piezoelectric actuator control inputs

\mathbf{u}_2 -suspension control inputs.

The measurement outputs are chosen as :

\mathbf{y}_1 -measurements by the piezoelectric strain sensors

\mathbf{y}_2 -accelerations of the vehicle body by conventional accelerometers.

Practically the controllers $K_1(s)$ and $K_2(s)$ can either be designed independently based on the corresponding decoupled parts of $G(s)$, or they can be designed sequentially, i.e. firstly design $K_1(s)$, then design $K_2(s)$ with the previously designed $K_1(s)$ implemented. The independent design is preferred when the system is decoupled in space ($G(s)$ is close to diagonal) while the sequential design is preferred when the system is decoupled in time. In this chapter, controllers $K_1(s)$ and $K_2(s)$ are to be designed independently.

7.3 Control design

Two combinations of control methods are applied: 1. $K_1(s)$ is designed with LQG control method, and $K_2(s)$ is designed with the approach of modal control with skyhook damping; 2. both $K_1(s)$ and $K_2(s)$ are designed with LQG control method.

Four actuator and sensor placement configurations (Figure 5.14) will be investigated. It should be noted that, on one common mounting position as shown in Figure 5.14, twenty piezo stack actuators are placed in parallel in order to produce the necessary moments.

7.3.1 Active structural damping (design of K_1)

Piezoelectric actuators will only influence the flexible modes and the piezoelectric sensors measure only the motion of the flexible modes. Therefore, the sub-controller $K_1(s)$ can be designed independently and only a model of the flexible modes of the flexible vehicle body is necessary for control design of $K_1(s)$. The control system is of the structure shown by Figure 7.2. $G_1(s)$ is the design model.

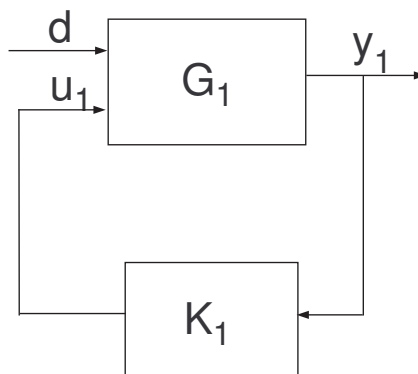


Figure 7.2: Control system for design of $K_1(s)$

The state-space representation of the design model, $G_1(s)$, is given as follows

$$\dot{\mathbf{x}}_f = \mathbf{A}_f \mathbf{x}_f + \mathbf{B}_{f1} \mathbf{u}_1 + \mathbf{B}_{f2} \mathbf{d} \quad (7.1)$$

$$\mathbf{y}_1 = \mathbf{C}_v \mathbf{x}_f \quad (7.2)$$

$$\mathbf{y}_f = \mathbf{C}_2 \mathbf{x}_f + \mathbf{D}_{12} \mathbf{u}_1 + \mathbf{D}_{22} \mathbf{d} \quad (7.3)$$

where \mathbf{A}_f is the $(n \times n)$ system matrix, where n is the number of states. \mathbf{B}_{f1} is the $(n \times 2)$ disturbance input matrix, \mathbf{B}_{f2} is the $(n \times n_p)$ input matrix, \mathbf{C}_v is the $(m_p \times n)$ measurement output matrix. \mathbf{u}_1 is the $(n_p \times 1)$ vector of control signals (from the piezoelectric actuators), \mathbf{d} is the (2×1) vector of disturbances (from secondary suspensions), \mathbf{y}_1 is the $(m_p \times 1)$ vector of measured variables (by piezoelectric sensors), \mathbf{y}_f is the vector of controlled variables.

Configuration 1 For configuration 1, The first two flexible modal coordinates and the first derivative of the modal coordinates are included as the states of the state-space model of G_1 .

$$\mathbf{x}_f = \begin{bmatrix} \dot{q}_1 & q_1 & \dot{q}_2 & q_2 \end{bmatrix}^T \quad (7.4)$$

The system matrix \mathbf{A}_f , the voltage input matrix \mathbf{B}_{f1} , the disturbance input matrix \mathbf{B}_{f2} and the measurement output matrix \mathbf{C}_v are in the following form:

$$\mathbf{A}_f = \begin{bmatrix} -2\zeta_1\omega_1 & -\omega_1^2 & 0 & 0 \\ 1 & 0 & 0 & 0 \\ 0 & 0 & -2\zeta_2\omega_2 & -\omega_2^2 \\ 0 & 0 & 1 & 0 \end{bmatrix} \quad (7.5)$$

$$\mathbf{B}_{f1} = \frac{K_a}{M_v} \begin{bmatrix} \Psi_{a11} & \Psi_{a12} & \Psi_{a13} \\ 0 & 0 & 0 \\ \Psi_{a21} & \Psi_{a22} & \Psi_{a23} \\ 0 & 0 & 0 \end{bmatrix} \quad (7.6)$$

$$\mathbf{B}_{f2} = \begin{bmatrix} \frac{\phi_1(x_L)}{M_v} & \frac{\phi_1(x_R)}{M_v} \\ 0 & 0 \\ \frac{\phi_2(x_L)}{M_v} & \frac{\phi_2(x_R)}{M_v} \\ 0 & 0 \end{bmatrix} \quad (7.7)$$

$$\mathbf{C}_v = \frac{K_s}{C_p} \begin{bmatrix} 0 & \Psi_{s1}(x_C) & 0 & \Psi_{s2}(x_C) \\ 0 & \Psi_{s1}(x_L) & 0 & \Psi_{s2}(x_L) \\ 0 & \Psi_{s1}(x_R) & 0 & \Psi_{s2}(x_R) \end{bmatrix} \quad (7.8)$$

Configurations 2 For configurations 2,3 and 4, piezoelectric actuators and sensors are placed at the centre of the vehicle for controlling the first flexible modes. The design model G_1 contains only the first flexible mode. The state vector is written as

$$\mathbf{x}_f = \begin{bmatrix} \dot{q}_1 & q_1 \end{bmatrix}^T \quad (7.9)$$

The system matrix and the disturbance input matrix are in the following form:

$$\mathbf{A}_f = \begin{bmatrix} -2\zeta_1 w_1 & -w_1^2 \\ 1 & 0 \end{bmatrix} \quad (7.10)$$

$$\mathbf{B}_{f2} = \begin{bmatrix} \frac{\phi_1(x_L)}{M_v} & \frac{\phi_1(x_R)}{M_v} \\ 0 & 0 \end{bmatrix} \quad (7.11)$$

The voltage input matrix and the measurement output matrix are as follows

$$\mathbf{B}_{f1} = \frac{K_a}{M_v} \begin{bmatrix} \Psi_{a11} \\ 0 \end{bmatrix} \quad (7.12)$$

$$\mathbf{C}_v = \frac{K_s}{C_p} \begin{bmatrix} 0 & \Psi_{s11} \end{bmatrix} \quad (7.13)$$

Configuration 3 There are three actuators and one sensor placed at the centre of the beam (railway vehicle body). For the state-space representation of the design model of G_1 , the state vector \mathbf{x}_f , the system matrix \mathbf{A}_f , the disturbance input matrix \mathbf{B}_{f2} and the measurement output matrix \mathbf{C}_v are in the same form as given for configuration 2. The input matrix \mathbf{B}_{f1} is as

follows

$$\mathbf{B}_{f1} = \frac{K_a}{M_v} \begin{bmatrix} \Psi_{a11} & \Psi_{a12} & \Psi_{a13} \\ 0 & 0 & 0 \end{bmatrix} \quad (7.14)$$

Configuration 4 There are three actuators and three sensor placed at the centre of the beam (railway vehicle body). For the state-space model of $G_1(s)$, the state vector \mathbf{x}_f , system matrix \mathbf{A}_f and the disturbance input matrix \mathbf{B}_{f2} are in the same form as given for configuration 2. The input matrix \mathbf{B}_{f1} is in the same form as given for configuration 3. The measurement output matrix is as follows

$$\mathbf{C}_v = \frac{K_s}{C_p} \begin{bmatrix} 0 & \Psi_{s11} \\ 0 & \Psi_{s12} \\ 0 & \Psi_{s13} \end{bmatrix} \quad (7.15)$$

Control design

The aim of the control design is minimizing the accelerations of flexible motion at the chosen performance positions, thereby improving the passenger ride quality of the vehicle. In other words, it is aimed to increase the damping ratio of the flexible modes. Though the approach of pole placement is straightforward to increase the damping ratios of the flexible modes, it is hard to control the control inputs. Therefore, LQG control method is adopted to design $K_1(s)$. Preliminaries on LQG control have been given in section 6.2.1.

The performance positions are chosen as the centre of the vehicle, x_C , position of left suspension, x_L , and position of the right suspension, x_R .

Accelerations of the flexible modes are chosen as the controlled variables. For configuration 1 the vector of controlled variables is given by

$$\mathbf{y}_f = \begin{bmatrix} \phi_1(x_C)\ddot{q}_1 + \phi_2(x_C)\ddot{q}_2 \\ \phi_1(x_L)\ddot{q}_1 + \phi_2(x_L)\ddot{q}_2 \\ \phi_1(x_R)\ddot{q}_1 + \phi_2(x_R)\ddot{q}_2 \end{bmatrix} \quad (7.16)$$

and for configuration 2,3,4, the vector of controlled variables is given by

$$\mathbf{y}_f = \phi_1(x_C)\ddot{q}_1 \quad (7.17)$$

The cost function is given as the following

$$J = \lim_{T \rightarrow \infty} E \left\{ \int_0^T [\mathbf{y}_f(t)^T \mathbf{Q}_y \mathbf{y}_f(t) + \mathbf{u}(t)^T \mathbf{R}_0 \mathbf{u}(t)] \right\} \quad (7.18)$$

where \mathbf{R}_0 is the input weighting matrix and its elements are fixed at 1. \mathbf{Q}_y is the output weighting matrix and are written in the form as follows for the four configurations:

for configuration 1

$$\mathbf{Q}_y = \text{diag}\{1/(q_{y1})^2, 1/(q_{y2})^2, 1/(q_{y3})^2\} \quad (7.19)$$

and for configuration 2,3,4

$$\mathbf{Q}_y = 1/(q_{y1})^2 \quad (7.20)$$

where q_1 , q_2 and q_3 are usually initially chosen as the expected values of the controlled variables and further tuned accordingly to achieve the best performance while maintaining the input voltages of the piezoelectric actuators within their limits.

Kalman filter is designed to estimate the states of the system. The system is subject to disturbances from the secondary suspensions \mathbf{d} . The variance of the disturbance obtained from the simulation results of the passive system of the railway system

$$\mathbf{W} = \text{diag}\{2.5 \times 10^{-4}, 2.5 \times 10^{-4}\} \quad (7.21)$$

The piezoelectric sensor patches measure the strain in the beam by feeding

back voltage signals. For configurations 1 and 4,

$$\mathbf{y}_1 = \begin{bmatrix} v_{s1} \\ v_{s2} \\ v_{s3} \end{bmatrix} \quad (7.22)$$

and for configurations 2 and 3,

$$\mathbf{y}_1 = \begin{bmatrix} v_{s1} \end{bmatrix} \quad (7.23)$$

The measurement noise is assumed to have an RMS value of one percent of the maximum value measured by the sensors. However the variance of the measurement noise is further tuned until the estimator can provide a good performance for the system. For configurations 1 and 4

$$\mathbf{V} = \text{diag}\{1 \times 10^{-18}, 1 \times 10^{-18}, 1 \times 10^{-18}\} \quad (7.24)$$

and for configurations 2 and 3

$$\mathbf{V} = \text{diag}\{1 \times 10^{-18}\} \quad (7.25)$$

Very small value have been chosen for \mathbf{V} , which implies that the sensors are almost perfect. This will cause potential robustness problems in practice.

Results and discussion

In the following, it is going to examine the closed-loop of the railway vehicle system $G(s)$ with the LQG controller $K_1(s)$.

The eigenvalues and modal damping ratios ξ_i for the controlled flexible modes are tabulated in Table 7.1. Damping ratio of the first two flexible modes of the passive system are $\xi_1 = 0.05$ and $\xi_2 = 0.051$. It shows that the damping ratios have been effectively increased by the controller.

Table 7.2 tabulates the RMS acceleration levels at the centre (x_C), left (x_L) and right (x_R) of the vehicle, the RMS suspension deflection values at left (x_L) and right (x_R) of the vehicle, and the RMS voltage input levels

7.3. CONTROL DESIGN

Table 7.1: Eigenvalues and damping ratios of the first two flexible modes of system $(G + K_1)$

config.	Eigenmode	eigenvalues	ξ_i	ω_i (Hz)
1	1 st flexible mode	$-9 \pm 53.4i$	0.166	8.83
	2 nd flexible mode	$-16.6 \pm 146i$	0.122	23.4
2	1 st flexible mode	$-4.78 \pm 53i$	0.0898	8.47
3	1 st flexible mode	$-23.7 \pm 57.8i$	0.3800	9.95
4	1 st flexible mode	$-16 \pm 55.1i$	0.279	9.14

of the piezoelectric actuators. They are optimum values found by varying the parameters (weights Q) for the LQG controller while keeping the voltage inputs to the piezoelectric actuators within the required range (i.e. 1000V).

Comparing the RMS results of configuration 1 and configuration 2, there is improvements only in the centre accelerations. This is due to the fact that the second flexible mode has little effect on the ride quality of the railway vehicle. Configuration 3 and 4 give almost the same lowest ride accelerations, but configuration 3 uses fewer sensors and achieves higher damping ratio for the first flexible mode. Therefore configuration 3 is considered the best based on the above

Table 7.2: RMS results for system $(G + K_1)$

conf.	Vertical Acc. (%g)			Susp. Def. (mm)		Piezo Act. Voltages (volts)		
	centre	left	right	left	right	A1	A2	A3
1	2.24	2.82	3.53	7.80	11.35	270.09	179.16	178.99
2	2.49	2.89	3.6	7.80	11.35	284.11	-	-
3	2.03	2.77	3.48	7.80	11.35	283.40	283.38	283.38
4	2.02	2.77	3.47	7.80	11.35	292.02	291.99	291.99

Figure 7.3,7.4 and 7.5 give power spectral densities (PSDs) for the centre (x_C), left (x_L) and right (x_R) accelerations of the railway vehicle with respect to random track disturbances. They show significant reductions of the accelerations in the first flexible mode region of 8.5Hz. Figure 7.6 is the piezoelectric actuator input voltage for configuration 3. It shows that the voltages are within the required range (i.e.1000V).

7.3. CONTROL DESIGN

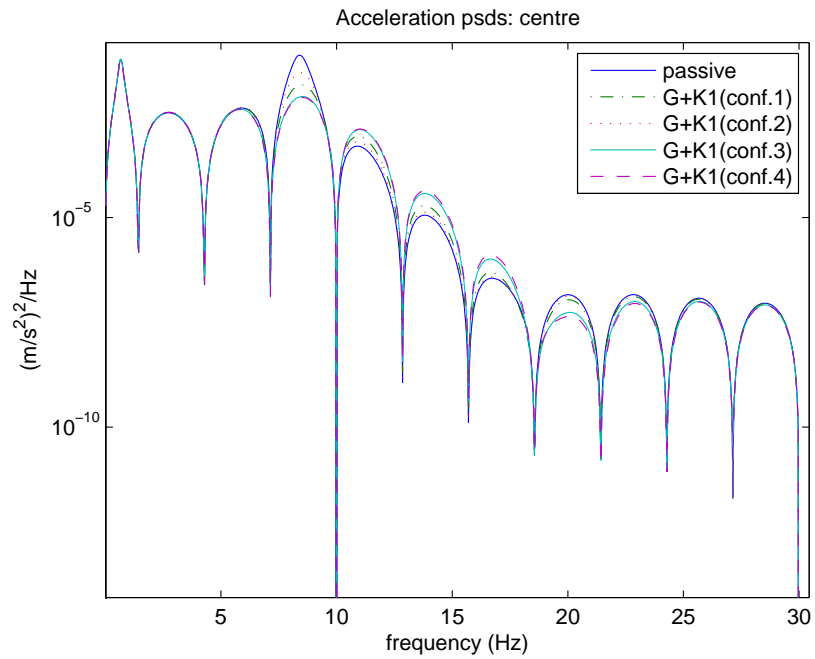


Figure 7.3: Closed-loop system with controller K_1 : centre acceleration PSDs

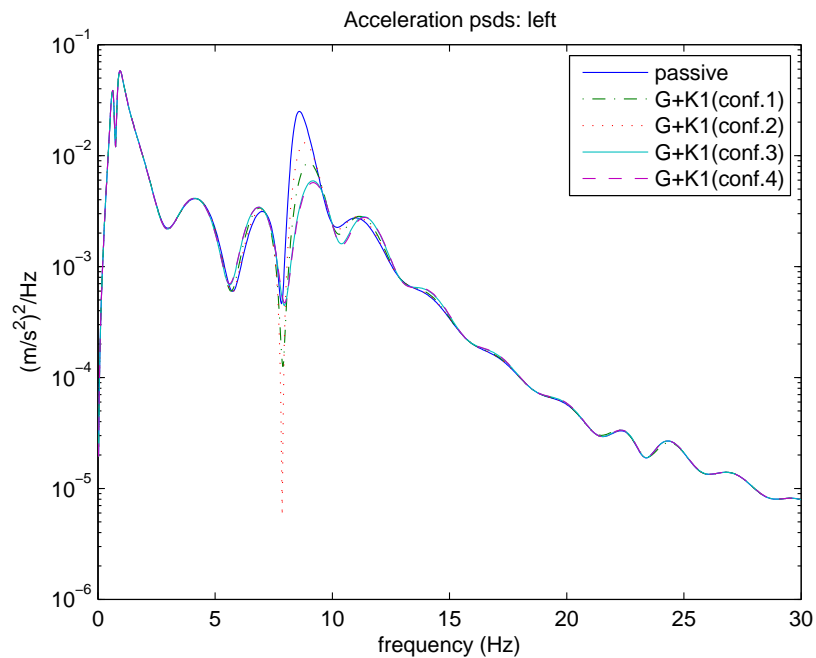


Figure 7.4: Closed-loop system with controller K_1 : left acceleration PSDs

7.3. CONTROL DESIGN

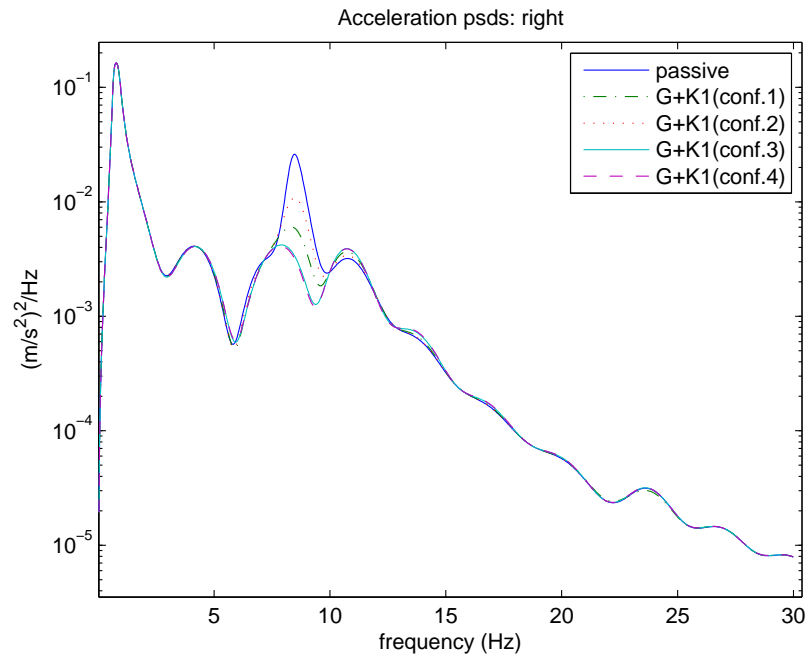


Figure 7.5: Closed-loop system with controller K_1 : right acceleration PSDs

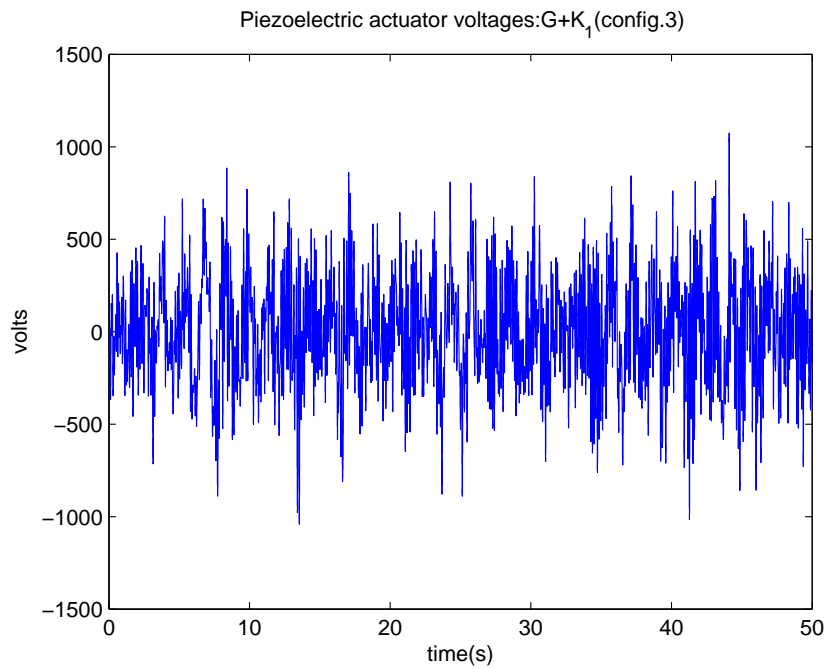


Figure 7.6: Piezoelectric actuator input voltages (configuration 3)

7.3.2 Active suspension control (design of K_2)

The structure of the control system is shown by Figure 7.7. $G(s)$ is the design

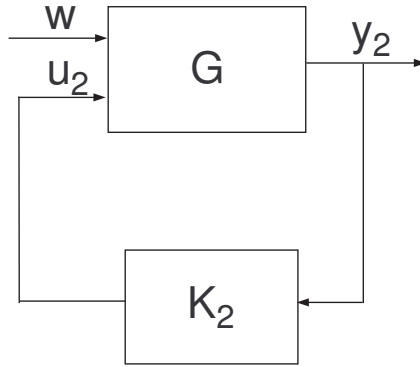


Figure 7.7: Control system for design of $K_2(s)$

model used for designing controller $K_2(s)$. \mathbf{y}_2 is the $m \times 1$ vector of measured variables, \mathbf{u}_2 is the 2×1 vector of control signals

$$\mathbf{w} = \begin{bmatrix} U_L \\ U_R \end{bmatrix} \quad (7.26)$$

where U_L and U_R are left and right suspension control forces respectively. And \mathbf{w} is the 2 vector of track disturbances.

$$\mathbf{w} = \begin{bmatrix} \dot{Z}_{0L} \\ \dot{Z}_{0R} \end{bmatrix} \quad (7.27)$$

Chapter 6 has described the design of the active suspension controller. Two approaches, modal control with skyhook damping and LQG control have been adopted, the resulting controllers are denoted as K_{sky} for modal controller with skyhook damping, K_{rLQG} for LQG controller designed with rigid model and K_{LQG} for LQG controller designed with the model including flexibilities.

7.4 Combined active damping and active suspension control

Previous section described the design of controllers K_1 and K_2 (Figure 7.1). Now it is to examine the performance of the system closed with the combined controller ($K_1 + K_2$) of active damping with piezoelectric actuators and sensors (K_1) and active suspension control(K_2).

7.4.1 $K_1 + K_{sky}$

Table 7.3 tabulates the RMS results of the closed-loop system with the overall controller K_1+K_{sky} ($c_1 = 12 \times 10^4$ and $c_2 = 2$) for the four configurations. The accelerations of the vehicle body are effectively reduced. Configuration 3 and 4 give the better performance.

Table 7.3: RMS results for system ($G + K_1 + K_{sky}$):

conf.	Vertical Acc. (%g)			Susp. Def. (mm)		susp. forces (kN)		Piezo Act.Voltages (volts)		
	centre	left	right	left	right	left	right	A1	A2	A3
1	1.65	1.55	1.54	11.66	7.09	3.74	2.69	212.73	141.03	141.06
2	1.87	1.61	1.65	11.66	7.09	3.74	2.70	209.71	-	-
3	1.46	1.48	1.46	11.66	7.09	3.74	2.68	219.95	219.93	219.93
4	1.44	1.48	1.45	11.66	7.09	3.74	2.68	228.24	228.22	228.22

Table 7.4 compare the results between systems $G + K_1$, $G + K_{sky}$ and $G + K_1 + K_{sky}$. Figure 7.8, 7.9 and 7.10 compares the power spectral densities of systems $G + K_1$ (config.3), $G + K_{sky}$ and $G + K_1 + K_{sky}$ (config.3). Both the RMS results and the PSDs show that controller K_{a1} for active structural damping and secondary suspension controller K_{sky} work in a complementary manner to each other to suppress the flexible modes and the rigid modes respectively.

7.4.2 $K_1 + K_{rLQG}$

Table 7.5 tabulates the RMS results for the closed-loop system $G + K_1 + K_{rLQG}$. It is shown that the vibration of the vehicle body is well suppressed.

7.4. COMBINED ACTIVE DAMPING AND ACTIVE SUSPENSION CONTROL

Table 7.4: RMS results: comparison between $G + K_1$ (config.3), $G + K_{sky}$ and $G + K_1 + K_{sky}$ (config.3)

Sys.	Vert. Acc. (%g)			Susp. Def. (mm)		susp. forces (kN)		Piezo Act. Voltages (volts)		
	centre	left	right	left	right	left	right	A1	A2	A3
$G + K_1$	2.04	2.77	3.47	7.80	11.35	-	-	281.95	281.95	281.92
$G + K_{sky}$	2.19	1.76	1.83	11.09	6.76	3.52	2.56	-	-	-
$G + K_1 + K_{sky}$	1.46	1.48	1.46	11.66	7.09	3.74	2.68	219.95	219.93	219.93

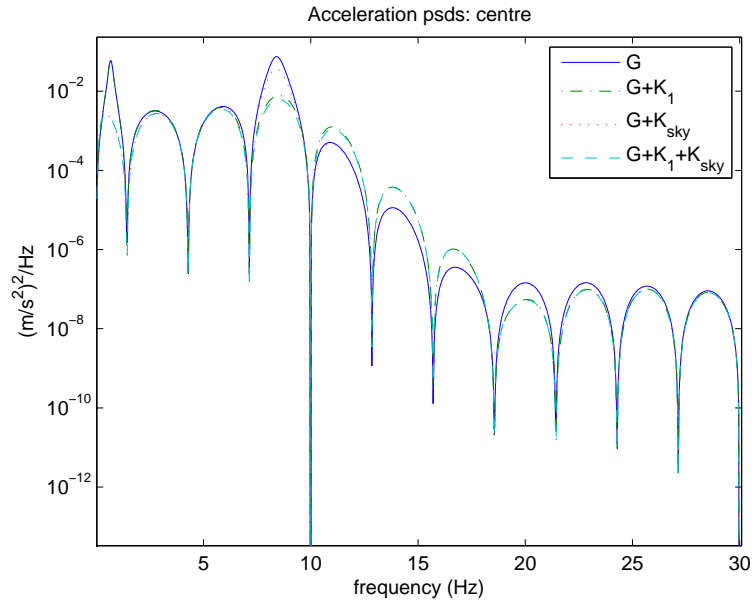


Figure 7.8: comparison between $G + K_1$ (config.3), $G + K_{sky}$ and $G + K_1 + K_{sky}$ (config.3) : centre acceleration PSDs

7.4. COMBINED ACTIVE DAMPING AND ACTIVE SUSPENSION CONTROL

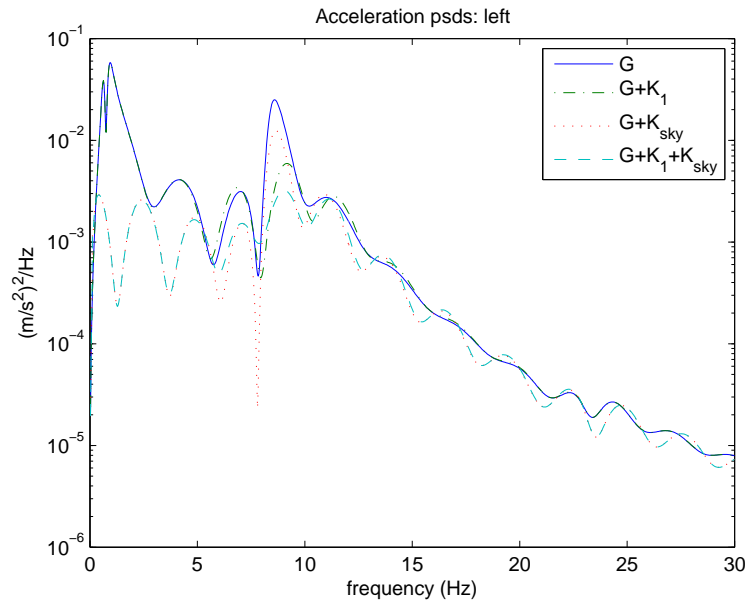


Figure 7.9: comparison between $G+K_1$ (config.3), $G+K_{sky}$ and $G+K_1+K_{sky}$ (config.3): left acceleration PSDs

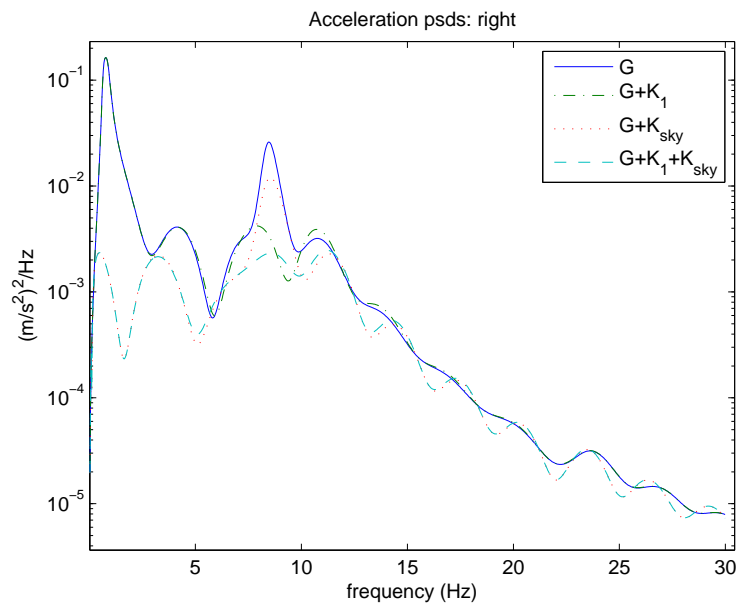


Figure 7.10: comparison between $G+K_1$ (config.3), $G+K_{sky}$ and $G+K_1+K_{sky}$ (config.3): right acceleration PSDs

7.4. COMBINED ACTIVE DAMPING AND ACTIVE SUSPENSION CONTROL

The RMS levels of the acceleration and suspension deflections achieved with the four actuator and sensor placement configurations are nearly the same, which is the best that can be achieved.

Table 7.5: RMS results for system $(G + K_1 + K_{rLQG})$:

config.	Vertical Acc. (%g)			Susp. Def. (mm)		susp. forces (kN)		Piezo Act.Voltages (volts)		
	centre	left	right	left	right	left	right	A1	A2	A3
1	0.36	0.51	0.54	10.27	10.70	3.82	3.97	99.29	66.21	66.02
2	0.37	0.52	0.55	10.27	10.70	3.82	3.97	144.04	-	-
3	0.37	0.52	0.55	10.28	10.70	3.82	3.97	48.22	48.22	48.22
4	0.37	0.52	0.54	10.27	10.70	3.82	3.97	58.77	58.76	58.76

Table 7.6 compare the results between the closed-loop systems $G + K_1$, $G + K_{rLQG}$ and $G + K_1 + K_{rLQG}$. It is found the decentralized controller $K_1 + K_{rLQG}$ give the lowest RMS accelerations levels.

Table 7.6: RMS results: comparison between $G + K_1$ (config.3), $G + K_{rLQG}$ and $G + K_1 + K_{rLQG}$ (config.3)

Sys.	Vert. Acce. (%g)			Susp. Def. (mm)		susp. forces (kN)		Piezo Actu.Voltages (volts)		
	centre	left	right	left	right	left	right	A1	A2	A3
$G + K_1$	2.04	2.77	3.47	7.80	11.35	-	-	281.95	281.95	281.92
$G + K_{rLQG}$	0.46	0.53	0.57	10.27	10.70	3.82	3.97	-	-	-
$G + K_1 + K_{rLQG}$	0.37	0.52	0.55	10.28	10.70	3.82	3.97	48.22	48.22	48.22

Figure 7.11, 7.12 and 7.13 compare between the power spectral densities of systems $G + K_1$ (config.3), $G + K_{rLQG}$ and $G + K_1 + K_{rLQG}$ (config.3). It is clearly found that the suspension controller K_{rLQG} , designed with the rigid model, is able to influence both the rigid modes and the flexible modes. The rigid modes have been sufficiently reduced, but its ability in reducing the flexible modes is limited. Controller K_1 only influences the flexible modes. Subsequently, the combined controller $K_1 + K_{rLQG}$, K_1 works in complementary to K_{rLQG} and a satisfactory performance in suppressing both the rigid and flexible modes is achieved.

Figure 7.14 shows the acceleration step responses of system $G + K_1 + K_{rLQG}$ (config.3). High frequency oscillation has been eliminated. It also proves that the flexible modes are well suppressed.

7.4. COMBINED ACTIVE DAMPING AND ACTIVE SUSPENSION CONTROL

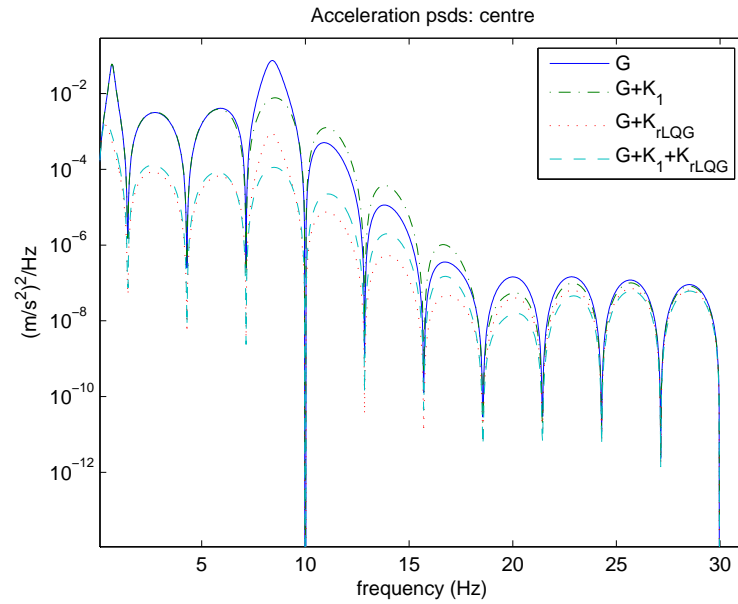


Figure 7.11: comparison between $G + K_1$ (config.3), $G + K_{rLQG}$ and $G + K_1 + K_{rLQG}$ (config.3): centre acceleration PSDs

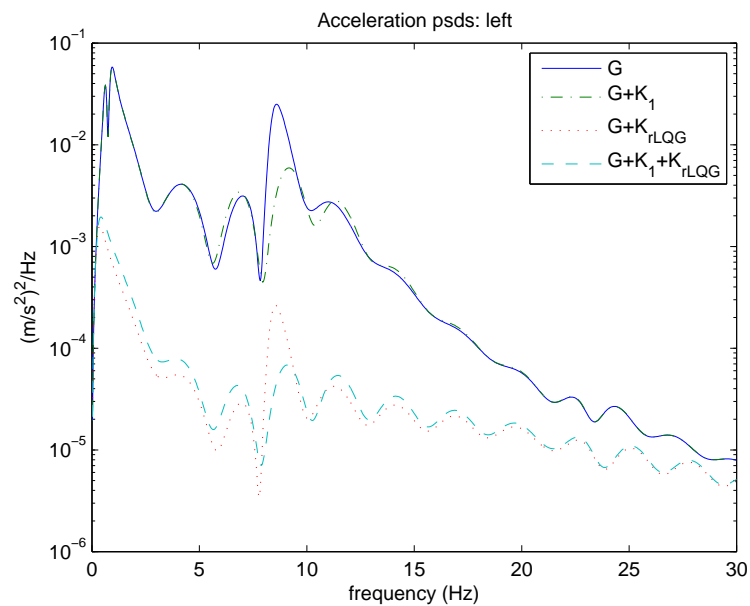


Figure 7.12: comparison between $G + K_1$ (config.3), $G + K_{rLQG}$ and $G + K_1 + K_{rLQG}$ (config.3): left acceleration PSDs

7.4. COMBINED ACTIVE DAMPING AND ACTIVE SUSPENSION CONTROL

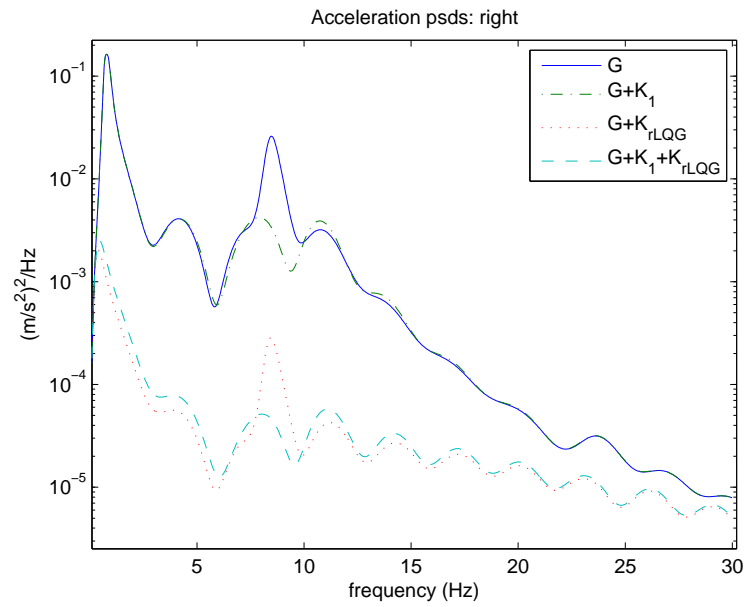


Figure 7.13: comparison between $G + K_1$ (config.3), $G + K_{rLQG}$ and $G + K_1 + K_{rLQG}$ (config.3): right acceleration PSDs

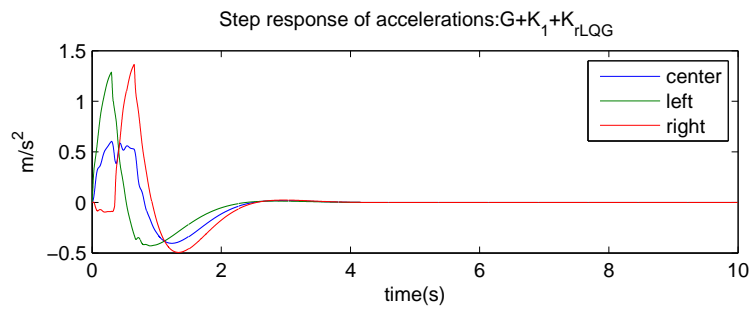


Figure 7.14: Acceleration step responses of system $G + K_1 + K_{rLQG}$ (config.3)

7.4.3 $K_1 + K_{LQG}$

K_{LQG} is the suspension controller designed with the model including flexibilities. RMS results of system $G + K_{LQG}$ and $G + K_1 + K_{LQG}$ (config.3) are tabulated in Table 7.7. Controller $K_1 + K_{LQG}$ provides little further improvement in ride quality compared with controller K_{LQG} , because both the rigid modes and flexible modes have already been well suppressed by controller K_{LQG} . In consequence, the voltage inputs to the piezoelectric actuators for system $G + K_1 + K_{LQG}$ are much smaller than the voltage inputs for system $G + K_1$. Figure 7.15,7.16 and 7.17 are acceleration PSDs of systems $G + K_1$, $G + K_{LQG}$ and $G + K_1 + K_{LQG}$.

Table 7.7: RMS results: comparison between $G + K_{LQG}$ and $G + K_1 + K_{LQG}$ (config.3)

Sys.	Vert. Acce. (%g)			Susp. Def. (mm)		Susp. forces (kN)		Piezo Actu.Voltages (volts)		
	centre	left	right	left	right	left	right	A1	A2	A3
$G + K_{LQG}$	0.36	0.50	0.54	10.33	10.79	3.87	4.02	-	-	-
$G + K_1 + K_{LQG}$	0.35	0.51	0.54	10.34	10.79	3.87	4.02	33.90	33.89	33.89

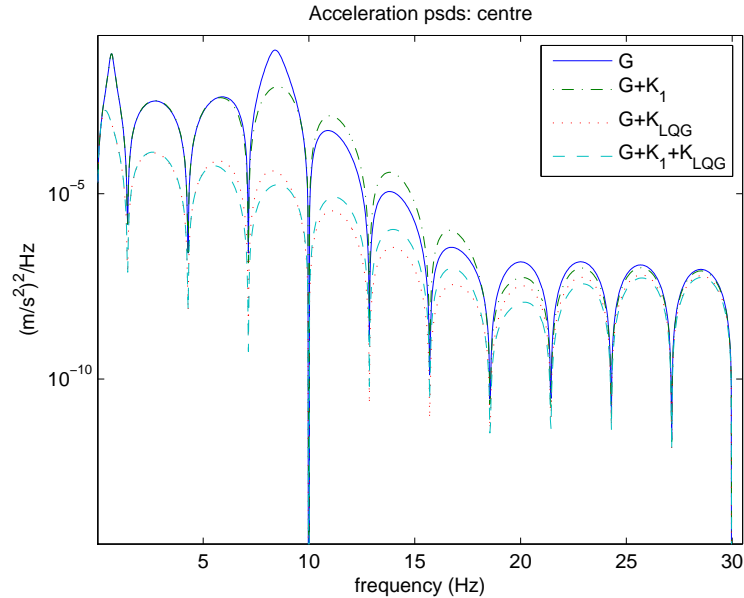


Figure 7.15: comparison between $G + K_1$ (config.3), $G + K_{LQG}$ and $G + K_1 + K_{LQG}$ (config.3): centre acceleration PSDs

7.4. COMBINED ACTIVE DAMPING AND ACTIVE SUSPENSION CONTROL

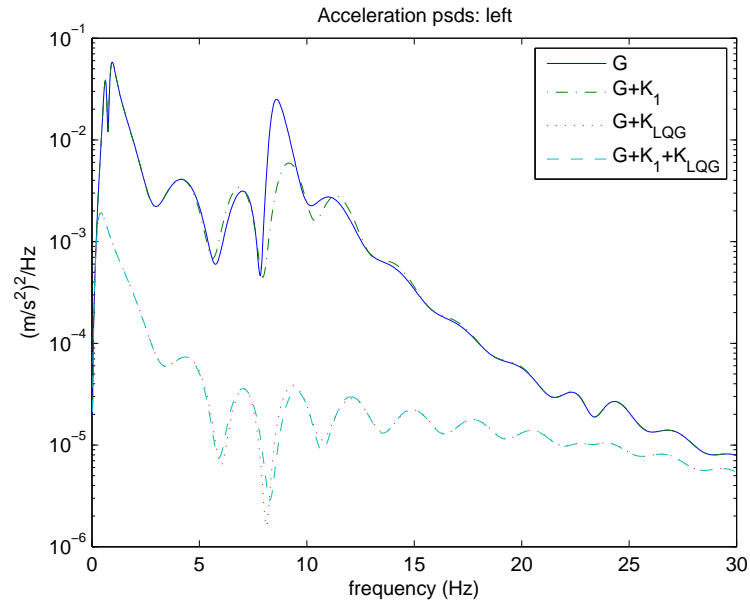


Figure 7.16: comparison between $G + K_1$ (config.3), $G + K_{LQG}$ and $G + K_1 + K_{LQG}$ (config.3): left acceleration PSDs

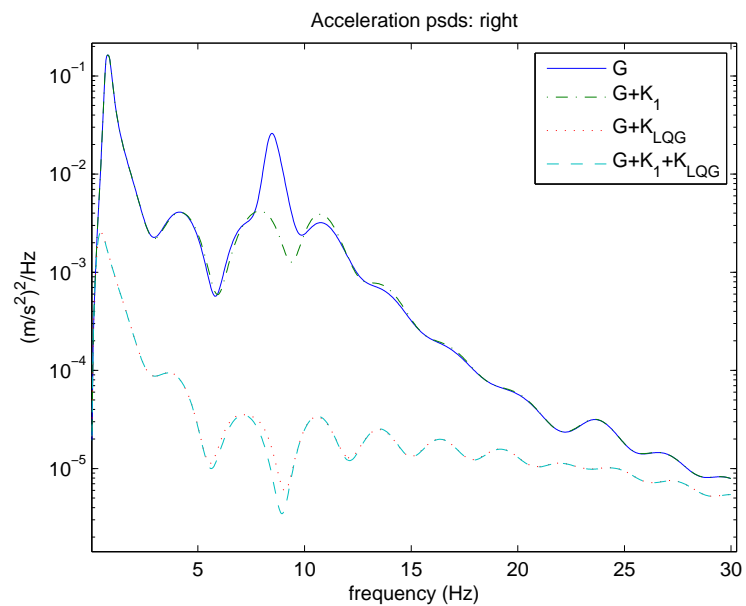


Figure 7.17: comparison between $G + K_1$ (config.3), $G + K_{LQG}$ and $G + K_1 + K_{LQG}$ (config.3): right acceleration PSDs

7.5 Summary

The control strategy of decentralized control has been successfully adopted for vibration control of the flexible-bodied railway vehicle.

The controller for active structural damping with piezoelectric actuators and sensors and the controller for active suspension control are designed independently for vibration suppression of the vehicle body. The couplings between the flexible motions and the rigid motions are neglected when the decoupled models are used for the design of the two sub controllers.

The second flexible mode has little effect on ride quality of the railway vehicle and hence is negligible. Four configurations of piezoelectric actuator and sensor placement have been investigated. Configuration 3 and 4 achieves better performances than configuration 1 and 2. Configuration 3 uses only one sensor so it would be considered the best for practice. The damping ratios of the flexible modes are effectively increased by controller K_1 . The results show that the two sub controllers (K_1 and K_2) are able to work in complementary manner to each other in achieving a satisfactory ride quality for the railway vehicle under consideration.

Chapter 8

Control Design II: Centralized Control

This chapter describes the centralized control strategy for vibration control of the flexible bodied railway vehicle. The control inputs consist of suspension control inputs and control inputs for active structural damping by piezoelectric actuators. The full model of the system is used for control design, which includes the rigid modes and flexible modes of the vehicle body and the coupling terms of the flexible and rigid modes. Three control methods will be considered : \mathcal{H}_2 optimal control, \mathcal{H}_∞ control and finally model predictive control technology based on mixed $\mathcal{H}_2/\mathcal{H}_\infty$ control approach.

8.1 Structure of centralized control

The structure of the centralized control strategy is shown in Figure 8.1, The full model $G(s)$ is used as design model. In state-space form, it is represented as follows

$$\dot{\mathbf{x}} = \mathbf{A}\mathbf{x} + \mathbf{B}_1\boldsymbol{\omega} + \mathbf{B}_2\mathbf{u} \quad (8.1)$$

$$(8.2)$$

8.1. STRUCTURE OF CENTRALIZED CONTROL

where the state vector \mathbf{x} is chosen as

$$\mathbf{x} = [\dot{Z}_{3C} \quad \dot{\theta} \quad \dot{Z}_{1L} \quad \dot{Z}_{1R} \quad Z_{3L} - Z_{1L} \quad Z_{3R} - Z_{1R} \quad Z_{2L} - Z_{1L} \quad Z_{2R} - Z_{1R} \\ Z_{1L} - Z_{0L} \quad Z_{1R} - Z_{0R} \quad \dot{q}_1 \quad q_1 \quad \dot{q}_2 \quad q_2] \quad (8.3)$$

where \mathbf{A} , \mathbf{B}_1 and \mathbf{B}_2 are the system matrix, track disturbance input matrix and control input matrix respectively.

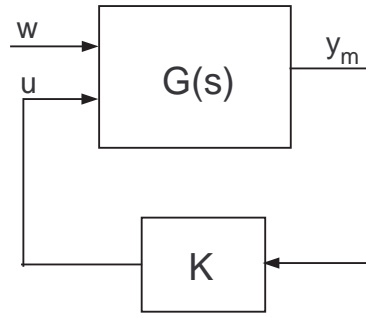


Figure 8.1: Structure of centralized control

$\boldsymbol{\omega}$ is the vector of exogenous inputs, which includes the track disturbances and the measurements noises, \mathbf{y}_m is the vector of measurement outputs. The accelerations of the vehicle body are measured. \mathbf{u} is the vector of control inputs and is as below

$$\mathbf{u} = \begin{bmatrix} \mathbf{u}_1 \\ \mathbf{u}_2 \end{bmatrix} \quad (8.4)$$

where \mathbf{u}_1 is the vector of suspension control inputs and \mathbf{u}_2 is the vector of voltage inputs to the piezoelectric actuators. As it is shown by Figure 8.2, three sets of piezoelectric actuators are placed at the centre of the vehicle body for suppressing the first flexible mode. On one common mounting position, twenty piezoelectric stack actuators are placed in parallel in order to produce the necessary moments. In this chapter, suppressing of the first flexible mode, which is the dominant flexible mode that affects the ride quality is, of the main concern.

$K(s)$ is the centralized controller to be designed. The aim of the control

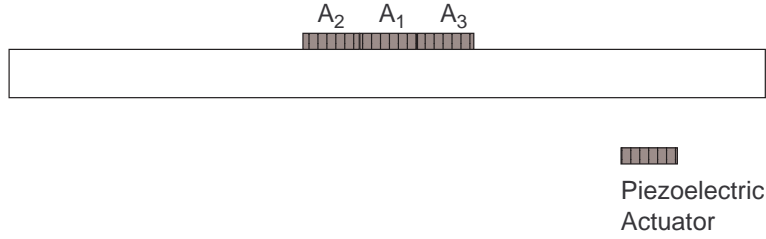


Figure 8.2: Configuration of piezoelectric actuators for centralized control

design is to reduce both the rigid and flexible accelerations of the vehicle body as much as possible while keeping the suspension deflections and the control inputs within the required range for practical reasons. The following sections present the application of several control methods for designing $K(s)$.

8.2 \mathcal{H}_2 and \mathcal{H}_∞ control preliminaries

The $\mathcal{H}_2 / \mathcal{H}_\infty$ optimization problem may be manipulated into the general problem formulation (Skogestad and Postletwaite [2005]). The generalized control configuration is presented by Figure 8.3 and can be described as follows

$$\begin{bmatrix} z \\ \mathbf{y} \end{bmatrix} = P(s) \begin{bmatrix} \mathbf{w} \\ \mathbf{u} \end{bmatrix} = \left[\begin{array}{c|cc} P_{11} & P_{12} \\ \hline P_{21} & P_{22} \end{array} \right] \begin{bmatrix} \mathbf{w} \\ \mathbf{u} \end{bmatrix} \quad (8.5)$$

$$\mathbf{u} = K(s)\mathbf{y}_m \quad (8.6)$$

The signals are: \mathbf{u} the control variables, \mathbf{y}_m the measured variables, \mathbf{w} the exogenous signals such as command signals, disturbances, and measurement noises, and \mathbf{z} the error signals, which are to be minimized to meet the control objectives. The state-space realization of the generalized plant P is given by

$$P = \left[\begin{array}{c|cc} A & B_1 & B_2 \\ \hline C_1 & D_{11} & D_{12} \\ C_2 & D_{21} & D_{22} \end{array} \right] \quad (8.7)$$

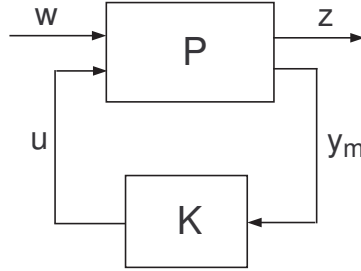


Figure 8.3: General control configuration

and

$$P_{ij}(s) = C_i(sI - A)^{-1}B_j + D_{ij} \quad (8.8)$$

The generalized plant P will include the plant model, the interconnection, and designer-specified weighting functions, which are chosen appropriately according to different control objectives. The closed-loop transfer function from w to z is given by the linear fractional transformation (LFT)

$$z = \mathcal{F}_l(P, K)\omega \quad (8.9)$$

where

$$\mathcal{F}_l(P, K) = P_{11} + P_{12}K(I - P_{22}K)^{-1}P_{21} \quad (8.10)$$

8.3 \mathcal{H}_2 optimal control for vibration control of railway vehicles

The standard \mathcal{H}_2 optimal control problem is to find a stabilizing controller K which minimizes

$$\|F(s)\|_2 = \sqrt{\frac{1}{2\pi} \int_{-\infty}^{\infty} \text{tr}[F(j\omega)F(j\omega)^H]d\omega} \quad (8.11)$$

An important special case of \mathcal{H}_2 optimal control problem is the LQG control problem (Skogestad and Postletwaite [2005]). So the LQG control problem can be cast as an \mathcal{H}_2 optimization problem in the general framework. The

unique optimal \mathcal{H}_2 controller can be found from the solution of two Riccati equations.

8.3.1 Control design with constant weights

Figure 8.4 shows the LQG control problem as a special case of \mathcal{H}_2 control problem with constant weights.

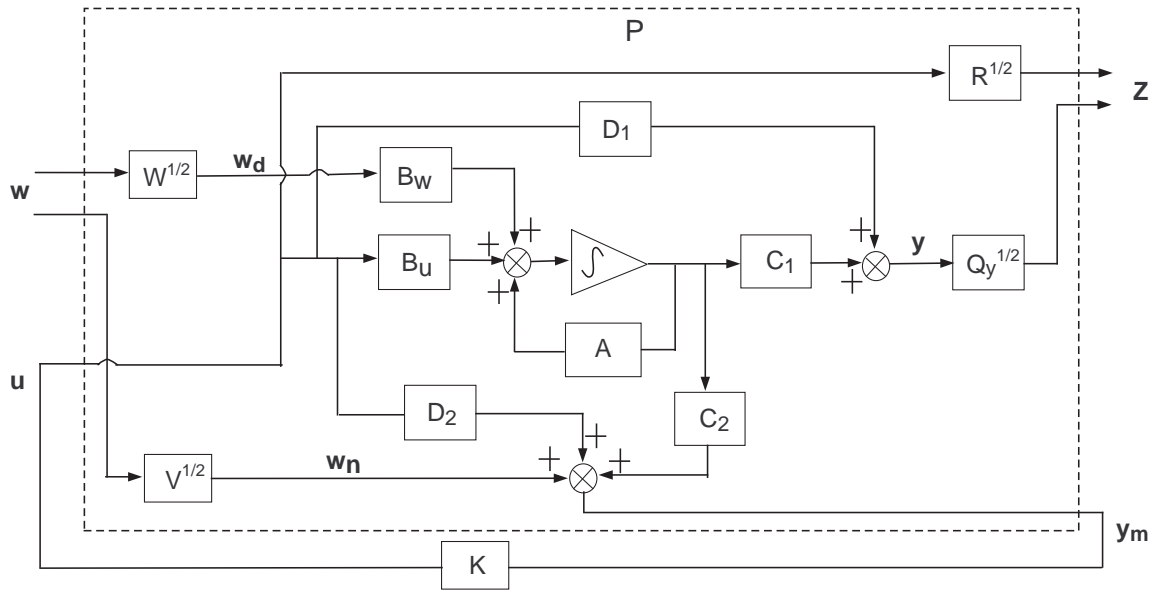


Figure 8.4: The LQG problem formulated in the general control configuration

The generalized plant can be written as

$$P = \left[\begin{array}{c|c} P_{11} & P_{12} \\ \hline P_{21} & P_{22} \end{array} \right] = \left[\begin{array}{c|cc|c} A & \mathbf{W}^{\frac{1}{2}}B_1 & 0 & B_2 \\ \hline \mathbf{Q}^{\frac{1}{2}}C_1 & 0 & 0 & 0 \\ 0 & 0 & 0 & \mathbf{R}^{\frac{1}{2}} \\ \hline C_2 & 0 & \mathbf{V}^{\frac{1}{2}} & D_{22} \end{array} \right] \quad (8.12)$$

where the measurement outputs \mathbf{y}_m are chosen as three accelerations of the vehicle body

$$\mathbf{y}_m = \left[\ddot{z}_{x_L} \quad \ddot{z}_{x_C} \quad \ddot{z}_{x_R} \right]^T \quad (8.13)$$

8.3. \mathcal{H}_2 OPTIMAL CONTROL FOR VIBRATION CONTROL OF RAILWAY VEHICLES

Piezoelectric sensors are not used in the centralized control design strategy. The three accelerations will not only pick up the accelerations of the rigid modes but also the flexibility effect associated with the three points (centre x_C , left x_L and right x_R).

The control input vector \mathbf{u} is given as below

$$\mathbf{u} = \begin{bmatrix} U_L & U_R & V_{a1} & V_{a2} & V_{a3} \end{bmatrix}^T \quad (8.14)$$

where U_L and U_R are the command forces for the secondary suspension actuators, and V_{a1} , V_{a2} and V_{a3} are the voltage inputs to the piezoelectric actuators. Here the actuators are all assumed ideal for controller design.

\mathbf{w}_d the vector of track disturbances, \mathbf{w}_n the vector of measurement noises and \mathbf{w} the vector of white noises of unit intensity are related by

$$\begin{bmatrix} \mathbf{w}_d \\ \mathbf{w}_n \end{bmatrix} = \begin{bmatrix} \mathbf{W}^{\frac{1}{2}} & 0 \\ 0 & \mathbf{V}^{\frac{1}{2}} \end{bmatrix} \mathbf{w} \quad (8.15)$$

where weights \mathbf{W} and \mathbf{V} are the covariances of \mathbf{w}_d and \mathbf{w}_n respectively. They are chosen as (please relate to the principles given in section 6.2.2).

$$\mathbf{W} = \begin{bmatrix} 5.4283 \times 10^{-4} & 0 \\ 0 & 5.4283 \times 10^{-4} \end{bmatrix} \quad (8.16)$$

$$\mathbf{V} = \begin{bmatrix} 1.3323 \times 10^{-5} & 0 & 0 \\ 0 & 1.3323 \times 10^{-5} & 0 \\ 0 & 0 & 1.3323 \times 10^{-5} \end{bmatrix} \quad (8.17)$$

The error signals \mathbf{z} are the weighted regulated variables

$$\mathbf{z} = \begin{bmatrix} \mathbf{Q}_y^{\frac{1}{2}} & 0 \\ 0 & \mathbf{R}^{\frac{1}{2}} \end{bmatrix} \begin{bmatrix} \mathbf{y} \\ \mathbf{u} \end{bmatrix} \quad (8.18)$$

where output variables \mathbf{y}_1 and the control inputs \mathbf{u} are chosen as the regulated variables, i.e. three accelerations of the vehicle body, two

suspension deflections and the five control inputs.

$$\begin{bmatrix} \mathbf{y} \\ \mathbf{u} \end{bmatrix} = \begin{bmatrix} \ddot{Z}_{xL} & \ddot{Z}_{xC} & \ddot{Z}_{xR} & Z_{Ld} & Z_{Rd} & U_L & U_R & V_{a1} & V_{a2} & V_{a3} \end{bmatrix}^T \quad (8.19)$$

\mathbf{Q}_y and \mathbf{R} are symmetric and definite weighting matrices and are tuned for performance and control efforts. For matrix \mathbf{Q}_y , the first three diagonal elements are on the three regulated accelerations of the vehicle body and the other two diagonal elements are on suspension deflections. For matrix \mathbf{R} , the first two diagonal elements are on control efforts from suspension control and the other three diagonal elements are on piezoelectric actuators. Their values have been tuned as follows, with which satisfying results in terms of performance and control efforts are achieved.

$$\mathbf{Q}_y = \text{diag}([50 \ 50 \ 50 \ 83.33 \ 83.33]) \quad (8.20)$$

$$\mathbf{R} = \text{diag}([0.001 \ 0.001 \ 0.0025 \ 0.0025 \ 0.0025]) \quad (8.21)$$

8.3.2 Control design with frequency dependent weights

To account for the limited bandwidth of the real actuators for suspension control and to constrain the control signals from the piezoelectric actuators within the desired frequency range, the case of \mathcal{H}_2 control with constant weights is extended to \mathcal{H}_2 control with dynamic weights.

Figure 8.5 shows the general structure diagram for \mathcal{H}_2 (or \mathcal{H}_∞) control design, where

$$\mathbf{W}_d = \mathbf{W}^{\frac{1}{2}} \quad (8.22)$$

$$\mathbf{W}_n = \mathbf{V}^{\frac{1}{2}} \quad (8.23)$$

the vector of error signals \mathbf{z} is given by

$$\mathbf{z} = \begin{bmatrix} \mathbf{W}_y & 0 \\ 0 & \mathbf{W}_u \end{bmatrix} \begin{bmatrix} \mathbf{y}_1 \\ \mathbf{u} \end{bmatrix} \quad (8.24)$$

8.3. \mathcal{H}_2 OPTIMAL CONTROL FOR VIBRATION CONTROL OF RAILWAY VEHICLES

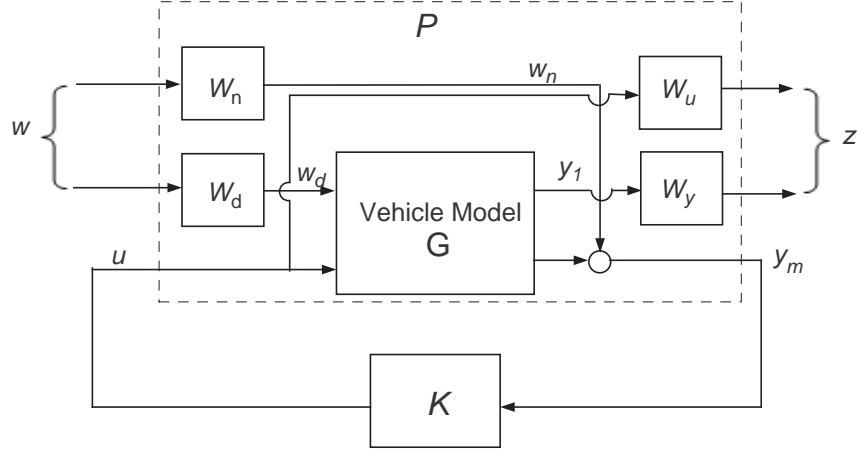


Figure 8.5: Structure diagram of \mathcal{H}_2 (/ \mathcal{H}_∞) control design

where W_u is the frequency dependent weighting matrix on control signals

$$\mathbf{W}_u = \text{diag}([W_{u1} \quad W_{u1} \quad W_{u2} \quad W_{u2} \quad W_{u2}]) \quad (8.25)$$

W_{u1} is the dynamic weight set to give a cut-off frequency around 10Hz as a constraint to account for the dynamics of the hydraulic actuators

$$W_{u1} = k_{u1} \frac{s^2 + 2\xi_{1a}\omega_{1a}s + \omega_{1a}^2}{s^2 + 2\xi_{1b}\omega_{1b}s + \omega_{1b}^2} \quad (8.26)$$

where $\xi_{1a} = 0.7$, $\xi_{1b} = 0.7$, $\omega_{1a} = 4\text{Hz}$, and $\omega_{1b} = 10\text{Hz}$.

W_{u2} is the dynamic weight chosen to reflect the desired frequency content of the control efforts by the piezoelectric actuators.

$$W_{u2} = k_{u2} \frac{s^2 + 2\xi_{2a}\omega_2s + \omega_2^2}{s^2 + 2\xi_{2b}\omega_2s + \omega_2^2} \quad (8.27)$$

where $\xi_{2a} = 0.2$, $\xi_{2b} = 0.7$, and $\omega_2 = 8.45\text{Hz}$. The coefficients k_{u1} and k_{u2} are tuned for the performance in improving the ride quality and control efforts. Satisfying performance have been achieved with $k_{u1} = 0.0045$ and $k_{u2} = 0.001$. Figure 8.6 plots the weights of W_{u1} and W_{u2} . Weight W_{u1} is a high pass filter with a cut-off frequency at 10Hz according to the limited bandwidth of the hydraulic actuator. Weight W_{u2} has decreased magnitude around

8.3. \mathcal{H}_2 OPTIMAL CONTROL FOR VIBRATION CONTROL OF RAILWAY VEHICLES

the frequency of 8.45Hz, which make the control efforts by the piezoelectric actuators more concentrated on the first flexible mode of the vehicle body.

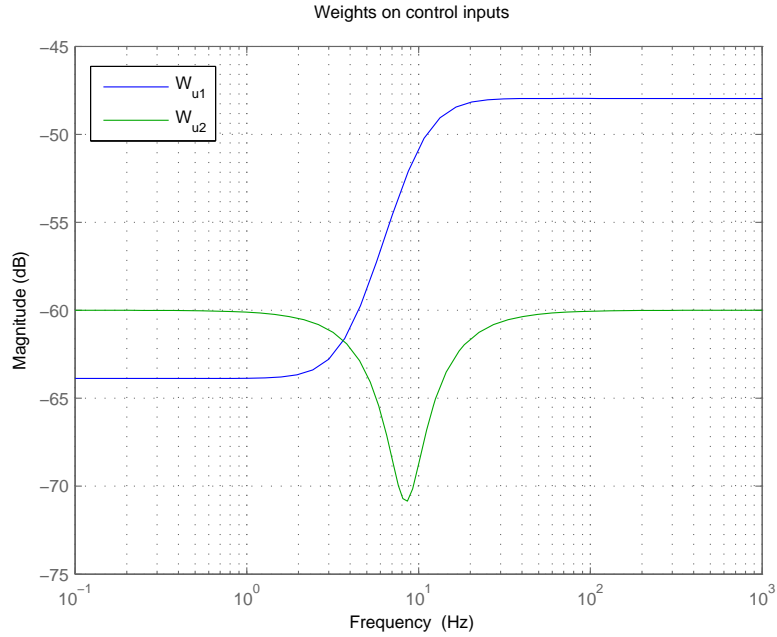


Figure 8.6: Weights on control inputs for \mathcal{H}_2 control with $k_{u1} = 0.004$ and $k_{u2} = 0.001$

8.3.3 Simulation results and analysis

This section analyzes the two \mathcal{H}_2 controllers designed above by constructing the closed-loop feedback systems. We are interested in analyzing the contribution of the piezoelectric actuators in further improving the ride quality, so comparisons are made between the closed-loop system with and without control from piezoelectric actuators.

Table 8.1 and Table 8.2 tabulate the RMS results of the accelerations of the vehicle body, suspension deflections and control inputs. In general, the vertical accelerations at these three positions of the vehicle body have been effectively reduced by the \mathcal{H}_2 controllers. Due to the limitations placed by the dynamic weights on the control inputs, it is not surprising to find that the

8.3. \mathcal{H}_2 OPTIMAL CONTROL FOR VIBRATION CONTROL OF RAILWAY VEHICLES

improvement in ride quality achieved by \mathcal{H}_2 controller with dynamic weights is less than that by the \mathcal{H}_2 controller with constant weights. It is also found that the acceleration levels with or without piezoelectric actuators are almost the same.

Figure 8.7-8.11 and Figure 8.12-8.16 show PSDs of the accelerations of the vehicle body and the control inputs of the two closed-loop systems with \mathcal{H}_2 controller designed with constant weights and of the closed-loop system with \mathcal{H}_2 controller designed with dynamic weights, respectively, with respect to the track disturbance inputs. For both \mathcal{H}_2 controllers, it is found that the whole PSDs of the accelerations of the vehicle body have been pushed down to a considerably lower level. With control from piezoelectric actuators, the PSDs of the accelerations are reduced at the natural frequency of the first flexible mode, i.e. 8.45Hz, and the whole plot becomes smoother with resonances eliminated. Figure 8.10 and Figure 8.15 show that, with control from piezoelectric actuators, the suspension control effort around the frequency of 8.5Hz decreases compared to that without control from piezoelectric actuators.

Table 8.1: RMS results for centralized control: \mathcal{H}_2 control with constant weights

Sys.	Vert. Acce. (%g)			Susp. Def. (mm)		Susp. forces (kN)		Piezo Actu. Voltages (volts)		
	centre	left	right	left	right	left	right	A1	A2	A3
without piezo	0.36	0.49	0.53	10.55	11.03	3.75	3.90	-	-	-
with piezo	0.36	0.50	0.53	10.47	10.91	3.68	3.83	65.10	65.09	65.09

Table 8.2: RMS results for centralized control: \mathcal{H}_2 control with dynamic weights

Sys.	Vert. Acce. (%g)			Susp. Def. (mm)		Susp. forces (kN)		Piezo Actu. Voltages (volts)		
	centre	left	right	left	right	left	right	A1	A2	A3
without piezo	0.45	0.61	0.63	10.82	11.35	3.76	3.94	-	-	-
with piezo	0.45	0.65	0.67	10.59	11.00	3.61	3.77	205.13	211.95	211.20

8.3. \mathcal{H}_2 OPTIMAL CONTROL FOR VIBRATION CONTROL OF RAILWAY VEHICLES

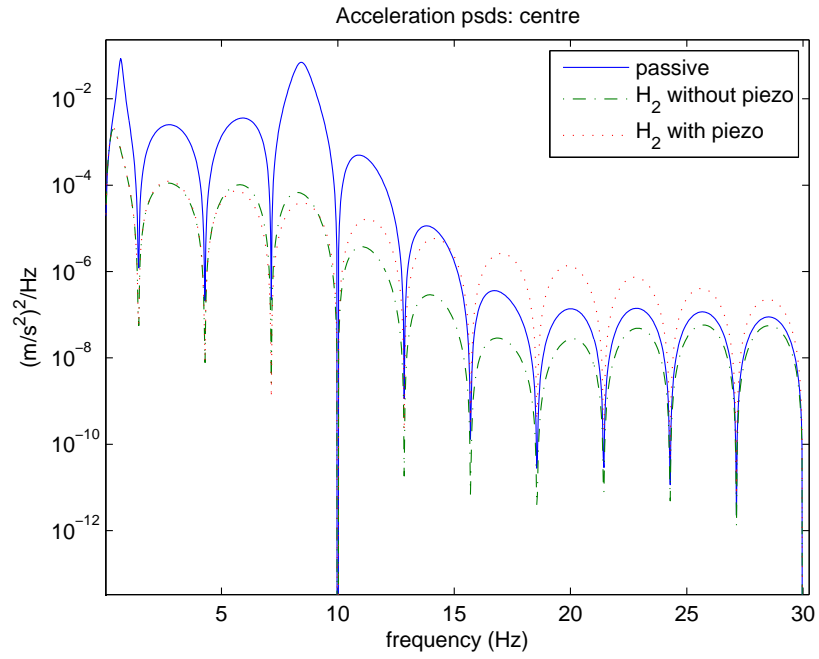


Figure 8.7: \mathcal{H}_2 control with constant weights: centre acceleration PSDs

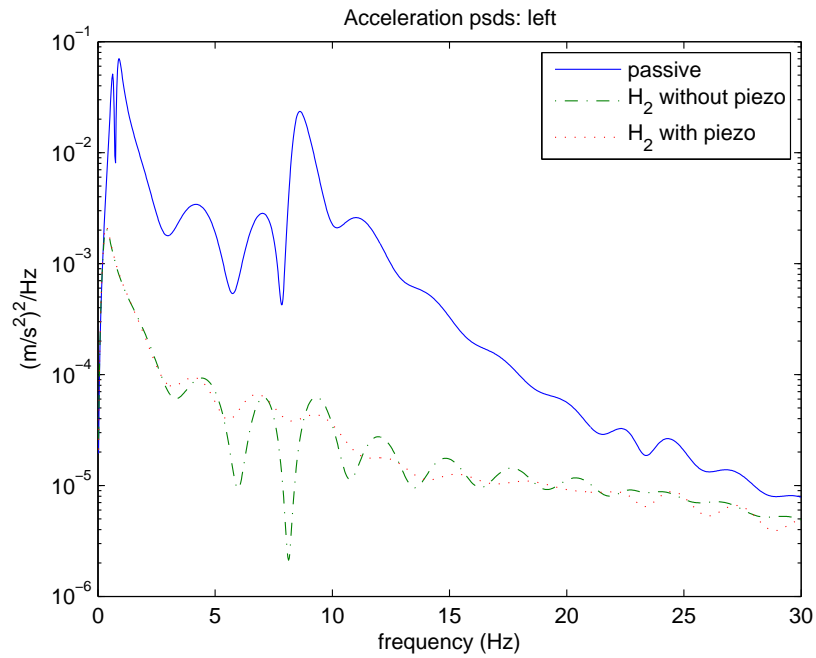


Figure 8.8: \mathcal{H}_2 control with constant weights: left acceleration PSDs

8.3. \mathcal{H}_2 OPTIMAL CONTROL FOR VIBRATION CONTROL OF RAILWAY VEHICLES

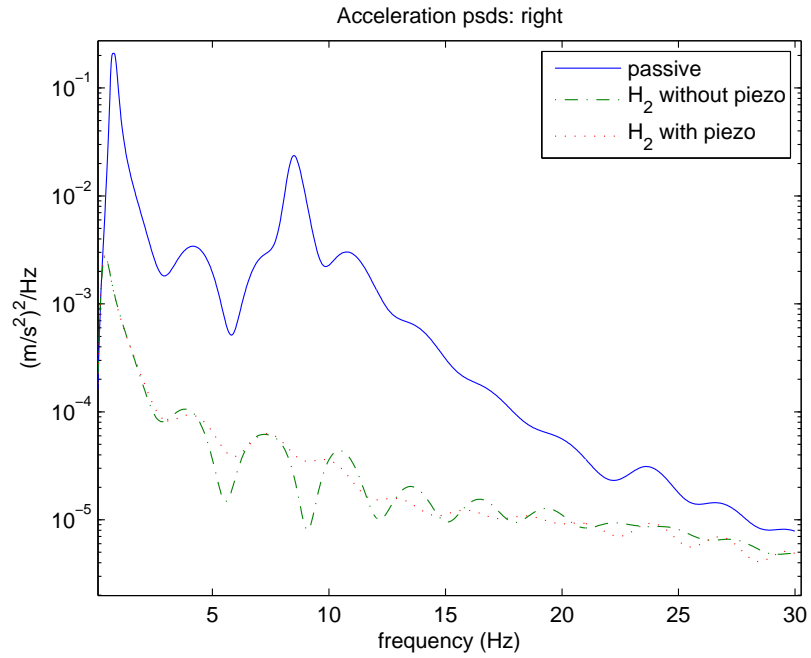


Figure 8.9: \mathcal{H}_2 control with constant weights: right acceleration PSDs

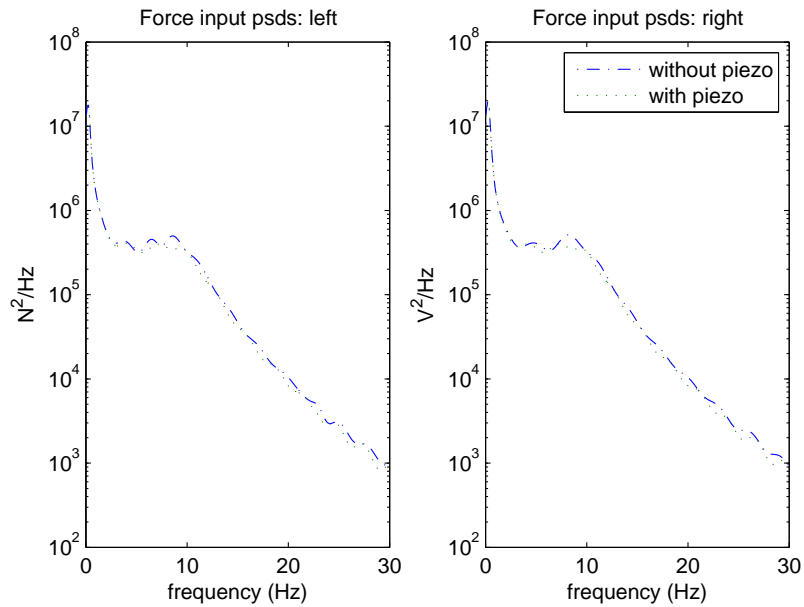


Figure 8.10: \mathcal{H}_2 control with constant weights: force PSDs

8.3. \mathcal{H}_2 OPTIMAL CONTROL FOR VIBRATION CONTROL OF RAILWAY VEHICLES

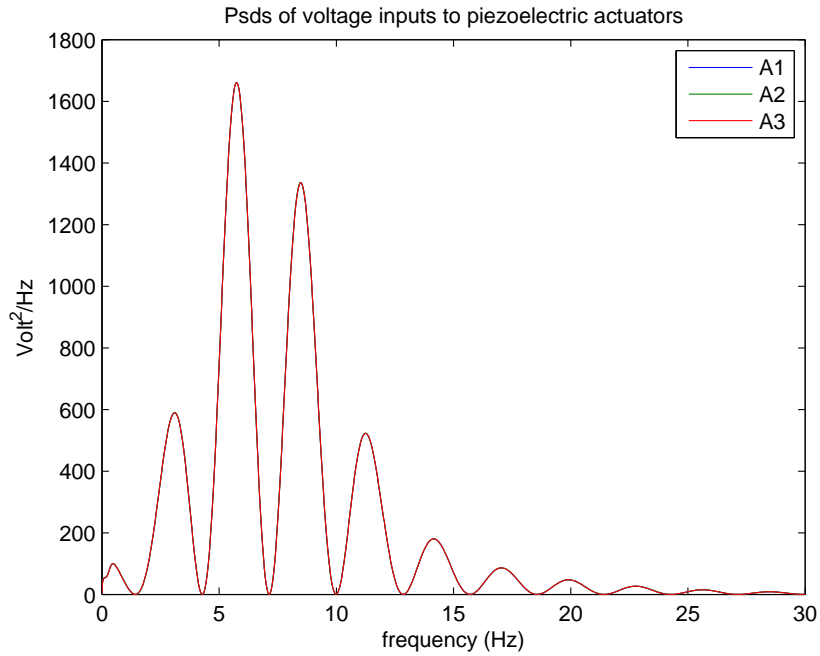


Figure 8.11: \mathcal{H}_2 control with constant weights: piezoelectric actuator voltage PSDs

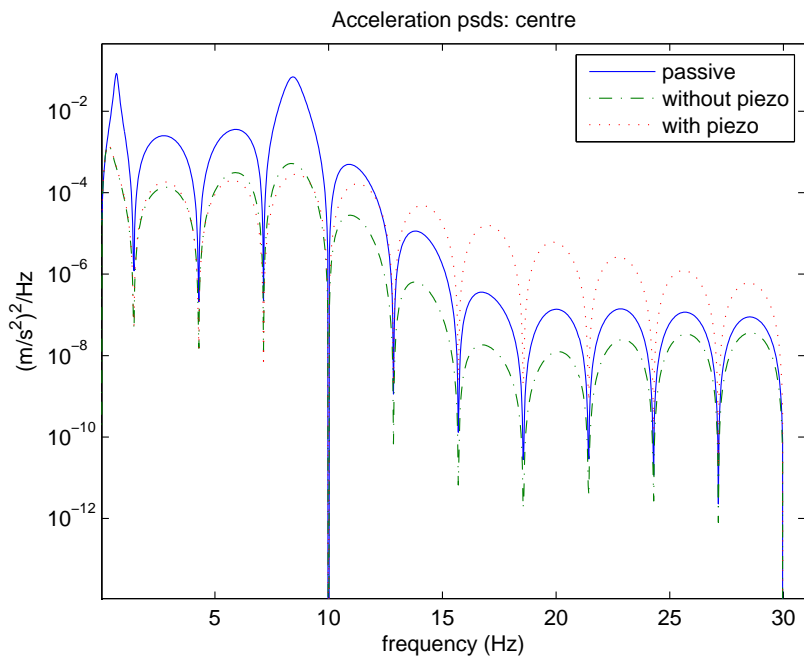


Figure 8.12: \mathcal{H}_2 control with dynamic weights: centre acceleration PSDs

8.3. \mathcal{H}_2 OPTIMAL CONTROL FOR VIBRATION CONTROL OF RAILWAY VEHICLES

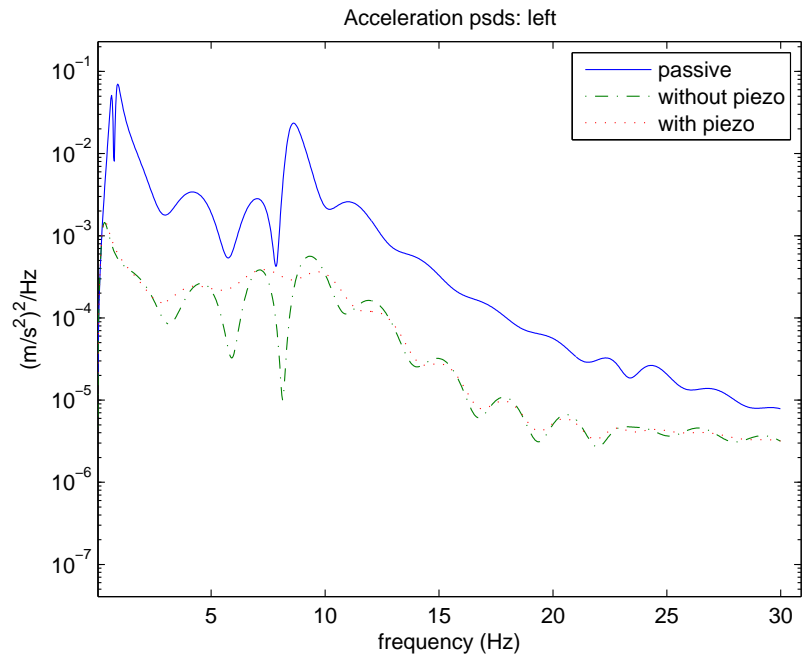


Figure 8.13: \mathcal{H}_2 control with dynamic weights: left acceleration PSDs

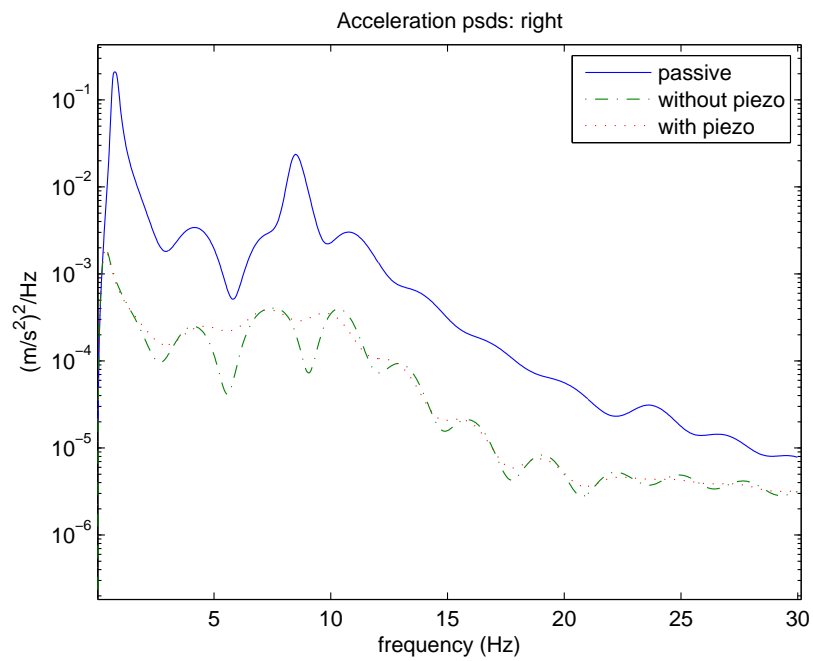


Figure 8.14: \mathcal{H}_2 control with dynamic weights: right acceleration PSDs

8.3. \mathcal{H}_2 OPTIMAL CONTROL FOR VIBRATION CONTROL OF RAILWAY VEHICLES

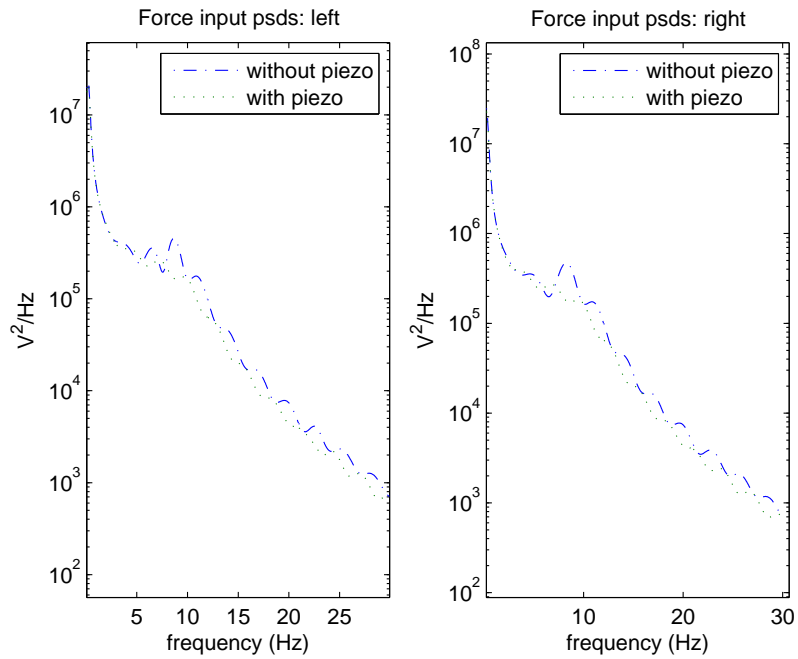


Figure 8.15: \mathcal{H}_2 control with dynamic weights: force PSDs

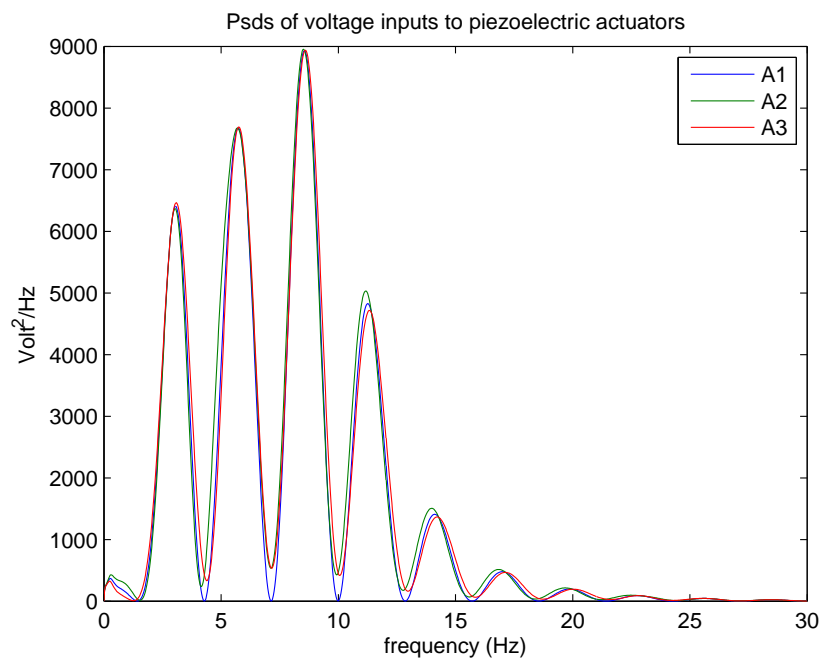


Figure 8.16: \mathcal{H}_2 control with dynamic weights: piezoelectric actuator voltage PSDs

8.3.4 Summary

In this section, it has been shown that the designed \mathcal{H}_2 controllers have successfully improved ride quality of the railway vehicle body against random irregularities of the track. By tuning the coefficients of the weights, satisfying acceleration levels are obtained in both the situations: with or without piezoelectric actuators. With piezoelectric actuators, the control effort around the frequencies of the first flexible mode decreases and the resonances in PSDs of the accelerations are eliminated.

It is known that \mathcal{H}_2 controllers push down all the singular values over all frequencies of the generalized plant. One of its shortcomings is that it has poor robustness properties attributed to the integral criterion in terms of the \mathcal{H}_2 norm. So next robust \mathcal{H}_∞ control technique will be considered for vibration control of the flexible-bodied vehicle body.

8.4 \mathcal{H}_∞ optimal control for vibration control of railway vehicles

The \mathcal{H}_∞ norm of a stable transfer function matrix $G(j\omega)$ is defined as its largest singular value over the entire frequency range

$$\|G(j\omega)\|_\infty = \sup_{\omega} \bar{\sigma}(G(j\omega)) \quad (8.28)$$

where $\bar{\sigma}$ represents the largest singular value of $G(j\omega)$.

For the \mathcal{H}_∞ based control design, the controller $K(s)$ is selected in such a way that it stabilizes the nominal system such that the \mathcal{H}_∞ norm of $F_l(P, K)$ is minimized or becomes smaller than a specified value γ .

$$\min_{K \in \mathcal{S}} \|F_l(P, K)\|_\infty < \gamma \quad (8.29)$$

Therefore, \mathcal{H}_∞ control pushes down the peak of the largest singular value.

Transfer function shaping approach (e.g. the mixed-sensitivity \mathcal{H}_∞ control) and the signal-based approach are the two distinguished methodologies

for \mathcal{H}_∞ controller design. The first methodology focuses on the size and bandwidth of the selected closed-loop transfer functions while the later focuses on the size of the error signals. The problem can be solved either by Riccati based approach or linear matrix inequalities (LMI) based approach. The computation required for designing \mathcal{H}_∞ controllers can be intense but the solution of the controller can be calculated with the available software MATLAB. One of the difficulty is the selection of weights, which is aimed to provide a good trade-off between conflicting objectives in various frequency ranges.

8.4.1 Choice of weight

The signal-based approach is used for designing the \mathcal{H}_∞ controller. The diagram for generalized plant for \mathcal{H}_∞ control is given by Figure 8.5. The robust \mathcal{H}_∞ controllers are to be designed with the nominal plant without considering the system uncertainty.

The control inputs \mathbf{u} , measurement outputs \mathbf{y}_m and regulated variables are chosen as following

$$\mathbf{u} = \begin{bmatrix} U_L & U_R & V_{a1} & V_{a2} & V_{a3} \end{bmatrix}^T \quad (8.30)$$

$$\mathbf{y}_m = \begin{bmatrix} \ddot{Z}_{x_L} & \ddot{Z}_{x_C} & \ddot{Z}_{x_R} \end{bmatrix}^T \quad (8.31)$$

$$\begin{bmatrix} \mathbf{y} \\ \mathbf{u} \end{bmatrix} = \begin{bmatrix} \ddot{Z}_{x_L} & \ddot{Z}_{x_C} & \ddot{Z}_{x_R} & Z_{Ld} & Z_{Rd} & U_L & U_R & V_{a1} & V_{a2} & V_{a3} \end{bmatrix}^T \quad (8.32)$$

where U_L and U_R are the force commands for the secondary suspension actuators, and V_{a1} , V_{a2} and V_{a3} are the voltage inputs to the piezoelectric actuators. \ddot{Z}_{x_L} , \ddot{Z}_{x_C} and \ddot{Z}_{x_R} are the three body accelerations which will pick up both the rigid accelerations and flexibility effect associated with the three points x_L , x_C and x_R .

Weights on the regulated variables are as follows

$$\mathbf{W}_y = \text{diag}([W_{z1} \quad W_{z1} \quad W_{z1} \quad k_{z2} \quad k_{z2}]) \quad (8.33)$$

$$\mathbf{W}_u = \text{diag}([W_{u1} \quad W_{u1} \quad W_{u2} \quad W_{u2} \quad W_{u2}]) \quad (8.34)$$

It is required that the first flexible mode be effectively reduced by the piezoelectric actuators, so W_{z1} the frequency dependent weight on accelerations, as shown in Figure 8.5, are set to produce an increased gain at the frequencies around 8.5Hz.

$$W_{z1} = k_{z1} \frac{s^2 + 2\xi_{1c}\omega_2 s + \omega_2^2}{s^2 + 2\xi_{1d}\omega_2 s + \omega_2^2} \quad (8.35)$$

where $\xi_{1c} = 0.7$, $\xi_{1d} = 0.3$ and $\omega_2 = 8.45\text{Hz}$.

W_{u1} are frequency dependent weights on the suspension control inputs to account for the limited bandwidth of the hydraulic actuators.

$$W_{u1} = k_{u1} \frac{s^2 + 2\xi_{1a}\omega_{1a}s + \omega_{1a}^2}{s^2 + 2\xi_{1b}\omega_{1b}s + \omega_{1b}^2} \quad (8.36)$$

where $\xi_{1a} = 0.7$, $\xi_{1b} = 0.7$, $\omega_{1a} = 4\text{Hz}$, and $\omega_{1b} = 10\text{Hz}$.

W_{u2} are frequency dependent weights chosen to reflect the desired frequency content of the control efforts by the piezoelectric actuators.

$$W_{u2} = k_{u2} \frac{s^2 + 2\xi_{2a}\omega_2 s + \omega_2^2}{s^2 + 2\xi_{2b}\omega_2 s + \omega_2^2} \quad (8.37)$$

where $\xi_{2a} = 0.4$, $\xi_{2b} = 0.7$, and $\omega_2 = 8.45\text{Hz}$.

The constant weights k_{z2} and the coefficients k_{z1} , k_{u1} and k_{u2} are tuned for performance in improving the ride quality and control efforts. Figure 8.17 shows the weights of W_{z1} , W_{u1} and W_{u2} with $k_{z1} = 50$, $k_{u1} = 0.0014$ and $k_{u2} = 0.01$, with which satisfying results have been achieved.

8.4.2 Simulation results

Table 8.3 tabulates the RMS results of acceleration levels, suspension deflections, suspension control forces and voltages inputs for piezoelectric actuators of the closed-loop system with the \mathcal{H}_∞ controller, which is solved by LMI based approach, where C_1 and C_2 denote the two controllers without piezoelectric inputs and with piezoelectric inputs respectively. It is shown that only a small further reduction in acceleration levels have been achieved

8.4. \mathcal{H}_∞ OPTIMAL CONTROL FOR VIBRATION CONTROL OF RAILWAY VEHICLES

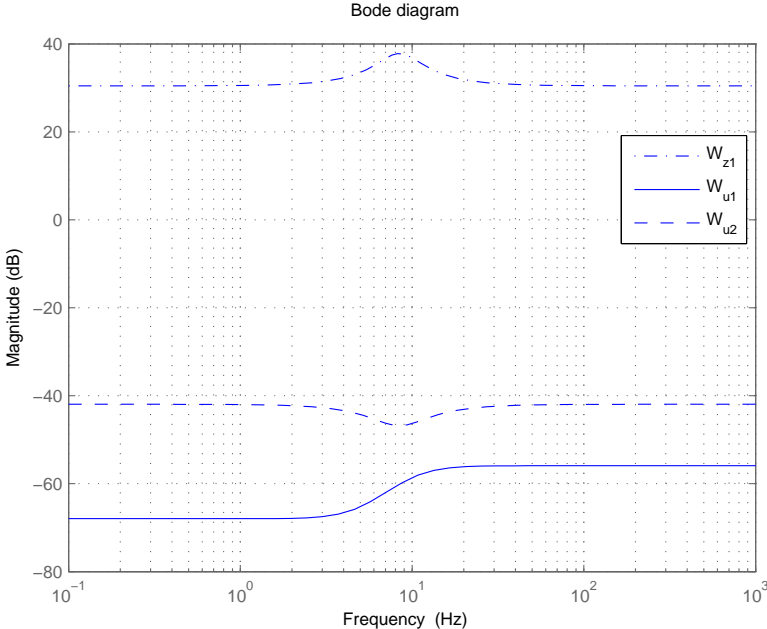


Figure 8.17: Weights on outputs for \mathcal{H}_∞ control with $k_{z1} = 33.33$, $k_{z2} = 50$, $k_{u1} = 0.0016$ and $k_{u2} = 0.005$

8.4. \mathcal{H}_∞ OPTIMAL CONTROL FOR VIBRATION CONTROL OF RAILWAY VEHICLES

by including piezoelectric control inputs.

Table 8.3: RMS results for \mathcal{H}_∞ control

Sys.	Vert. Acce. (%g)			Susp. Def. (mm)		susp. forces (kN)		Piezo Actu.Voltages (volts)		
	centre	left	right	left	right	left	right	A1	A2	A3
C_1	0.69	0.83	0.78	8.91	9.54	3.2	3.61	-	-	-
C_2	0.57	0.67	0.62	9.59	9.56	3.50	3.78	100.94	103.05	101.26

Figure 8.18, 8.19, 8.20, 8.21 and 8.22 show PSDs for the centre, left and right accelerations, suspension control inputs and piezoelectric control inputs respectively of the closed-loop system with controllers C_1 and C_2 with respect to random track disturbances. Comparing C_1 and C_2 , accelerations are further reduced with piezoelectric control inputs.

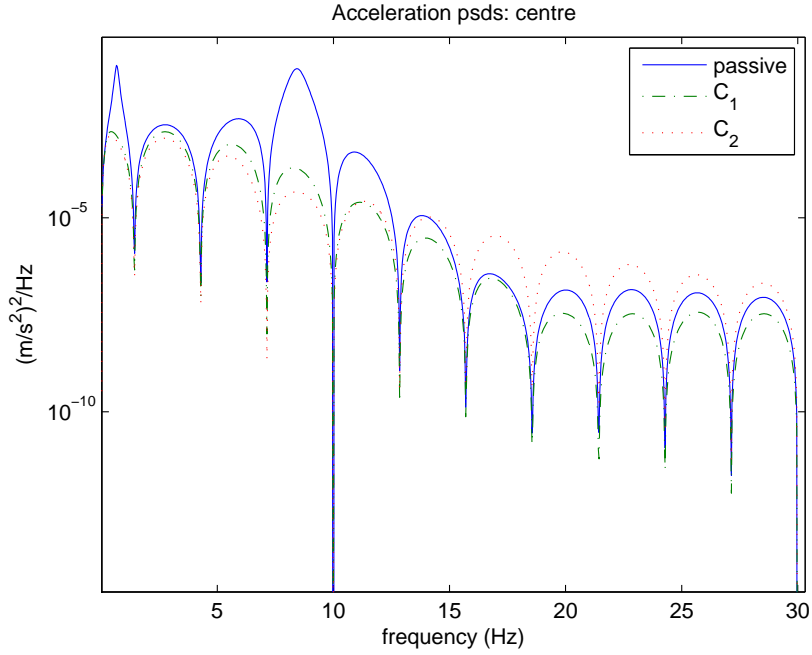


Figure 8.18: \mathcal{H}_∞ control: centre acceleration PSDs

8.4.3 Summary

\mathcal{H}_∞ controllers are designed for vibration suppressing of the flexible-bodied railway vehicle. The RMS results and the PSDs plots have shown that

8.4. \mathcal{H}_∞ OPTIMAL CONTROL FOR VIBRATION CONTROL OF RAILWAY VEHICLES

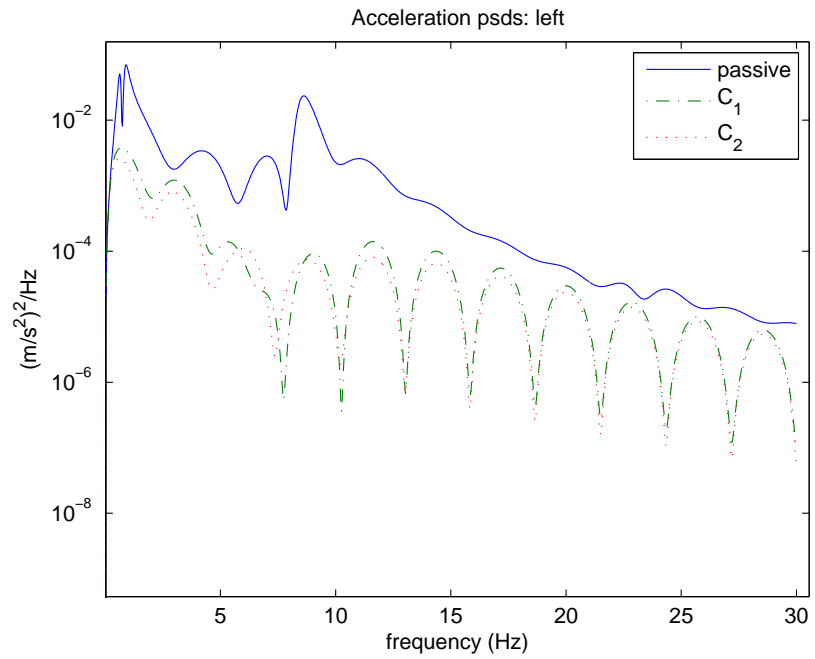


Figure 8.19: \mathcal{H}_∞ control: left acceleration PSDs

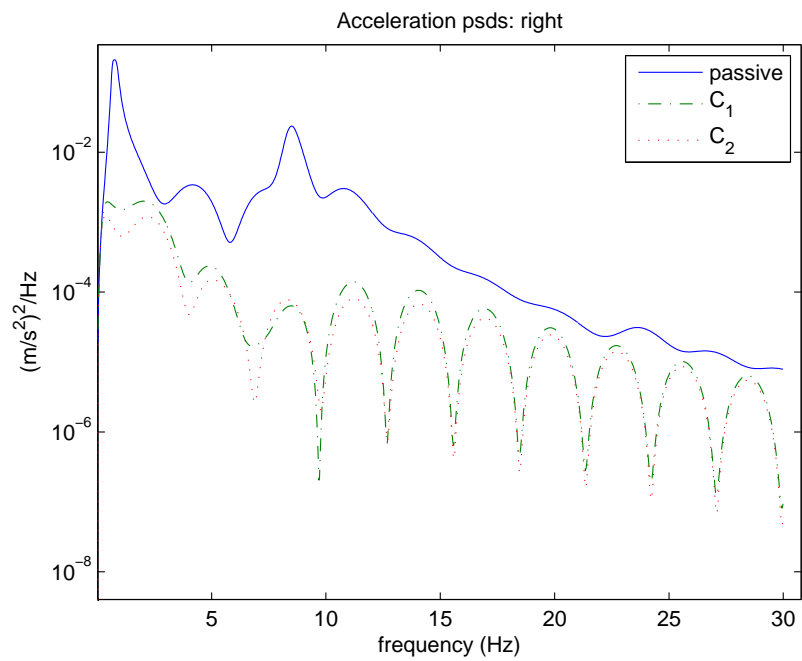


Figure 8.20: \mathcal{H}_∞ control: right acceleration PSDs

8.4. \mathcal{H}_∞ OPTIMAL CONTROL FOR VIBRATION CONTROL OF RAILWAY VEHICLES

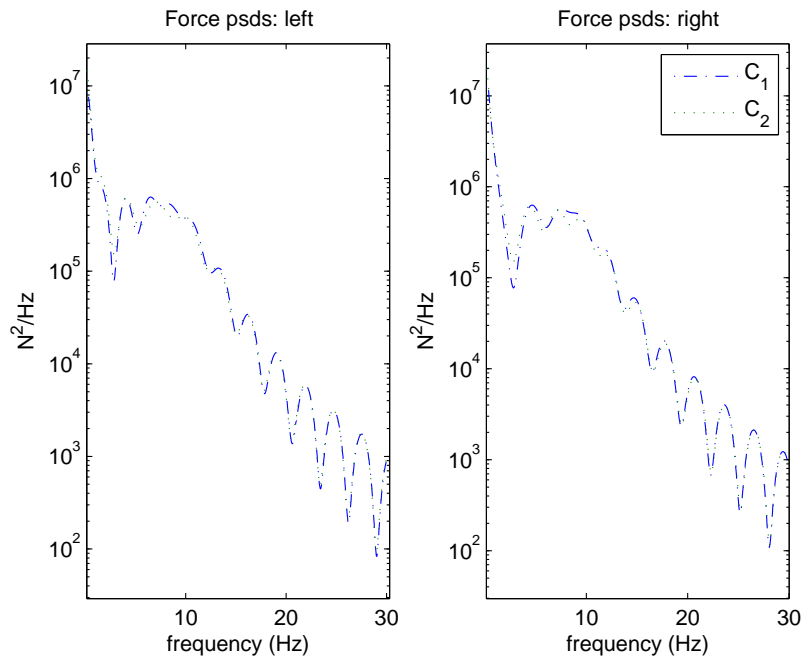


Figure 8.21: \mathcal{H}_∞ control: force PSDs

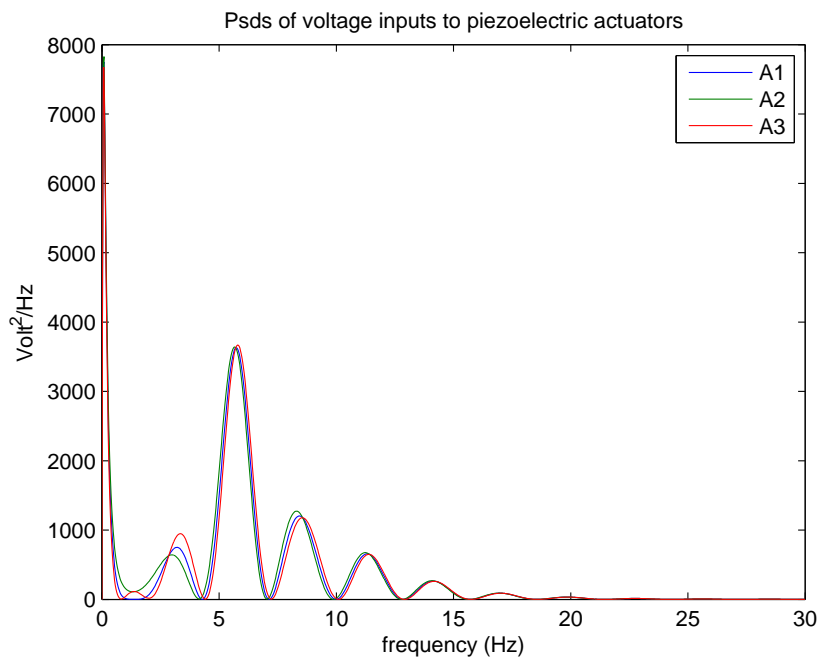


Figure 8.22: \mathcal{H}_∞ control: piezoelectric actuator voltage PSDs

further reduction in accelerations is achieved with the inclusion of control by piezoelectric actuators. One of the shortcomings of \mathcal{H}_∞ control is that it can be conservative because \mathcal{H}_∞ norm of a system represents the worst-case energy transfer between disturbances to regulated outputs and trade-off exists between performance and robustness. In the next section, a new control method based on mixed $\mathcal{H}_2/\mathcal{H}_\infty$ control approach is going to be introduced and applied to the vibration control problem of the flexible-bodied railway vehicles.

8.5 Model predictive control based on mixed $\mathcal{H}_2/\mathcal{H}_\infty$ control approach for vibration control of railway vehicles ¹

This part of work is an application of model predictive control using mixed $\mathcal{H}_2/\mathcal{H}_\infty$ control approach for active vibration control of railway vehicles, with the aim to improve the ride quality of the railway vehicle.

Model Predictive Control (MPC) technology based on mixed $\mathcal{H}_2/\mathcal{H}_\infty$ control approach (Orukpe et al. [2007]) is utilized for active vibration control of a railway vehicle. The suitability of the proposed approach stems from the fact of considering both performance and robustness issues within a unified framework. The work is based on Linear Matrix Inequalities (LMI), in particular develops an LMI linear in the state feedback. The interested reader can see more details on LMIs in paper by Scherer and Weiland [2000]. LMIs are inequalities linear in sets of matrix variables. From a control engineering point of view, one of the main attractions of LMIs is that they can be used to solve problems which involve several matrix variables, with different structures imposed on these matrix variables. Another attractive feature of LMI methods is that they form a flexible approach, thus it is usually

¹This work was in collaboration with Dr. Patience E. Orukpe, Imperial College London. A common paper was published, details: Patience E. Orukpe, X.Zheng, I.M.Jaimoukha, A.C.Zolotas and R.M.Goodall Model predictive control based on mixed control approach for active vibration control of railway vehicles *Vehicle System Dynamics*, 46:1, 151-160,2008

rather straightforward to pose a multitude of problems as LMI problems. An advantage of LMIs is that they are able to unite many previous existing results in a common framework. In this section, the potential of improving the ride quality of the railway vehicle and overall performances of the system will be investigated.

8.5.1 Control design

MPC is a form of control in which the current control action is obtained by solving on-line, at each sampling instant, an open-loop optimal control problem. Using the current states of the plant as the initial states; the optimization yields an optimal control sequence and the first control in this sequence is applied to the plant. The main advantages of MPC include the ability to handle constraints and the capability for controlling multivariable plants, although computational requirements increase due to the online computation and problem dimension.

The following discrete-time state-space representation of the linear time invariant railway vehicle model is considered

$$\begin{aligned}
 x(k+1) &= Ax(k) + B_1w(k) + B_2u(k) \\
 y(k) &= Cx(k) + D_{1w}w(k) + D_{1u}u(k) \\
 z(k) &= \begin{bmatrix} \sqrt{R_{LQ}}u(k) \\ \sqrt{Q_{LQ}}y(k) \end{bmatrix} \\
 x(0) &= x_0
 \end{aligned} \tag{8.38}$$

where the state $x(k) \in \mathcal{R}^{12}$ and the track disturbance $w(k) \in \mathcal{R}^2$ are the same as given for flexible model in chapter 5. The control inputs, $u(k) \in \mathcal{R}^5$, are

$$u = \begin{bmatrix} U_L & U_R & V_{a1} & V_{a2} & V_{a3} \end{bmatrix}^T \tag{8.39}$$

where U_L and U_R are the command forces for the secondary suspension actuators, and V_{a1} , V_{a2} and V_{a3} are the voltage inputs to the piezoelectric

8.5. MODEL PREDICTIVE CONTROL BASED ON MIXED $\mathcal{H}_2/\mathcal{H}_\infty$ CONTROL APPROACH FOR VIBRATION CONTROL OF RAILWAY VEHICLES

actuators. The output $y(k) \in \mathcal{R}^5$ is chosen to be

$$y = [\ddot{Z}_{x_C} \quad \ddot{Z}_{x_L} \quad \ddot{Z}_{x_R} \quad Z_{Ld} \quad Z_{Rd}] \quad (8.40)$$

where

$$\begin{aligned} Z_{Ld} &= Z_{3l} - Z_{1l} \\ Z_{Rd} &= Z_{3r} - Z_{1r} \end{aligned} \quad (8.41)$$

$z(k) \in \mathcal{R}^{10}$ the controlled output, i.e. a combination of inputs and outputs of the system, and A , B_1 , B_2 , \sqrt{R}_{LQ} , \sqrt{Q}_{LQ} , C , D_{1w} and D_{1u} are matrices of appropriate dimensions based on system dynamics and physical constraints.

The aim is to find a control strategy $\{u(k)\}$ in \mathcal{L}_2 , where \mathcal{L}_2 is the time domain Lebesgue space, to minimize the following \mathcal{H}_2 cost function J

$$J = \sum_{k=0}^{\infty} z^T(k)z(k), \quad (8.42)$$

subject to the specified level of disturbance rejection γ

$$\|T_{zw}\|_\infty < \gamma \quad (8.43)$$

for any $\gamma > 0$, where T_{zw} represents the transfer matrix from w to z .

Input and state constraints can be added as follows:

For given $H_1, \dots, H_{m_u} \in \mathcal{R}^{n_h \times n_u}$ and $\bar{u}_1, \dots, \bar{u}_{m_u} > 0$ the general quadratic input constraints are satisfied

$$u^T(k)H_j^T H_j u(k) \leq \bar{u}_j^2, \quad \forall k; \text{ for } j = 1, \dots, m_u, \quad (8.44)$$

where H_j $j = 1, \dots, m_u$ are given matrices with appropriate dimensions and m_u is the number of control inputs. Also, for given $E_1, \dots, E_{m_x} \in \mathcal{R}^{n_e \times n}$ and $\bar{x}_1, \dots, \bar{x}_{m_x} > 0$ the general quadratic state/output constraints are satisfied

$$x^T(k+1)E_j^T E_j x(k+1) \leq \bar{x}_j^2, \quad \forall k; \text{ for } j = 1, \dots, m_x, \quad (8.45)$$

where $E_j, j = 1, \dots, m_x$ are given matrices with appropriate dimensions and m_x is the number of states.

8.5.2 Problem Formulation

For state feedback $u(k) = Fx(k)$, the state equation (8.38) becomes

$$x(k+1) = \overbrace{(A + B_2F)}^{A_{cl}} x(k) + B_1w(k).$$

The disturbance is assumed to be bounded by

$$\sum_{k=0}^{\infty} w^T(k)w(k) \leq \bar{w}^2,$$

or $\|w\|_2 \leq \bar{w}$.

The cost in (8.42) is considered and can be expressed as

$$J = x_0^T P x_0 + \gamma^2 \sum_{k=0}^{\infty} w^T(k)w(k) + \sum_{k=0}^{\infty} \begin{bmatrix} x(k) \\ w(k) \end{bmatrix}^T K \begin{bmatrix} x(k) \\ w(k) \end{bmatrix}$$

where K is defined as

$$K = \begin{bmatrix} k_{11} & A_{cl}^T P B_1 + F^T D_{1u}^T Q_{LQ} D_{1w} + C^T Q_{LQ} D_{1w} \\ B_1^T P A_{cl} + D_{1w}^T Q_{LQ} D_{1u} F + D_{1w}^T Q_{LQ} C & B_1^T P B_1 + D_{1w}^T Q_{LQ} D_{1w} - \gamma^2 I \end{bmatrix} \quad (8.46)$$

where

$$k_{11} = A_{cl}^T P A_{cl} - P + C^T Q_{LQ} C + F^T R_{LQ} F + 2F^T D_{1u}^T Q_{LQ} C + F^T D_{1u}^T Q_{LQ} D_{1u} F \quad (8.47)$$

An application of the bounded real lemma (Dumitrescu [2005]) shows that A_{cl} is stable and (8.43) is satisfied if and only if $K < 0$ and $P > 0$. These condition can be reduced to LMIs as shown in Theorem 8.5.1 below. Thus the desired upper bound of the cost function is (for details of derivation,

please refer to the paper by Orukpe et al. [2007])

$$J \leq x_0^T P x_0 + \gamma^2 \sum_{k=0}^{\infty} w^T(k) w(k) \leq x_0^T P x_0 + \gamma^2 \bar{w}^2. \quad (8.48)$$

Hence, the goal of the robust mixed $\mathcal{H}_2/\mathcal{H}_\infty$ MPC is to compute, at each time step, a state-feedback control law $u(k) = Fx(k)$, to minimize this upper bound and the first of the computed inputs is implemented. The problem concerned in this case is finding a state feedback control law $u = Fx$ with F of appropriate dimension, such that

1. The matrix $A_{cl} = A + B_2 F$ is stable (for stability);
2. The closed loop transfer function, T_{zw} from w to z satisfies (8.43) for $\gamma > 0$, or equivalently, $K < 0$ (for disturbance rejection);
3. The upper bound (8.48) is minimized (for performance).

Such an F is called an admissible state feedback gain.

The next result gives sufficient conditions in the form of easily computable LMIs for the existence of an admissible state feedback gain.

Theorem 8.5.1. *Consider the system defined in (8.38). Then, F is an admissible state feedback gain if $F = YQ^{-1}$ where $Q > 0$ and Y are obtained from the solution, if it exists, of the following LMI minimization problem:*

$$\begin{aligned} & \min_{\alpha^2, Q, Y} \alpha^2 \\ & \text{subject to} \quad \begin{bmatrix} 1 & \star & \star \\ \gamma^2 \bar{w}^2 & \alpha^2 \gamma^2 \bar{w}^2 & \star \\ x_0 & 0 & Q \end{bmatrix} \geq 0 \end{aligned} \quad (8.49)$$

$$\begin{bmatrix} -Q & \star & \star & \star & \star \\ 0 & -\alpha^2\gamma^2I & \star & \star & \star \\ AQ + B_2Y & \alpha^2B_1 & -Q & \star & \star \\ D_{1u}Y + C_2Q & \alpha^2D_{1w} & 0 & -\alpha^2I & \star \\ C_1Q & 0 & 0 & 0 & -\alpha^2I \end{bmatrix} < 0 \quad (8.50)$$

$$\begin{bmatrix} \bar{w}_j^2I & \star \\ Y^T H_j^T & Q \end{bmatrix} \geq 0, \quad j = 1, \dots, m_u \quad (8.51)$$

$$\begin{bmatrix} \bar{x}_j^2I - (1 + \bar{w}^2)E_j B_1 B_1^T E_j^T & \star \\ QA^T E_j^T + Y^T B_2^T E_j^T & \frac{Q}{(1 + \bar{w}^2)} \end{bmatrix} \geq 0, \quad j = 1, \dots, m_x \quad (8.52)$$

where \star represents terms readily inferred from symmetry.

The proof is similar to the proof of Theorem 1 of the paper by Orukpe et al. [2007] and, hence, is omitted.

Remark 8.5.1. *The variables F, Y and Q in LMI minimization problem of Theorem 8.5.1 are computed at time k , the subscript k is omitted for convenience.*

Remark 8.5.2. *In this formulation, γ^2 is a parameter that can be tuned using simulations, while α^2 , Q and Y are variables determined by the solution to the LMI. Moreover, α^2 is a measure of the contribution of the H_2 cost, while γ^2 measures the contribution of the H_∞ cost, and determines the disturbance rejection level of the control system.*

Remark 8.5.3. ²

We can give the following interpretation to the result obtained. Since the upper bound on J is given by $x_0^T P x_0 + \gamma^2 \bar{w}^2$, and since $x_0^T P x_0 + \gamma^2 \bar{w}^2 \leq \alpha^2$, it follows that $x_0^T P x_0$ may be regarded as the contribution of the initial state to the total cost while $\gamma^2 \bar{w}^2$ may be regarded as the corresponding

²This remark is duplicated here from the paper by Orukpe et al. [2008] in its original form as the author of the thesis considers this being an integral part of the work to properly explain the use of the use of the technique to the readers

contribution of the disturbance. By guaranteeing $x_0^T \alpha^{-2} P x_0 + \alpha^{-2} \gamma^2 \bar{w}^2 \leq 1$, this is a normalized mixed performance objective, where $\alpha^{-2} \gamma^2 \bar{w}^2$ is the contribution of the \mathcal{H}_∞ cost and $x_0^T \alpha^{-2} P x_0$ is the contribution of the \mathcal{H}_2 cost. Therefore condition (8.49) might be considered as the normalized mixed objective function. This is a more natural combination of the control objectives since it emphasizes the trade-off between the normalized \mathcal{H}_2 cost and the normalized \mathcal{H}_∞ bound.

8.5.3 Simulation results and discussion

In this simulation, we considered the discrete-time model of the railway vehicle as given by (8.38), with a sampling time of 0.001 second. The static state are taken as the initial state, so the initial values of the states are

$$\mathbf{x}_0 = [0; 0; 0; 0; 0; 0; 0; 0; 0; 0; 0; 0]. \quad (8.53)$$

8.5.4 Parameter tuning

Tuning of R_{LQ} and γ^2

The term R_{LQ} is given by

$$R_{LQ} = \text{diag}([r_1 \ r_1 \ r_2 \ r_2 \ r_2]) \quad (8.54)$$

The weight for suspension control inputs, r_1 and the weight for voltage inputs for piezoelectric actuators, r_2 , are tuned in order to achieve proper scaled control inputs and the best performance for the system. The choice of γ^2 is based on Remark 8.5.2. It measures the contribution of the \mathcal{H}_∞ cost in (8.42), and determines the disturbance rejection level of the control system.

It is found that γ^2 needs to be adjusted accordingly so that LMI could find a feasible solution while it is desired to be small to maintain high disturbance rejection level. For example, when stricter constraints on control inputs are imposed with a relatively bigger value for r_1 and r_2 , γ^2 may need to be increased too if LMI becomes infeasible.

Tuning of Q_{LQ}

The term Q_{LQ} is given by

$$Q_{LQ} = \text{diag} \left[\begin{array}{ccccc} q_1 & q_1 & q_1 & q_2 & q_2 \end{array} \right] \quad (8.55)$$

where q_1 is the weight for accelerations and q_2 is the weight for suspension deflections. They are initially determined based on the physical constraints of the system, and further tuned to achieve the best performance.

From experience, it is known that the requirements for acceleration and suspension deflections are in conflict with each other. So when it shows there is space for the deflections to be increased, weight q_2 can be decreased in order to achieve better ride quality. After changing the value for q_2 , it may be necessary to go back to tune R_{LQ} again as q_2 will have an effect on the control inputs too.

Results and discussion

Based on the principles given above, parameters of γ^2 , R_{LQ} and Q_{LQ} are chosen as: $\gamma^2 = 1000$, $r_1 = 1 \times 10^{-8}$, $r_2 = 1 \times 10^{-7}$, $q_1 = 1/(0.15)^2$ and $q_2 = 1/(0.02)^2$. RMS results of the vertical accelerations in gravity%, deflections in millimetres and control in Newton are tabulated in Table 8.4. It shows that the accelerations of the vehicle body have been successfully reduced with the designed controllers. With piezoelectric control, no obvious further improvement in ride quality is found compared to the case without piezoelectric control.

The time domain responses of the accelerations of the vehicle body and control inputs to the random track disturbances are shown in Figure 8.23-8.27. The PSDs of accelerations of the vehicle body, which are calculated in time domain, are shown in Figure 8.28-8.30. The PDS results agrees with the RMS results that the accelerations have been successfully reduced, however, no big further improvements have been achieved by including piezoelectric actuators for structural damping.

8.5. MODEL PREDICTIVE CONTROL BASED ON MIXED $\mathcal{H}_2/\mathcal{H}_\infty$ CONTROL APPROACH FOR VIBRATION CONTROL OF RAILWAY VEHICLES

Table 8.4: RMS results for MPC control based on mixed $\mathcal{H}_2/\mathcal{H}_\infty$ control approach

System	Vertical Acce. (%g)			Susp. Defle (mm)		Susp. forces (kN)		Piezo Actu.Voltages (volts)		
	centre	left	right	left	right	left	right	A1	A2	A3
without piezo	0.48	0.65	0.68	5.65	7.71	2.40	3.0	-	-	-
with piezo	0.45	0.69	0.69	8.36	7.88	3.08	2.98	107.1	107	107

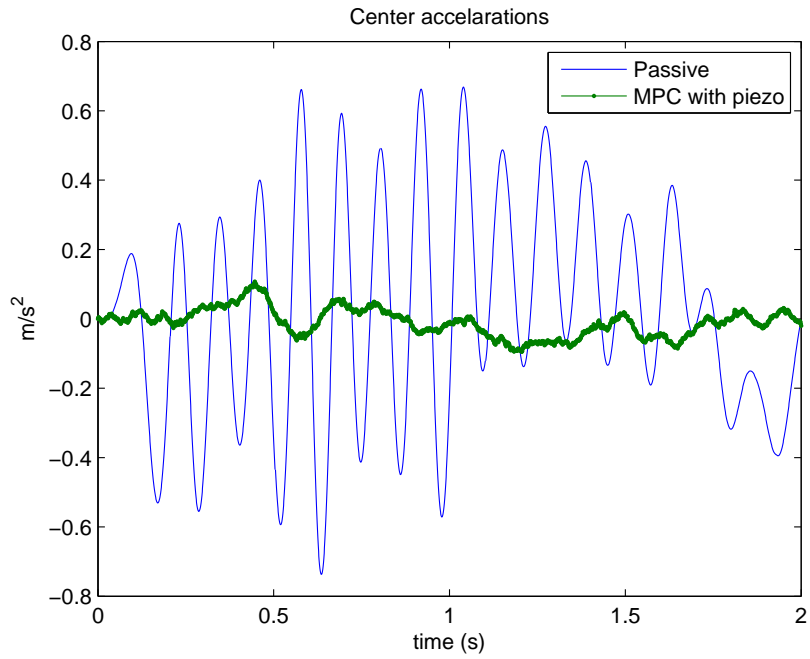


Figure 8.23: MPC with piezoelectric actuators: centre acceleration

8.5. MODEL PREDICTIVE CONTROL BASED ON MIXED $\mathcal{H}_2/\mathcal{H}_\infty$ CONTROL APPROACH FOR VIBRATION CONTROL OF RAILWAY VEHICLES

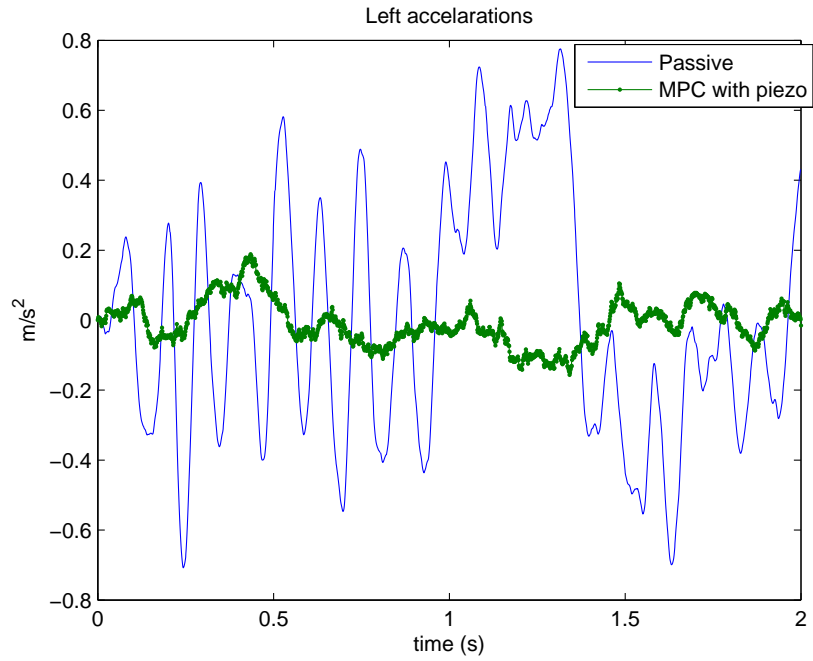


Figure 8.24: MPC with piezoelectric actuators: left acceleration

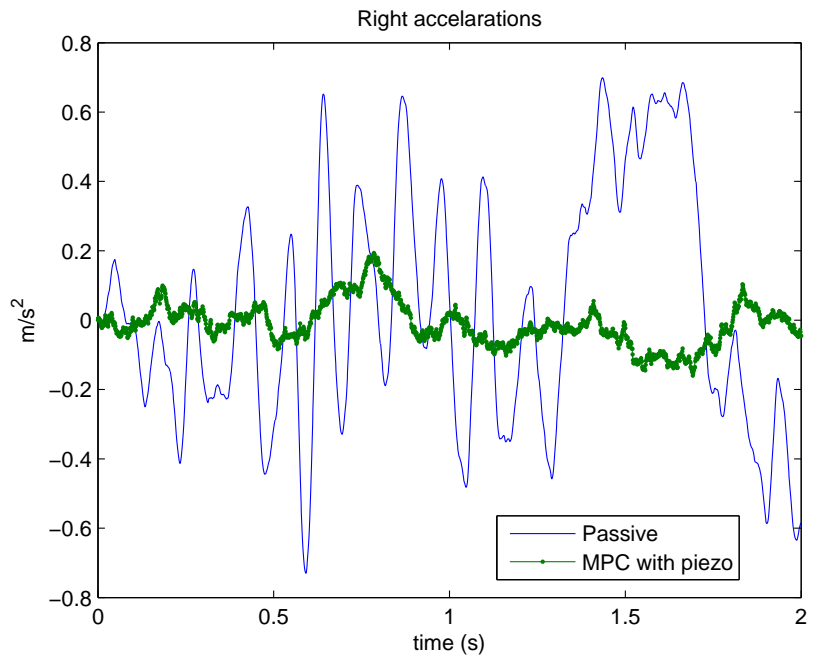


Figure 8.25: MPC with piezoelectric actuators: right acceleration

8.5. MODEL PREDICTIVE CONTROL BASED ON MIXED $\mathcal{H}_2/\mathcal{H}_\infty$ CONTROL APPROACH FOR VIBRATION CONTROL OF RAILWAY VEHICLES

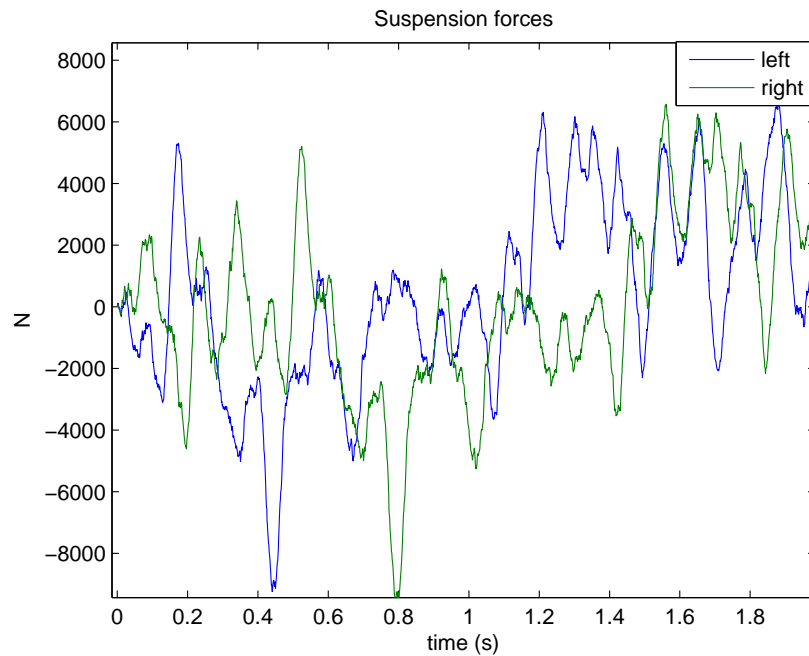


Figure 8.26: MPC with piezoelectric actuators: suspension forces

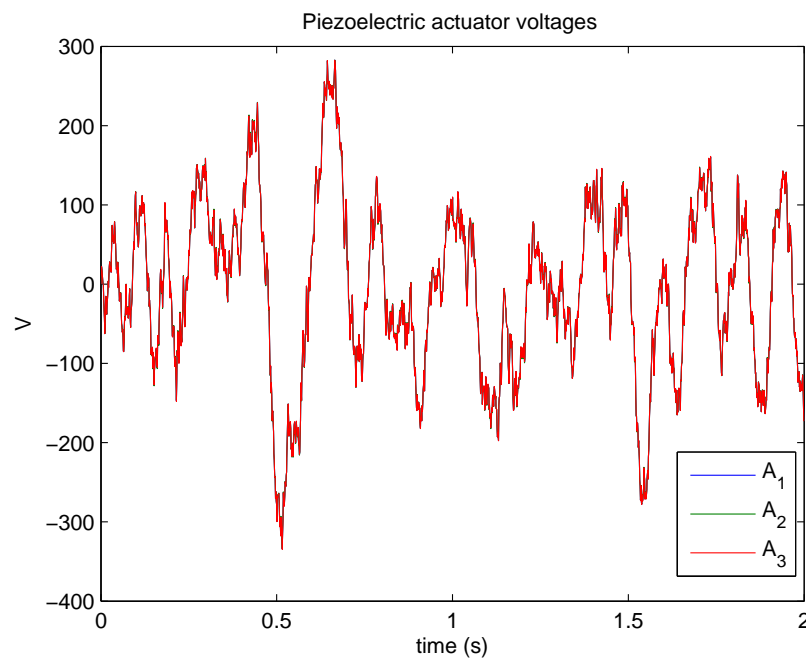


Figure 8.27: MPC with piezoelectric actuators: piezoelectric actuator voltages

8.5. MODEL PREDICTIVE CONTROL BASED ON MIXED $\mathcal{H}_2/\mathcal{H}_\infty$ CONTROL APPROACH FOR VIBRATION CONTROL OF RAILWAY VEHICLES

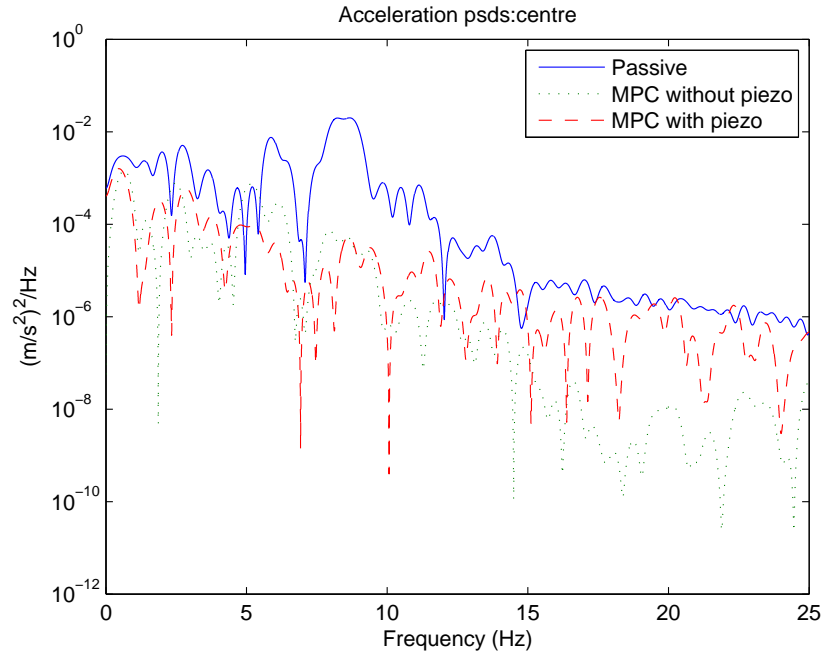


Figure 8.28: Comparisons between MPC controllers: Center acceleration PSDs

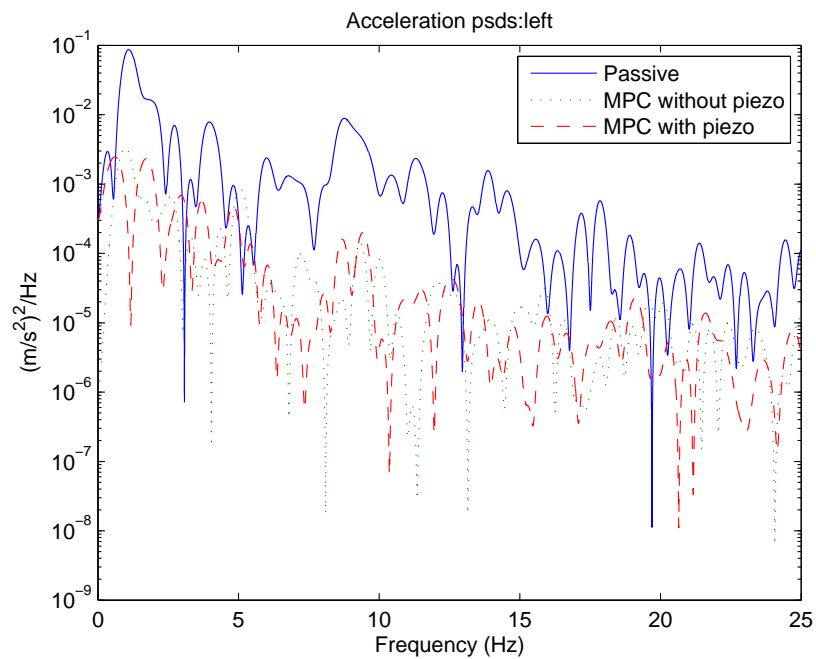


Figure 8.29: Comparisons between MPC controllers: Left acceleration PSDs

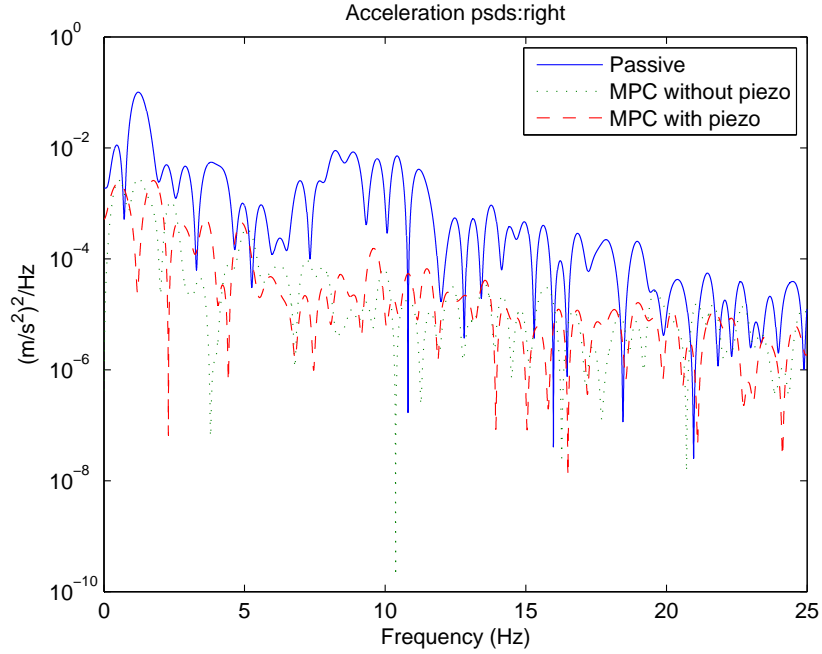


Figure 8.30: Comparisons between MPC controllers: Right acceleration PSDs

8.5.5 Conclusions

A novel method of MPC based on a mixed $\mathcal{H}_2/\mathcal{H}_\infty$ control approach (Orukpe et al. [2007]) is introduced and successfully applied to the vibration control problem of flexible-bodied railway vehicles. With parameters properly tuned, satisfying online control is accomplished that the accelerations of the vehicle body are effectively reduced and it is more capable in keeping the suspension deflection small compared to the other control methods. From research point of view, this modern control method shows the capability of achieving a very complicated multi-objective control and balance well between different or even conflicting performance requirements. However, there are no obvious further improvements in ride quality with piezoelectric control inputs. The reasons for this will be further discussed in the following section.

8.6 Concluding remarks

This chapter has considered the design of centralized controllers for vibration control of the flexible bodied railway vehicle. The full model that includes rigid modes, flexible modes and the coupling terms between the rigid modes and flexible modes is used as design model. Three control approaches have been investigated: \mathcal{H}_2 optimal control, \mathcal{H}_∞ optimal control and model predictive control based on a mixed $\mathcal{H}_2/\mathcal{H}_\infty$ control approach.

In general, vibrations of the vehicle body have been effectively suppressed with combined active suspension control and active structural damping with piezoelectric actuators. It is found that the contribution of the piezoelectric actuators in reducing the flexible modes can be limited. This may be due to several reasons: 1) the full model is used for control design and modern control methods are able to use full information of the system provided by the design model; 2) active suspension controller designed with modern methods in this case are effective in suppressing both the vertical rigid modes and vertical bending modes, for there is a close connection between the vertical rigid modes and vertical bending modes, which are the main flexible mode portion of concern in this thesis. Piezoelectric actuators could be complementary in reducing the effects of the flexible modes. Nevertheless, the investigation in this chapter is a good preparation for future research in vibration control of the railway vehicles when more flexible modes of the vehicle body are taken into account.

Chapter 9

Conclusions and Future Work

9.1 Conclusions

Previous research on active secondary suspension has proved that it is an effective way for vibration control of the railway vehicle to improve the ride quality. However, its ability in suppressing the flexible modes is limited by the dynamics of real actuators (e.g. hydraulic actuators) that are used for suspension control and by the fact that the real vehicle body is complex because it includes various flexible modes: vertical bending mode, horizontal bending mode, torsional mode and diagonal distortion mode. Literature in suppressing of the flexible modes of railway vehicles has been concentrated on the application of piezoelectric actuators and sensors for structural damping without including suspension control. Therefore, it is motivated to study the combined control approach with both active suspension control and active structural damping for improving the ride quality of the railway vehicles. Active structural damping is realized by integrating piezoelectric actuators and sensors onto the vehicle body together with appropriate control strategies.

This thesis describes the modeling and control design for vibration suppression of a typical flexible-bodied railway vehicle. The work is based on a simplified side-view model of the railway vehicle with the vehicle body assumed as a free-free beam. It is aimed to improve the vertical ride quality

9.1. CONCLUSIONS

of the railway vehicle. Hence bounce and pitch (rigid modes) of the vehicle body and the vertical bending mode of the vehicle body are the modes of concern for suppressing. The main contributions of this thesis are listed as follows:

1. Rigorous modeling and related analysis of a flexible-bodied railway vehicle with the so called smart structure, i.e. the vehicle body (assumed as a free-free beam) integrated with piezoelectric actuators and sensors. The modal analysis technique has been utilized for deriving the equations of motion of the flexible modes and the derivation of couplings terms between the rigid motion and flexible motion. The link between the rigid motion and flexible motion suggests that it would be more effective to consider the combined control of active suspension control and active structural damping.

2. The effect of flexibility of the vehicle body upon the ride quality is investigated. Two controllers, i.e. modal controller with skyhook damping and LQG controller, were designed using the rigid model as the design model. The simulation of the closed-loop system with the controller that ignores the flexibility in design stage shows degradation in ride quality which is caused by flexibility of the vehicle body. So it is indicated that it is necessary to introduce extra control for suppressing the flexibility of the vehicle body.

3. The procedure for placement of piezoelectric actuators and sensors on the vehicle body with the application of the $\mathcal{H}_2/ \mathcal{H}_\infty$ norms of flexible structures(Gawronski [1998]) is presented. The candidate positions for piezoelectric actuators and sensors are determined and four placement configurations are chosen.

4. The investigation of two control strategies, i.e. decentralized control and centralized control, for the combined active suspension control and active structural damping with piezoelectric actuators.

With decentralized control, the couplings between the flexible motions and the rigid motions are not taken into account during control design when decoupled models are used for control design. In this case, the controller for active suspension and the controller for structural damping are designed independently for suppressing the rigid motion and the flexible motion respectively. Two combinations of control methods have been investigated

9.1. CONCLUSIONS

: 1) modal control with skyhook damping for suspension control and LQG control for structural damping with piezoelectric actuators and sensors. 2) two individual LQG controllers for structural damping with piezoelectric actuators and sensors and suspension control respectively. The damping ratios of the flexible modes are effectively increased with the designed controllers. The advanced control method achieves better ride quality than classical control methods. The results show that the two sub controllers are able to work in a complementary manner to each other in achieving a satisfactory ride quality for the railway vehicle under consideration. When the LQG controller for suspension control is designed with the full model, it is shown that the contribution by the piezoelectric actuators is not evident due to the fact that the suspension controller has already suppressed the first bending flexible mode sufficiently.

5. With centralized control, the full model that includes rigid modes, flexible modes and the coupling terms between the rigid modes and flexible modes are used for control design. It presented the application of three advanced control methods, i.e. \mathcal{H}_2 optimal control, \mathcal{H}_∞ optimal control and model predictive control (MPC) based on a mixed $\mathcal{H}_2/\mathcal{H}_\infty$ control approach for designing the centralized controller.

Two \mathcal{H}_2 controllers have been designed with constant weights and with frequency dependent weights respectively. The \mathcal{H}_2 controller with constant weights achieves the lowest acceleration levels. When dynamic weights are chosen to account for the limited bandwidth of hydraulic actuators and to reflect the desired frequency range of the piezoelectric actuators, a degradation is seen in the ride quality of the system. With piezoelectric control included, its contribution in reducing the acceleration is not obvious, however, it is seen that resonances in PSDs are eliminated, the flexibility of the first flexible mode is further attenuated, and the control effort from the actuators around the frequency of the first flexible mode is reduced. Then the \mathcal{H}_∞ controller is designed via the signal based approach. Satisfactory results have been obtained and improvements in ride quality are achieved by including piezoelectric control inputs. Finally a novel method of MPC

based on a mixed $\mathcal{H}_2/\mathcal{H}_\infty$ control approach is investigated¹. It has been shown that the vibrations of the vehicle body are effectively suppressed with this new method. However the improvement in ride quality provided by the piezoelectric actuators is not evident.

The overall summary of the results is presented in Table 9.1. D_1 represents the decentralized controller, $K_1 + K_{sky}$, where K_1 is the LQG controller for active structural damping(with configuration 3) and K_{sky} is the modal controller with skyhook damping for suspension control. D_2 represents the decentralized controller, $K_1 + K_{rLQG}$, where K_{rLQG} is the LQG controller designed with rigid model for suspension control.

In general, the advanced control approaches achieves better ride quality than classical control approach. The \mathcal{H}_∞ controller is more conservative than \mathcal{H}_2 /LQG controllers in improving the ride quality while accomplish better stability robustness. The MPC based on mixed $\mathcal{H}_2/\mathcal{H}_\infty$ control approach shows the capability of achieving multi-objective control that the level of acceleration achieved is comparable to that achieved by \mathcal{H}_2 controller with dynamic weights with better robustness properties in disturbance rejection.

Table 9.1: Percentage improvement in ride quality compared with the passive system

Strategy	Center (%)	Left (%)	Right (%)
D_1	51.97	51.32	61.07
D_2	87.83	82.89	85.33
\mathcal{H}_2 cons. weights	88.16	83.55	85.87
\mathcal{H}_2 dyn. weights	85.20	78.62	82.13
\mathcal{H}_∞	81.25	77.96	83.47
MPC	85.20	77.30	81.60

9.2 Suggestions for future work

The vehicle body was viewed as a free-free beam and only the vertical bending modes were considered. In future research, more flexible modes

¹This has been joint work between the author of the thesis and Dr. Orukpe,P.E (Orukpe et al. [2008])

(e.g vertical bending mode, horizontal bending mode, torsional mode and diagonal distortion mode) may be included in the vehicle model. This will add to the complexity of the placement of the piezoelectric actuators and sensors and the modeling of the flexible structure of the vehicle body integrated with piezoelectric actuators and sensors and it is expected to see that the piezoelectric actuators will possibly play a more important role in active damping of the flexible structure.

Uncertainty was not included in the control design. Variations in values of parameters such as of mass, damper and flexible frequency and mode shapes will have an effect on the stability and performance of the system. Besides, in theory, there is an infinite number of flexible modes, so the neglected high-frequency modes may cause stability problems and degradation of performance. Therefore, structured and unstructured uncertainties may be introduced to the linear model in future control design. However, this will yield a quite complex robust stability and robust performance problem as well as larger scale models that may require a form of model reduction to be performed. From the control design point of view, techniques such as μ -synthesis may be employed to cater for worst case designs.

References

Mehdi Ahmadian and Andrew P. DeGuilio. Recent advances in the use of piezoceramics for vibration suppression. *The Shock and Vibration Digest*, 33(1), 2001.

Osama J. Aldraihem. Realistic determination of the optimal size and location of piezoelectric actuator/sensors. *Proceedings of the 1997 IEEE International Conference on Control Application*, Hartford,CT(October 5-7), 1997.

C. Benatzky, M. Kozek, and C. Bilik. Experimental control of a flexible beam using a stack-bending actuator principle. *Institute of Mechanics and Mechatronics, Division of Control and Process Automation, Vienna University of Technology*.

Christian Benatzky and Martin Kozek. Influence of actuator size and location on robust stability of actively controlled flexible beams. *Proceedings of the 17th World Congress The International Federation of Automatic Control, Seoul, Korea*, 2008.

Christian Benatzky, Martin Kozek, and Hanns Peter Jorgl. Comparison of controller design methods for a scaled metro vehicle - flexible structure experiment. *Proceedings of the 2007 American Control Conference, New York, USA*, 2007.

R.E.D. Bishop and D.C. Johnson. *The Mechanics of Vibration*. University Press Cambridge, Cambridge, UK, 1960.

REFERENCES

- Chr Boller. State of the art and trends in using smart materials and systems in transportation vehicles. *Proceeding of Institution of Mechanical Engineers*, 212:149–158, 1998.
- G. Capitani and M. Tibaldi. Reduced-order controllers for active suspension of vehicles with flexible body. *System Modelling and Simulation*, pages 201–206, 1989.
- Inderjit Chopra. Review of state of art of smart structures and integrated systems. *AIAA Journal*, 40(11):2145, 2002.
- R.W. Clough and J. Penzien. *Dynamics of Structures*. McGraw-Hill, New York, 1975.
- B. Dumitrescu. Bounded real lemma for fir mimo systems. *IEEE Signal Process. Lett.*, 12(7), 2005.
- D.J. Ewins. *Modal Testing*. 2nd edition, Research Studies Press, Baldock, England, 2000.
- E. Foo and R.M. Goodall. Active suspension control of flexible-bodied railway vehicles using electro-hydraulic and electro-magnetic actuators. *Control Engineering Practice*, 8:507–518, 2000.
- Edwin Foo and R. M. Goodall. Active suspension control strategies for flexible-bodied railway vehicles. *UKACC International conference on control '98*, pages 1300–1305, 1998.
- T. H. E. Foo. *Active Suspensions for Flexible-bodied Rail Vehicles*. PhD thesis, Loughborough University, Jun 2000.
- Henri P. Gavin. Control of seismically excited vibration using electrorheological materials and lyapunov methods. *IEEE transaction on control systems technology*, 9(1), Jan 2001.
- W. Gawronski. *Advanced structural dynamics and active control of structures*. New York:Springer, 2004.

REFERENCES

- W. Gawronski. Letters to the editor: simultaneous placement of actuators and sensors. *Journal of Sound and Vibration*, 228(4):915–922, 1999.
- Wodek K. Gawronski. *Advanced Structural Dynamics and Active Control of Structures*. Springer, New York, 1998.
- William B. Gevarter. Basic relations for control of flexible vehicles. *AIAA Journal*, 8(4):666–672, April 1970.
- R. M. Goodall. Active railway suspensions: Implementation status and technological trends. *Vehicle System Dynamics*, 28(1997):87–117, 1997.
- R. M. Goodall and W. Kortum. Mechatronic developments for railway vehicles of the future. *Control Engineering Practice*, 10(8):887–898, 8 2002.
- A. Hac. Stochastic optimal control of vehicles with elastic body and active suspension. *Journal of Dynamics Systems, Measurement and Control*, 108(2):106–110, 1986.
- A. Hac. Suspension optimization of a 2-DOF vehicle model using a stochastic optimal control technique. *System Modelling and Simulation*, pages 201–206, 1989.
- A. Hac and L. Liu. Sensor and actuator location in motion control of flexible structures. *Journal of Sound and Vibration*, 167(2):239–261, 10/22 1993.
- Aleksander Hac, Iijoong Youn, and Hsien H. Chen. Control of suspensions for vehicles with flexible bodies-part I: Active suspensions. *Journal of Dynamic Systems, Measurement, and Control*, 118:509–517, 1996a.
- Aleksander Hac, Iijoong Youn, and Hsien H. Chen. Control of suspensions for vehicles with flexible bodies-part II: Semi-active suspensions. *Journal of Dynamic Systems, Measurement, and Control*, 118:519–525, 1996b.

REFERENCES

- Duant Halim. *Vibration analysis and control of smart structures*. PhD thesis, The University of Newcastle, New South Wales, Australia, 2002.
- Dunant Halim and S.O. Reza Moheimani. Spatial h_2 control of a piezoelectric laminate beam: experimental implementation. *IEEE transactions on control systems technology*, 10(4), 2002.
- Dunant Halim and S.O. Reza Moheimani. Spatial resonant control of flexible structures - application to a piezoelectric laminate beam. *IEEE transactions on control systems technology*, 9(1), 2001.
- J. Hansson, M. Takano, T. Takigami, Tomioka, and Y.Suzuki. Vibration suppression of railway vehicle carbody with piezoelectric elements (a study by using a scale model). *JSME International Journal Series C.*, 47(2), 2003.
- S. Hurlebaus and L. Gaul. Smart structure dynamics. *Mechanical Systems and Signal Proceeding*, 2005.
- W.B. Spillman Jr, J.S. Sirkis, and P.T. Gardiner. Smart materials and structures: what are they? *Smart Materials and Structures*, (5):247–254, 1996.
- Marke Kallio, Tatu Muukkonen, Seija Hietanen, Ismo Vessonen, Kari Tammi, and Mikko Lehtonen. *Smart Materials and Structures : VTT research program 2000-2002*. VTT Technical research centre of Finland, Vuorimiehentie, Finland, 2002.
- Takayoshi Kamada, Takayuki Tohtake, Tetsuro Aiba, and Masao Nagai. Active vibration control of the railway vehicles by smart structure concept. *Proceedings of International Symposium on Speed-up and Service Technology for Railway and Maglev Systems*, 2005.
- Takayoshi Kamada, Ryohei Kiuchi, and Masao Nagai. Suppression of railway vehicle vibration by shunt damping using stack type piezoelectric transducers. *Vehicle System Dynamics*, 46(Supplement):561–570, 2008.

REFERENCES

- D.C. Karnopp. Are active suspension really necessary. *The American Society of Mechanical Engineers Winter Meeting(San Francisco)*, Paper 78-WA/DE-12, 1978.
- D.C. Karnopp. Active and semi-active vibration control. Technical report, Department of Mechanical and Aeronautical Engineering, University of California, 1974.
- Martin Kozek, Christian Benatzky, Alexander Schirrer, and AntonStribersky. Vibration damping of a flexible car body structure using piezo-stack actuators. *Control Engineering Practice*, doi:10.1016/j.conengprac.2009.08.001, 2009.
- WW Law, WH Liao, and Huang. Vibration control of structures with self-sensing piezoelectric actuators incorporating adaptive mechanisms. *Smart Materials and Structures*, 12(5), 2003.
- S. Leleu, H. Abou-Kandil, and Y. Bonnasieux. Piezoelectric actuators and sensors location for active control of flexible structures. *IEEE transactions on Instrumentation and Measurement*, 50(6):1577–1582, 2001.
- H. Li and R. M. Goodall. Linear and non-linear skyhook damping control laws for active railway suspensions. *Control Engineering Practice*, 7(7): 843–850, 1999.
- S.O. Reza Moheimani. Resonant control of structural vibration using charge-driven piezoelectric actuators. *IEEE transactions on control systems technology*, 13(6), 2005.
- S.O. Reza Moheimani. A survey of recent innovations in vibration damping and control using shunted piezoelectric transducers. *IEEE transactions on control systems technology*, 11(4), 2003.
- N. Nagai and Y. Sawada. Active suspension for flexible structure control of high speed ground vehicles. In *10th World Congress on Automatic Control*, pages 197–202, 1987.

REFERENCES

- Patience E. Orukpe, Xiang Zheng, I.M. Jaimoukha, A.C. Zolotas, and R.M. Goodall. Model predictive control based on mixed control approach for active vibration control of railway vehicles. *Vehicle System Dynamics*, 46(1):151–160, 2008.
- P.E. Orukpe, I.M. Jaimoukha, and H.M.H. El-Zobaidi. Model predictive control based on mixed \langle_2/\langle_∞ control approach. *Proceedings of American Control Conference, New York, USA*, pages 6147–6150, 2007.
- Anneli Orvnas. Methods for reducing vertical carbody vibrations of a rail vehicle: A literature survey. *KTH Engineering Sciences, Sweden*, 2010.
- Anneli Orvnas. *Active secondary suspension in trains: A literature survey of concepts and previous work*. Royal Institutue of Technology, Stockholm, 2008. ISBN 978-91-7415-144-2.
- J.E. Paddison. *Advance Control Strategies For Maglev Suspension Systems*. PhD thesis, Loughborough University, 1995.
- S. Popprath, C. Benatzky, C. Bilki, M. Kozek, A. Stribersky, and J. Wassermann. Experimental modal analysis of a scaled car body for metro vehicles. *The Thirteenth International Congress on Sound and Vibration, Vienna, Austria*, July 2006.
- I. Pratt. *Active Suspensions Applied to Railway Trains*. PhD thesis, Loughborough University, UK, 1996.
- L.R. Ray. Robust linear-optimal control laws for active suspension systems. *Transactions of ASME, Journal of Dynamic Systems, Measurement, and Control*, 114(4):592–598, 1992.
- Y.M. Sam and K.Hudha. Modelling and force tracking control of hydraulic actuator for an active suspension system. *IEEE*, 2006.
- Gerhard Schandl, Peter Lugner, Christian Benatzky, Martin Kozek, and Anton Stribersky. Comfort enhancement by an active vibration

REFERENCES

- reduction system for a flexible railway car body. *Vehicle System Dynamics*, 45(9), 2007.
- C. Scherer and S. Weiland. Linear matrix inequalities in control. *DISC course lecture notes*, 2000.
- A. Schirrer and M. Kozek. Co-simulation as effective method for flexible structure vibration control. *16th Mediterranean Conference on Control and Automation, Ajaccio, France*, 2008.
- Sigurd Skogestad and Ian Postletwaite. *Multivariable Feedback Control: Analysis and design*. John Wiley & Sons, Ltd., 2005.
- Yoshiki Sugahara, Tadao Takigami, and Mitsuji Sampei. Suppressing vertical vibration in railway vehicles through primary suspension damping force control. *Journal of System Design and Dynamics*, 1(2), 2007.
- Tadao Takigami and Takahiro Tomioka. Investigation to suppress bending vibration of railway vehicle carbodies using piezoelectric elements. *QR of RTRI*, 46(4), 2005.
- Tadao Takigami and Takahiro Tomioka. Bending vibration suppression of railway vehicle carbody with piezoelectric elements(experimental results of excitation tests with a commuter car). *Journal of Mechanical Systems for Transportation and Logistics*, 1(1), 2008.
- Takayuki Tohtake, Masao Nagai, Takayoshi Kamada, and Hidehisa Yoshida. Active vibration control of the railway vehicles by smart structure. *Proceedings of International Symposium on Speed-up and Service Technology for Railway and Maglev Systems*, 2005.
- H. Tsunashima and S. Morichika. Ride quality improvement of agt vehicle by active secondary suspension. *Vehicle System Dynamics Supplement*, 41:764–773, 2004.

REFERENCES

- H.S. Tzou and J.J. Hollkamp. Collocated independent modal control with self-sensing orthogonal piezoelectric actuators(theory and experiment). *Smart Materials and Structures*, 3(1994), 1994.
- R. A. Williams. *Comparison of Classical and Optimal Active Suspension Control System*. PhD thesis, Loughborough University, 1986.
- P. Wu, J. Zeng, and H. Dai. Dynamic responses analysis of railway passenger car with flexible carbody model based on semi-active suspensions. *Vehicle System Dynamics Supplement*, 41:774–783, 2004.
- Hazlina Md Yusof, Roger M. Goodall, and Roger Dixon. Controller strategies for active secondary suspension actuators. *IAVSD*, 2011.

Appendices

Appendix A

Railway Vehicle parameters

Parameter	Symbol	Value
Mass of the vehicle	M_v	38000(kg)
Mass of the bogie	M_b	2500(kg)
Body pitch Inertia	I_{vc}	$2.31 \times 10^6 ((kgm)^2)$
Primary spring stiffness per axle	K_p	4.935(MN/m)
Primary damping per axle	B_p	0.05074(MNs/m)
Secondary spring stiffness per bogie	K_s	1.016(MN/m)
Secondary area stiffness per bogie	K_a	0(N/m)
Secondary reservoir stiffness per bogie	K_{sr}	0.508MN/m
Secondary damping per bogie	B_{sr}	0.06411 (MN/m)
Bogie center	L_{bc}	19(m)
Vehicle+gangway	L_v	27(m)
Speed of the train	v	198 (km/h)

Source: Foo and Goodall [2000],Phd thesis, Loughborough University (UK)

Appendix B

Actuator and sensor parameters

Table B.1: Specifications of electro-servo hydraulic actuator

Parameter	Symbol	Value
Spool mass	m_s	0.075(kg)
Spool stiffness	k_s	185000(Nm ⁻¹)
Spool damping	c_s	471 (Nsm ⁻¹)
Torque motor gain	k_i	142 (NmA ⁻¹)
Oil supply pressure	p_s	2×10^7 (Nm ⁻²)
Linearised parameter	dqaddxv	0.00935
Linearised parameter	dqbddxv	0.01218
Linearised parameter	dqaddpa	2.022×10^{-12}
Linearised parameter	dqbddpb	-1.9232×10^{-12}
Oil compressibility	β	1.38×10^9
Annulus cylinder volume	v_a	$5.063 \times 10^{-6}(m^3)$
Bore cylinder volume	v_b	$9.039 \times 10^{-6}(m^3)$
Annulus side area	a_a	$2.25 \times 10^{-4}(m^2)$
Bore side area	a_b	$4.02 \times 10^{-4}(m^2)$
Ram damping	c_d	$1.2 \times 10^3(Nsm^{-1})$

Source: Pratt [1996],Phd thesis, Loughborough University (UK)

Table B.2: Specification of piezoelectric stack actuator

Manufacture	PIEZOMECHANIK
Type	Pst1000/35/200VS45
Maximum force	50,000N
Length, L_{px}	0.194m
Thickness of one disk	5×10^{-4} m
Diameter of disk	0.045m
Piezoelectric constant, d_{33}	6.80×10^{-10} m/volts
Compliance, s_{33}^E	23×10^{-12} m^2/N

Table B.3: Specification of piezoelectric sensor patch

Length	0.02 m
Thickness	2.5×10^{-4} m
Width	0.025 m
Young's Modulus, E_p	6.70×10^{10} N/m^2
Capacitance, C_p	1.05×10^{-7} F
Electromechanical coupling factor, k_{31}	0.34
Voltage constant, g_{31}	-1.15×10^{-2} Vm/N

Appendix C

Publications of research work

[1] Patience E. Orukpe, X.Zheng, I.M.Jaimoukha, A.C.Zolotas and R.M.Goodall Model predictive control based on mixed control approach for active vibration control of railway vehicles *Vehicle System Dynamics*, 46:1, 151-160,2008

[2] X.Zheng and A.C.Zolotas and R.M.Goodall Modeling of flexible-bodied railway vehicles for vibration suppression *ICSE*, Coventry, UK, Sep 2006

[3]X.Zheng and A.C.Zolotas and H.Wang. Mathematica implementation of output-feedback pole assignment for uncertain systems via symbolic algebra *International Journal of Control*, Vol. **79**, No.11, 1431-1446, Nov 2006